CONVECTION PROCESSES IN TURBULENT IMPINGING JETS

by

Micha Wolfshtein

Thesis submitted for the degree of
Doctor of Philosophy
in the Faculty of Engineering
University of London

November, 1967

To my wife, my parents and my children, without whose cooperation, help and understanding this thesis would have never been written.

Abstract

A finite-difference method for the solution of the elliptic equations governing the steady transfer of momentum, heat and matter in turbulent flows is presented. The method ensures that the laws of conservation are satisfied over arbitrarily large or small control volumes. Accuracy, convergence and economy of the method are discussed, and shown to be satisfactory in cases of practical interest. The phenomenon of "false diffusion" is discussed, and related to local quantities.

On the physical side, the Kolmogorov-Prandtl hypothesis of turbulence is extended to two-dimensional flows and to viscous sublayer near solid walls. The empirical input to the hypothesis is obtained from various sets of data, for experimental situations approximating to Couette flows. Numerical solutions for Couette flows with augmented turbulence have been computed and cast in the form of wall-functions, for use in two-dimensional problems.

The finite-difference method, the viscosity hypothesis and the wall-functions are then used to obtain solutions for the problem of a plane, turbulent jet impinging normally to a flat surface. Comparisons with experimental results are made, and the influence of the Reynolds and Prandtl numbers is studied. The distribution of the

kinetic energy of the turbulent velocity-fluctuations is studied and discussed as well.

Finally, the results of the project are discussed, and suggestions for the continuation of the research are made.

Preface

This thesis constitutes the main result of the research activities which I have pursued in the Mechanical Engineering Department of Imperial College during the last three years. The tentative subject of this research was the provision of prediction methods for heat transfer in impinging jets. During the early days of the work, this project was supposed to be centered around the numerical solution of the parabolic equations governing wall-jet and boundary-layer flows, as well as experimental work on the wall jet itself. Therefore, I tried to collect and correlate data from different sources (Wolfshtein, 1966), and to adapt to the wall-jet problem solution-methods of the boundary-layer equations by integral methods (Patankar and Wolfshtein, 1966). But, at about the same time, I realised that the most un-explored part of the impinging jet system is, by far, the impingement region itself, and I decided to concentrate on it.

During 1966 I became more and more engaged in work on the solution of the elliptic, complete Navier-Stokes equations, by which the required solution could be obtained. Some of the results of this work were reported already in earlier papers by Runchal and Wolfshtein (1966), Runchal, Spalding and Wolfshtein (1967), Wolfshtein (1967), and Runchal and Wolfshtein (1967). In part II of the

present thesis, a full account of the final outcome of my work in this direction is given. For the sake of completeness I had to include some material which was reported in the earlier papers, but I usually presented such material in brief form only, quoting the appropriate reference.

Thus, towards the end of 1966, it became evident that solution to the impinging jet problem came within easy reach. The weak link in the chain was the turbulent viscosity law, and I had planned to fill this gap by measuring the turbulent heat-diffusion-coefficient in the impinging jet and incorporating correlations of these measurements in the computations. However, a road-accident prevented this experimental work. Instead, I had to obtain a viscosity law on the basis of the experimental data which were available, for other types of flow. In practice, this was done by the extension of the Kolmogorov-Prandtl hypothesis to two-dimensional flows, by a study of Couette flows with augmented turbulence, and by the development of special procedures for the treatment of flow near solid walls. All this work is reported in part III of the paper, as well as the impinging jet solutions which I was, eventually, able to get.

No account of my work will be complete without the mention of my supervisor, Professor D.B. Spalding. Professor Spalding took an active part in the research

project all along the way, supplying a constant stream of new ideas and suggestions, and in general, creating a very stimulating atmosphere among the whole group of research workers around him. The greatest tribute which I may pay to him, is, in my opinion, that Professor Spalding did not act only as my supervisor in this research, but was also a teacher, both in the subject of turbulent flows, and in more remote topics, such as technical writing, doing research, etc., etc. Last, but not least in the list was Professor Spalding's help to me in a time of personal hardship.

During a considerable period I was working in close contact with Mr. A.K. Runchal. Our collaboration and friendship was very fruitful, both in the results achieved, and in the satisfaction which I got from it. The credit for the development of the finite-difference method and the computer programme should be shared by both of us.

There are many others to whom my thanks are due. But I wish to mention specifically Mr. N. Mitchell, Dr. S.V. Patankar, Dr. W.M. Pun and Dr. E. Baker, who were always willing to help, and Miss M.P. Steele, who was always ready to solve administrative problems. The project became possible by the generous allocation of computer time by the Center for Computing and Automation of Imperial College.

During the time of this project I was financed by a research assistantship from the Imperial College. My travel to this country was covered by a loan from the Technion, Israel Institute of Technology. I was also assisted by a grant from the Committee for the Encouragement of the Research and Further Study of the Executive Committee of the General Federation of Jewish Labour in Israel.

Contents

List of figures

Part I : Introduction

1. Introduction

1.1 A general description of the problem

The recent advent of fast computing machines, accompanied by a rapid development of numerical analysis, has had a very strong influence on fluid-dynamics. Not only has it enabled us to obtain solutions for much more complex problems of potential and boundary-layer flow than we could some ten years ago, but also we may now venture into the relatively new field of the complete, non-linear, elliptic equations of flow. True enough, such solutions were obtained before as well, notably by Thom (1933), and then by some others in the early fifties; but these early solutions did not result in standard solution methods. All these early solutions were too laborious and limited in their scope.

The present thesis describes a new general computational scheme for the solution of the elliptic equations of fluid flow, and its application to the problem of a plane, turbulent, impinging jet. Among the interesting features of the thesis are the application and extension of the Kolmogorov-Prandtl hypothesis of turbulence. Another contribution in the present thesis is the suggestion of some new lines of research, which have become possible and necessary as a result of the new development.

The impinging jet deserves a special note. As far as the author is aware, this is the first time that a complete theoretical solution could be obtained for this phenomenon. Perhaps the most important feature of this solution is that it is derived from basic principles, and that none of the empirical input into it was extracted from impinging jet studies (or indeed, even from free-jet ones). Thus the impinging jet solutions serve two purposes simultaneously. Firstly, a demonstration is given, that impinging jet flow may be predicted. Secondly, the impinging jet solution serves as a test-ground for the validity of the method of solution and the turbulence hypothesis. The latter is probably the most promising prospect of the new method. We are now able to test new turbulence hypotheses without having to apply restrictions and simplifications to the basic equations.

1.2 An outline of previous knowledge

1.2.1 The plane impinging jet

Studies of impinging jets have attracted many researchers because of the high rates of heat-transfer which are found in the impingement region. Some of the heat-transfer experiments are summarised in table 1.2-1 below:

Author and year	Coefficients measured	Prandtl number	Range	
			$Re_c \times 10^{-3}$*	h_c/d_c
Glaser (1961)	mean mass-transfer	0.58	.9-10	2-16
Metzger (1962)	mean heat-transfer	0.71	1.5-4	2-20
Schauer and Eustis (1963)	local heat-transfer	0.71	40.8	40
Gardon and Akifrat (1965)	local heat-transfer	0.71	.45-22	2-45
Kroger and Krizek (1966)	local mass-transfer	2.5	8.3-44	.5-40

Table 1.2-1. Summary of heat-transfer measurements in impinging jets

Accurate comparison between these various sources is difficult because in most cases the measured parameters of the flow (such as the Reynolds number, the Prandtl number etc.) are not accurately reported. Still it was found useful to plot the stagnation point heat-transfer coefficient, St_o, versus the slot Reynolds number, Re_c, in figure 1.2-1 for

---

* All symbols are defined in chapter 9.

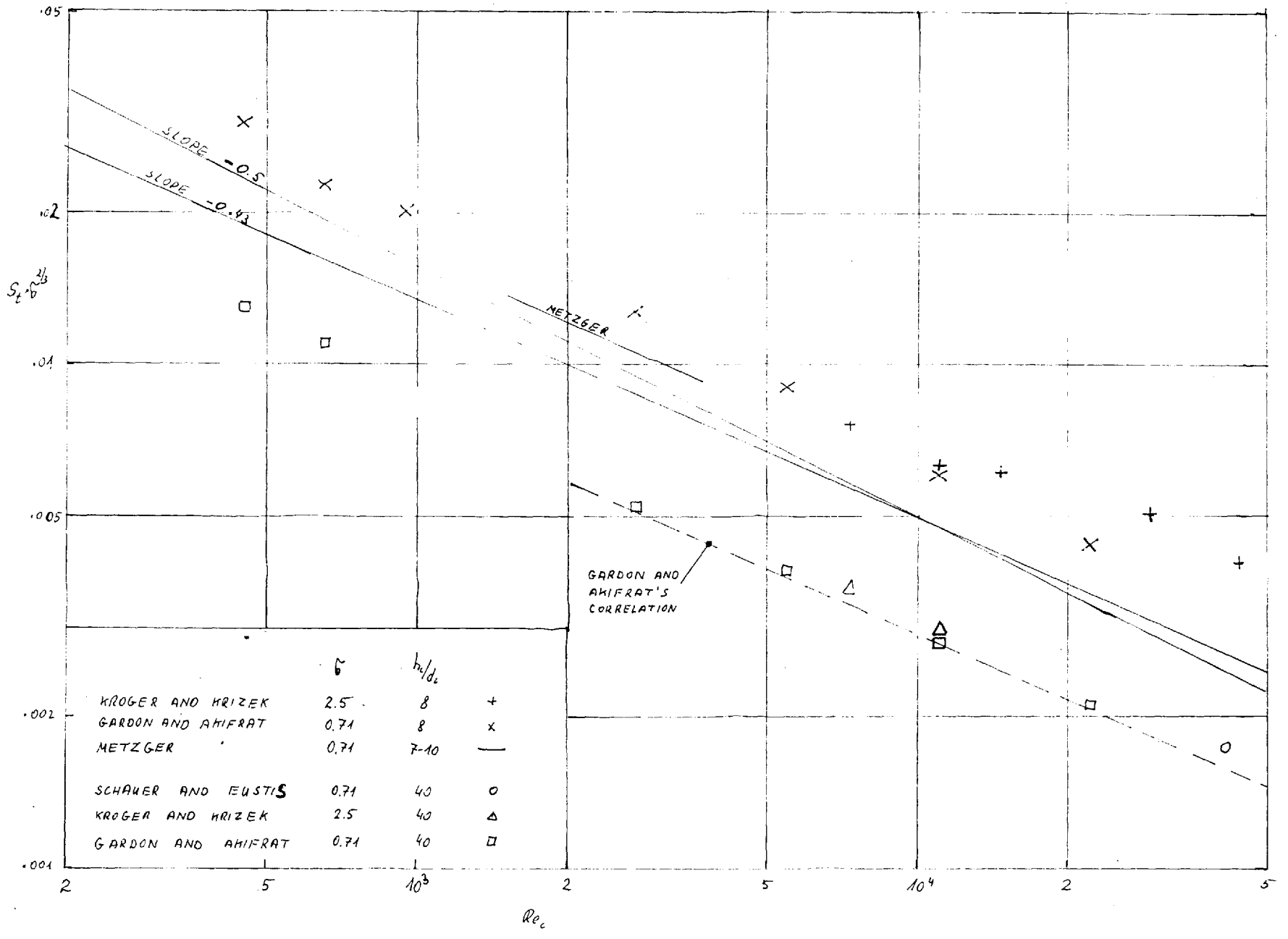

FIG 1.2-1: THE STANTON NUMBER AT THE STAGNATION POINT OF AN IMPINGING JET VERSUS THE REYNOLDS NUMBER.

the two nozzle-to-surface distances of $h_c/d_c = 8$ and $h_c/d_c = 40$.

There has been a wide spread-belief that the flow in the stagnation region is laminar. Therefore Metzger deduced that the $St_o \sim Re_c$ relation should have the form

$$St_o = \text{const.} \times Re_c^{\,a} \qquad (1.2\text{-}1)$$

where $a = \frac{1}{2}$.

This deduction was not supported, however, by experiments. Both Metzger's measurements and figure 1.2-1 suggest that the $Re_c \sim St_o$ relation may be correlated by equation (1.2-1) only if a is taken to be around 0.43. Apparently, the power a is independent of the Reynolds number.

Another interesting feature of the flow has been reported by Gardon and Akifrat, who found that augmentation of the turbulence intensity in the jet increases the heat-transfer in the stagnation region. Sutera et al. (1963) reported very similar trends in stagnation flow.

Skin-friction, surface static pressure, and maximum velocity measurements in the impingement region were reported by Schauer and Eustis, for a Reynolds number of about 43000, and a slot-to-plate distance of 40 slot widths.

Theoretical works on the impinging jet have not been very numerous: an interesting solution to the problem of laminar impingement was obtained by Chung and Viegas (1961); but their solution was heavily dependent on some simplifying

assumptions. Strand (1962) obtained an analytical solution to the velocity and pressure distributions in an irrotational inviscid impinging jet. Schauer and Eustis attempted a theoretical solution for the turbulent impinging jet problem. However, their solution was so much based on experimental information, that it could hardly be regarded as anything more than a complex correlation.

Sutera et al. (1963) devised a complex model to explain the increase in heat transfer in the stagnation point by the presence of turbulence in the flow. They obtained numerical solutions by which they showed that a relatively small increase in the level of turbulence might cause a much larger increase in heat-transfer rate.

Finally, Spalding (1967a) has shown that in turbulent stagnation flow the power a in equation (1.2-1) may be 0.4 and not 0.5.

1.2.2 Numerical solutions of the Navier-Stokes equation

The early solutions obtained by Thom (in a series of papers which terminated in 1933) to the full Navier-Stokes equations have already been mentioned. Thom eliminated the pressure by using the vorticity and stream-function as the dependent variables. This practice was later followed by most other workers*, and is also used in the present

---

* Some solution methods, notably those developed in Los-Alamos for non-steady flows, take the pressure and the velocity components as the dependent variables.

paper. Another important contribution made by Thom was the formulation of the vorticity boundary condition on solid walls. Thom related the wall vorticity to the stream function distribution near the wall by a Taylor series expansion of the stream function near the wall. This practice is, in fact, identical to the assumption of a constant vorticity near the wall, a forerunner of the method to be recommended in section 3.2 of the present thesis. On the other hand, Thom's early work, performed before the computer era, demanded too much labour, and was not continued for about twenty years.

In the fifties the interest in the Navier-Stokes equations was re-stimulated, and numerous solutions were obtained, employing various finite-difference techniques. Soon, it became apparent that the use of central differences (as they are usually applied to, say, Laplace's equation) resulted in divergence whenever the Reynolds number became large. Burgraff (1966) suggested overcoming this difficulty by employing a severe under-relaxation. But, apart from the arbitrariness inherent in the selection of his under-relaxation parameter, this practice resulted in excessive computing time.

A different approach was introduced by some workers to un-steady flow problems: they found that a flow-oriented finite-difference formulation resulted in stable

procedures even for very high Reynolds numbers (e.g. Barakat and Clark, 1965) and Runchal and Wolfshtein (1966) showed that this approach is useful also in steady-flows.

1.2.3 The Kolmogorov-Prandtl hypothesis of turbulence

The most successful theory of turbulence has been that of the mixing-length, suggested by Prandtl in 1925. The applicability of this hypothesis has been questioned, however, many times, Its main deficiency is that it relates the turbulence to one free parameter only, the mixing-length. As this parameter is very strongly dependent on the geometry of the flow, this theory is not directly sensitive to changes in the turbulence level inside the flow. Moreover, we cannot usually apply the same set of empirical constants to all flow conditions when we use the mixing-length hypothesis. These deficiencies may be overcome by the use of the turbulent kinetic energy hypothesis, which was introduced by Kolmogorov (1942) and Prandtl (1945). In this theory, one assumes that the turbulence is described by two parameters; a length scale, and the level of kinetic energy of the turbulent fluctuations. Emmons (1954) used this newer concept, and was able to obtain reasonable predictions for a variety of cases, while Spalding (1967a) was able to explain the hitherto unexplained phenomenon of high heat transfer in a reattachment region. Spalding (1967b)

also showed how the turbulent kinetic energy hypothesis reduced to the 1925 mixing-length law for Couette flow and for free jets.

1.3 The present contribution

The present thesis describes research activities which were directed towards three ends;

(i) The development of a computational method and a computer programme for the solution of the elliptic equations governing two-dimensional variable-property flows.

(ii) The recommendation of turbulent-property laws, which are universally valid for any flow, in all the regions of such a flow.

(iii) The predictions of the velocity field and heat transfer in impinging jets.

These three ends are interconnected with one another. When we have the computer programme, we may study and test complex turbulent viscosity hypotheses. The impinging jet is, then, a natural test ground for such hypotheses, being different from regular boundary layers, which have been successfully predicted even with the earlier mixing-length hypothesis. But, on the other hand, the very existence of the programme is sufficient to stimulate interest in the impinging jet problem, provided that a proper viscosity law is available.

The impinging jet results are interesting for several reasons. First because the impinging jet has not yielded to more conventional prediction methods in a satisfactory way. But these computations are of interest also because they display some features of the turbulent impinging jet flow, which have not yet been reported either experimentally or theoretically.

Restrictions: The present thesis is restricted to plane constant property flow on smooth walls, and without chemical reaction. These restrictions do not represent the limitations of the method, which may be applied to any two-dimensional flow (with the possible exception of supersonic flows). Some other restrictions, applied to particular cases, will be discussed in the appropriate sections.

Outline of the thesis: The thesis is divided into the following six parts:

Part I : Introduction to the subject.

Part II : The mathematical problem.

Part III : An application of the method to turbulent flows.

Part IV Closure.

Part V : Nomenclature and references.

Part VI : Appendices.

These parts are further subdivided into chapters. Part II is concerned with the method of solution. In

chapter 2 the differential equations, boundary conditions and auxiliary relations are presented. Then, in chapter 3 these are recast in a finite-difference form. A general finite-difference equation of conservation is derived and the solution procedure is described. A procedure for the evaluation of the wall vorticity is presented as well, followed by some remarks on the computer programme. In chapter 4 the method is checked for convergence, accuracy and economy, by trial solutions of laminar Couette flow and impinging jets. The appearance of the "smearing effect"* due to "false diffusion" is discussed as well, and it is shown that this false diffusion may be related to the local flow and grid properties.

The achievements of part II are exploited in part III, where solutions for the impinging jet problem are obtained. It is necessary, however, to present first a model of turbulence. This is done in chapter 5, where the Kolmogorov-Prandtl hypothesis is presented and extended, so as to give a good agreement with all the available data on turbulent Couette flows. The main achievement in chapter 5 is probably the demonstration that we may choose a single set of constants, which is adequate, together with the turbulent energy hypothesis,

---

* The term "smearing effect" is used in the present thesis to describe the spreading of a conserved property, which is not caused by the physical diffusivity, but is a direct outcome of the finite-difference process. Further details may be found in section 4.4.

in such a wide variety of flow regimes. The results of chapter 5 are further elaborated in chapter 6, where solutions for Couette flows with augmented turbulence are obtained, and cast in the form of wall functions. These wall functions replace the regular boundary conditions in the computational scheme, as was explained in section 3.2; but they also display some interesting features of Couette flows with augmented turbulence. Chapter 7 is the final check the method with the turbulence hypothesis and the wall functions, is applied to a turbulent impinging jet. The results are good enough to justify an optimistic view of the method, but some disagreements arise as well, demanding modifications in the method, and suggesting their possible direction. The problem of such modifications is discussed in part IV of the thesis.

The main contributions of the present thesis may be summarised as follows

(i) The finite-difference method, and the checks on its accuracy, convergence and economy, reported in chapters 3 and 4 respectively.

(ii) The fitting of universal constants in the Kolmogorov-Prandtl hypothesis, and the turbulent Couette flow solutions reported in chapter 5 and 6 respectively.

(iv) The impinging jet solutions in chapter 7.

Part II: The mathematical problem

Part II of the thesis is concerned with the mathematical presentation of the problem. It will be shown in chapter 2, that we can write a set of simultaneous, elliptic, second-order, partial differential equations, which control the transfer of momentum and conserved property in two-dimensional flows. Some ordinary differential equations and algebraic relations will be added, in order to make the number of equations equal to the number of unknowns. A short discussion of the boundary conditions will be presented as well. In chapter 3 a numerical method for the solution of the equations will be presented. The method is a finite-difference, iterative one. The advantages of this method are that it is very stable, and that the conservation laws are satisfied in an arbitrarily large or small control volume. The convergence, accuracy and economy of the method will be discussed in section 4, by reference to trial solutions of laminar and turbulent Couette flows and impinging jets. The influence of such factors as mesh size and mesh distribution will be studied as well.

2. The basic equations

In this chapter we shall list, examine and re-arrange the mathematical equations governing the transport of momentum and conserved properties in an incompressible flow. First we shall deal with the differential equations, then the boundary conditions will be reviewed, and finally all the necessary auxiliary relations will be described.

2.1 Differential equations

The differential equations with which we are concerned are basically those, describing the conservation of mass, momentum and conserved properties, which, in a cartesian coordinate system may be written as:

$$\frac{\partial u_i}{\partial x_i} = 0 \qquad (2.1\text{-}1)$$

$$\rho u_j \frac{\partial u_i}{\partial x_j} = - \frac{\partial p}{\partial x_i} + \frac{\partial \tau_{ij}}{\partial x_j} \qquad (2.1\text{-}2)$$

$$\rho u_j \frac{\partial \phi}{\partial x_j} = - \frac{\partial J_j}{\partial x_j} + S_\phi \qquad (2.1\text{-}3)$$

where ϕ is a conserved property, τ_{ij} is the shear stress, p is the pressure, $\underline{J}$ is the heat flux vector and S_ϕ is a ϕ-source. Other symbols are explained in the nomenclature, chapter 9. The indexes i and j may take the values 1,2,3, and the summation convention is used (i.e. $a_i b_i = a_1 b_1 + a_2 b_2 + a_3 b_3$).

The fluxes are given by

$$\tau_{ij} = \mu_{eff}\left(\frac{\partial u_i}{\partial x_j} + \frac{\partial u_j}{\partial x_i}\right) \qquad (2.1\text{-}4)$$

$$J_j = -\frac{\mu_{eff}}{\sigma_{eff}}\frac{\partial \phi}{\partial x_j} \qquad (2.1\text{-}5)$$

μ_{eff} is the sum of the laminar (or molecular) and the turbulent (or eddy) viscosities. It is introduced here, because we shall later solve problems of turbulent flow. However, the use of an effective viscosity in the present chapter may be regarded as a matter of convenient notation only. The treatment in the following pages is general in its nature, and is adequate for any problem with a variable viscosity due to turbulence, changes in the temperature, or, perhaps, because the fluid is non-Newtonian. The same remark applies also to the effective Prandtl number, σ_{eff}, which is a function of the laminar and turbulent Prandtl numbers. This function will be given in section 5.5.

It will be noted that eqn (2.1-2) is in fact three equations corresponding to the three values of i. These three equations must be solved simultaneously with eqn (2.1-1), for the four variables, p and u_i. We must therefore decide, which equation to use for which variable. Unfortunately, there does not seem to be a general answer to this question: there are situations when eqn (2.1-1) is used to compute the pressure, while

in others it may be used to compute the non-streamwise velocity component (say in a boundary-layer). However, in two-dimensional flows, it is possible to replace the equations (2.1-1) and (2.1-2) with two new equations: one for the stream-function, ψ , and another for the vorticity, ω.

These quantities are defined by

$$\omega = \frac{\partial v}{\partial x} - \frac{\partial u}{\partial y} \qquad (2.1\text{-}6)$$

$$\psi/\rho = \int u\, dy = -\int v\, dx \qquad (2.1\text{-}7)$$

The appropriate derivation for plane flows is given in appendix A.1. The resulting equations are:

$$\rho u_j \frac{\partial \omega}{\partial x_j} = \frac{\partial^2}{\partial x_j^2}\left(\mu_{eff}\,\omega\right) + S_\omega \qquad (2.1\text{-}8)$$

$$\frac{\partial^2 \psi}{\partial x_j^2} + \rho\omega = 0 \qquad (2.1\text{-}9)$$

where $$S_\omega = 2\frac{\partial^2}{\partial x \partial y}\left[\mu_{eff}\left(\frac{\partial v}{\partial y} - \frac{\partial u}{\partial x}\right)\right] + 2\frac{\partial^2}{\partial x^2}\left(\mu_{eff}\frac{\partial u}{\partial y}\right) - 2\frac{\partial^2}{\partial y^2}\left(\mu_{eff}\frac{\partial v}{\partial x}\right) \qquad (2.1\text{-}10)$$

Clearly S_ω equals zero in a uniform viscosity flow, and in boundary layers. But even in other types of flow it is not very important generally, and its neglect will usually not introduce serious errors.

We may now substitute eqn (2.1-5) in (2.1-3) to get

$$\rho u_j \frac{\partial \phi}{\partial x_j} = \frac{\partial}{\partial x_j}\left(\frac{\mu_{eff}}{\sigma_{eff}}\frac{\partial \phi}{\partial x_j}\right) + S_\phi \qquad (2.1\text{-}11)$$

The similarity between eqns (2.1-8) and (2.1-11) is apparent. Moreover, even eqn (2.1-9) is very similar

to the right-hand side of the other two equations. Because of this similarity we may write a general conservation equation:

$$\rho u_j \frac{\partial \phi}{\partial x_j} = \frac{\partial}{\partial x_j}\left[\Gamma \frac{\partial(\mu\phi)}{\partial x_j}\right] + S_\phi \qquad (2.1\text{-}12)$$

All the three equations, (2.1-8), (2.1-9) and (2.1-11), may now be considered as particular cases of eqn (2.1-12).

We shall always have to solve eqns (2.1-8) and (2.1-9) for the vorticity and stream-functions. If we are concerned with heat or mass transfer, we shall have to solve also equation (2.1-11) which will govern the temperature or concentration distribution.

It will be shown in chapter 5, that in case of a turbulent flow, we have to solve also eqn (2.1-11) for the kinetic energy of the turbulent fluctuations. The expression for its source, S_k and diffusivity, Γ_k, will be presented in chapter 5 as well.

2.2 The boundary conditions

The differential equations which we have to solve, (2.1-8), (2.1-9) and (2.1-11) are second-order elliptic equations. Therefore we have to specify the value of each variable (or its first derivative, normal to the boundary) on each boundary. In general such specification will depend on the case considered, and needs no explanation now. We shall, however, consider two parti-

cular kinds of boundaries: the solid wall, and the axis of symmetry.

The solid wall

On a solid wall the velocity is always known. In the present paper we deal mainly with stationary impermeable walls where both velocity components are zero. It follows then, that

$$\psi_s = const \tag{2.2-1}$$

$$\left(\frac{\partial \psi}{\partial n}\right)_s = 0 \tag{2.2-2}$$

where n is the normal to the boundary. It will be noted that we have, in fact, two boundary conditions for ψ, and none for ω. However, these two quantities are coupled through eqn (2.1-9), which on the boundary reduces to

$$\left(\frac{\partial^2 \psi}{\partial n^2}\right)_s = -\rho \omega_s \tag{2.2-3}$$

Therefore, eqn (2.2-1) is a sufficient boundary condition for ψ, and eqn (2.2-2) may be used to derive a boundary condition for ω. Details will be given in section 3.2. The wall fluxes are given by

$$\tau_s = \mu \left(\frac{\partial u}{\partial n}\right)_s \tag{2.2-4}$$

$$J_s = \frac{\mu}{\theta}\left(\frac{\partial \phi}{\partial n}\right)_s \tag{2.2-5}$$

Axis of symmetry

On an axis of symmetry we have, by definition,

$$\omega = 0 \tag{2.2-6}$$

$$\psi = const \tag{2.2-7}$$

$$\frac{\partial \phi}{\partial n} = 0 \tag{2.2-8}$$

where n is the normal to the axis of symmetry.

2.3 Auxiliary relations

The second order partial differential equations, (2.1-8), (2.1-9) and (2.1-11) together with the first order equation (2.1-7), constitute the set of equations which we have to solve. There are, however, some auxiliary relations which must be added to the set of equations, as well, and they will be discussed now:

Physical input

Appropriate physical laws must be specified, in order to describe the viscosity μ_{eff}, the diffusion coefficient Γ_{eff}, and the source terms S representing generation of ϕ. (Sometimes we may prefer to specify the Prandtl number σ_{eff} rather than Γ_{eff}.) In any case μ_{eff}, Γ_{eff}, or σ_{eff} should represent the effective values, which were mentioned in section 2.1.

In the present thesis we deal with constant property laminar and turbulent flows. In the laminar cases μ_{eff},

Γ_{eff} and σ_{eff} are constant (the vorticity source term is zero as well). But in the turbulent cases we must employ some physical hypotheses, which will be discussed in part III of the paper. By these hypotheses we shall compute μ_{eff}, and Γ_{eff} or σ_{eff} which will then replace μ, Γ and σ in our equations.

The pressure differences

The pressure may be related to the other variables by means of equation (2.1-2). It is important to realise however, that equation (2.1-2) is in fact a first-order differential equation for the pressure. Further, this equation requires the gradients of other quantities. On the boundaries of the region these gradients are not necessarily known beforehand, nor obtained by our solution, therefore we cannot apply equation (2.1-2)there. Thus we may compute the pressure differences inside the field only. For convenience, we shall rearrange eqn (2.1-2), to get:

$$\frac{\partial p}{\partial x} = \rho v \omega + \frac{\partial}{\partial x}\left(-\rho\frac{V^2}{2} + 2\mu_{eff}\frac{\partial u}{\partial x}\right) + \frac{\partial}{\partial y}\left[\mu_{eff}\left(\frac{\partial u}{\partial y} + \frac{\partial v}{\partial x}\right)\right] \qquad (2.3\text{-}1)$$

$$\frac{\partial p}{\partial y} = -\rho u \omega + \frac{\partial}{\partial y}\left(-\rho\frac{V^2}{2} + 2\mu_{eff}\frac{\partial v}{\partial y}\right) + \frac{\partial}{\partial x}\left[\mu_{eff}\left(\frac{\partial u}{\partial y} + \frac{\partial v}{\partial x}\right)\right] \qquad (2.3\text{-}2)$$

where

$$V^2 = u^2 + v^2 \qquad (2.3\text{-}3)$$

These equations may now be integrated starting from any arbitrary point inside the control volume, until all the

points inside the control volume have been covered.

Other relations

There are some other quantities which are used in the present work, mainly as an aid to improve the physical interpretation of the solutions. They are:

The dynamic pressure:

$$p_d = \frac{1}{2}\rho(u^2+v^2) = \frac{1}{2}\rho V^2 \qquad (2.3\text{-}4)$$

The shear stress

$$\tau_{xy} = \tau_{yx} = \mu_{eff}\left(\frac{\partial u}{\partial y} + \frac{\partial v}{\partial x}\right) \qquad (2.3\text{-}5)$$

The mass velocity

$$\underline{G} = \rho\,\underline{u} \qquad (2.3\text{-}6)$$

Some other relations which are connected with the turbulence energy will be discussed in chapter 5.

3. The finite-difference equations

In chapter 2 we have seen the differential equations, which we have to solve. Generally, there is only one practical method to obtain solution of these equations, and this is by finite-difference techniques. We cover our control volume with a mesh, which is rectangular in the present work. In each mesh point we replace each differential equation with a finite-difference, algebraic equation. To obtain the solution we solve all these equations simultaneously; because of the large number of algebraic equations involved the solution method must usually be iterative. The purpose of the present chapter, is to describe the finite-difference equations and the method of their solution.

3.1 The conserved property finite-difference equation

As already mentioned in chapter 2, we have to consider the general conservation equation (2.1-12) rather than the particular equations (2.1-8), (2.1-9) and (2.1-11).

The finite-difference substitution to this equation will be obtained by integration of the equation over small rectangles, surrounding each mesh point. These rectangles are so defined, that their sides lie half-way between the mesh points, parallel to the x and y axes (see fig 3.1-1). In appendix A.2 the integration of

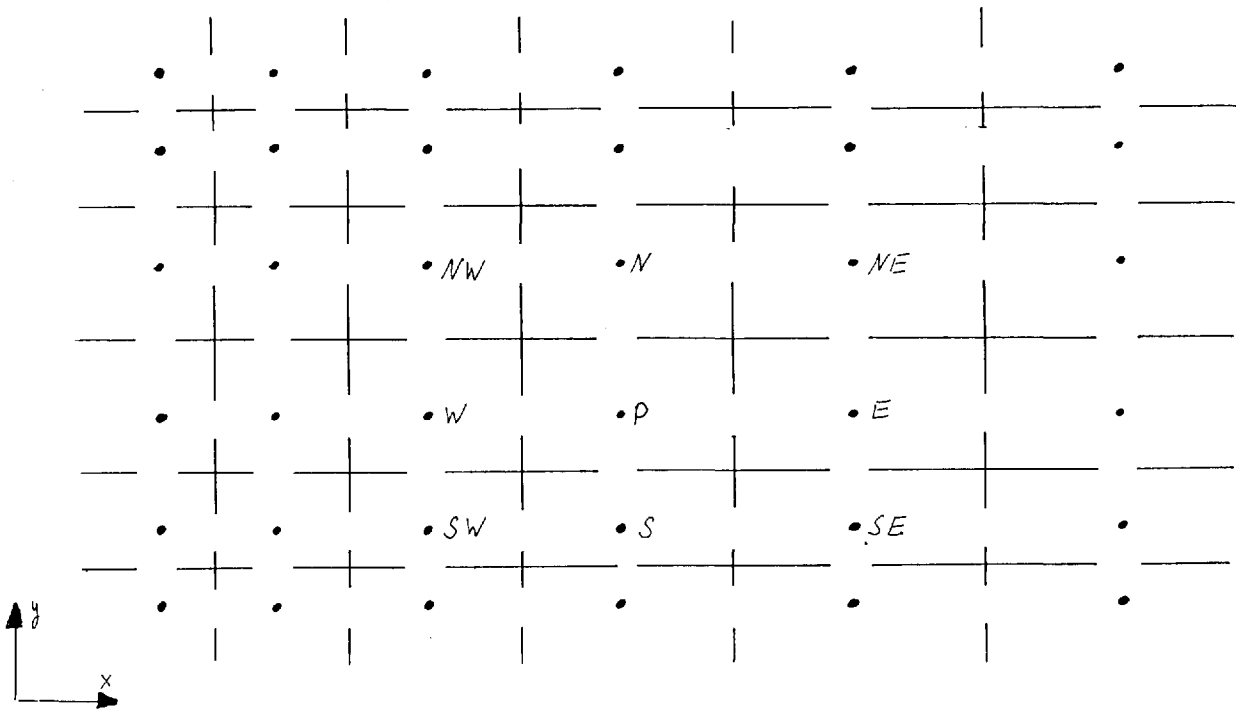

FIG 3.1-1 : THE DISTRIBUTION OF MESH POINTS AND TANKS

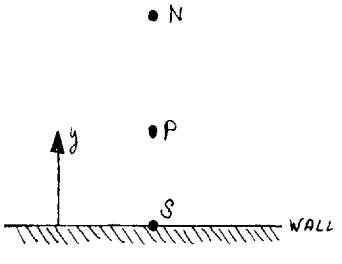

FIG 3.2-1 : THE POINTS NEAR A WALL

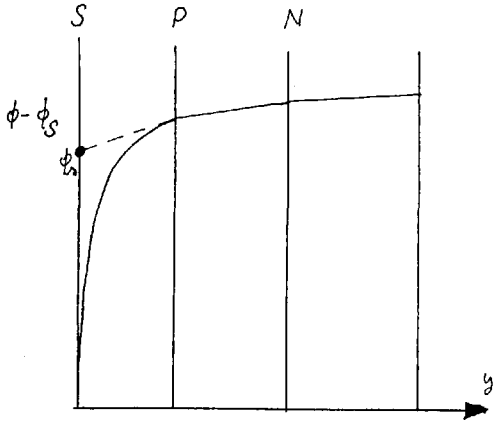

FIG 3.2-2 : THE SLIP VALUE

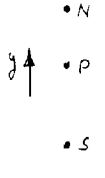

FIG 3.3-1 : CALCULATION OF THE FIRST DERIVATIVES.

equation (2.1-11) over these control volumes is performed, step after step. Here it will suffice to present the final result, for the value of ϕ at point P, surrounded by the points E, W, N, S, as follows

$$\phi_P = \frac{C_E \phi_E + C_W \phi_W + C_N \phi_N + C_S \phi_S + A_u + S_{u,P}}{C_E + C_W + C_N + C_S + Z_c} \qquad (3.1\text{-}1)$$

where $$C_E = \frac{\Gamma_E + \Gamma_P}{2} \cdot \frac{y_N - y_S}{2(x_E - x_P)} \qquad (3.1\text{-}2)$$

and C_W, C_N, C_S are similar expressions.

$$A_u = a_E \phi_E + a_W \phi_W + a_N \phi_N + a_S \phi_S \qquad (3.1\text{-}3)$$

$$Z_c = a_E + a_W + a_N + a_S \qquad (3.1\text{-}4)$$

$$a_E = \frac{1}{8}\left[(\psi_{NE} + \psi_N - \psi_{SE} - \psi_S) + |\psi_{NE} + \psi_N - \psi_{SE} - \psi_S|\right] \qquad (3.1\text{-}5)$$

and a_W, a_N, a_S are similar expressions.

$$S_{u,P} = \frac{S_P (x_E - x_W)(y_N - y_S)}{4} \qquad (3.1\text{-}6)$$

The expressions containing the terms C_E, C_W, C_N, C_S describe the transport of ϕ by diffusion. Those containing a_E, a_W, a_N, a_S describe the ϕ-transport by convection, and $S_{u,P}$ describes generation of ϕ. A further discussion of this equation was presented by Runchal et al. (1967).

3.2 Boundary conditions

The only boundary conditions which really need attention here, are those on solid walls. The differential form of the wall boundary conditions was presented in section 2.2. However, the transformation of these

differential conditions to finite-difference ones is not a straight forward process, due to two reasons: (i) the coupling of the vorticity and stream-function boundary condition, and (ii) the existence of thin boundary-layers, with steep gradients, and non-linear distributions where the usual finite-difference procedures are highly inaccurate. Moreover, due to the existence of boundary-layers, simple computation of the wall fluxes is impossible. Our aim in the present section will thus be three fold.

(i) To devise an expression for the wall vorticity.

(ii) To connect the wall fluxes and quantities (subscripted "S") to the quantities in a near wall point (subscripted "P"), which is as far as possible from the wall.

(iii) To apply the necessary corrections to the finite-difference scheme, as to offset the errors introduced by the non-linearity of the profiles.

We immediately note, that the wall vorticity, ω_s is of no interest to us, but for its appearance in the equation for ω_p . Therefore we may devise a direct expression for ω_p , rather than one for ω_s. The second remark is, that the only practical way to achieve our aims is by the use of some sort of a boundary-layer theory. The

theory adopted in the present thesis is a Couette flow theory, which has the advantage of simplicity. The solutions obtained by this theory depend on the viscosity hypotheses used and may require numerical integration. Still, the important thing about them, is that they can always be obtained. Chapter 6 of the thesis contains, in fact, such solutions for a turbulent flow. But at present we are not interested in any particular hypothesis: our interest lies in deriving such expressions as

$$\omega_p = \omega_p \{ y_p, \gamma_p, u_p, \mu_{eff,p}, \ldots \}$$

$$\tau_s = \tau_s \{ y_p, \gamma_p, u_p, \mu_{eff,p}, \ldots \}$$

$$\frac{\partial p}{\partial x} = p' \{ y_p, \gamma_p, u_p, \mu_{eff,p}, \ldots \}$$

Where the dots stand for any quantity inside the field of integration.

The Couette flow relations

In a Couette flow, without mass transfer, the equations of motion (2.1-2) reduce to

$$\frac{\partial p}{\partial y} = 0 \qquad (3.2\text{-}1)$$

$$\frac{\partial p}{\partial x} = \frac{\partial \tau}{\partial y} \qquad (3.2\text{-}2)$$

and the shear stress and vorticity are given by

$$\tau = \mu_{eff} \frac{du}{dy} \qquad (3.2\text{-}3)$$

$$\omega = -\frac{du}{dy} \qquad (3.2\text{-}4)$$

Integration of eqn (3.2-2) gives

$$\tau = \tau_s + p' y \tag{3.2-5}$$

where

$$p' = \frac{dp}{dx} = const \tag{3.2-6}$$

and τ_s is the wall shear stress.

We may now substitute (3.2-5) into (3.2-3), to get

$$\frac{du}{dy} = \frac{\tau_s}{\mu_{eff}} + \frac{p' y}{\mu_{eff}} \tag{3.2-7}$$

Integrating once, we get

$$u = \tau_s \int_0^y \frac{d\eta}{\mu_{eff}} + p' \int_0^y \frac{\eta\, d\eta}{\mu_{eff}} \tag{3.2-8}$$

and on a second integration we get

$$\frac{\psi}{\rho} = \int_0^y u\, d\eta = \tau_s \int_0^y \int_0^\eta \frac{d\xi\, d\eta}{\mu_{eff}} + p' \int_0^y \int_0^\eta \frac{\xi\, d\xi\, d\eta}{\mu_{eff}} \tag{3.2-9}$$

It will be noted, that the wall boundary conditions, eqn (2.2-1) and (2.2-2) were used during these integrations; that y is measured from the wall; and that the wall velocity and stream-function are zero.

The conserved property equation, (2.1-11), reduces, in a Couette flow, to:

$$J_\phi = J_{\phi s} = const \tag{3.2-10}$$

but on the other hand, eqn (2.1-5) may now be written as

$$J_\phi = -\frac{\mu_{eff}}{\sigma_{eff}} \frac{d\phi}{dy} \tag{3.2-11}$$

Combining the two equations and integrating we get

$$\phi - \phi_s = J_{\phi,s} \int_0^y \frac{\sigma_{eff}\, d\eta}{\mu_{eff}} \qquad (3.2\text{-}12)$$

The dimensionless form of the equations

We shall now define the following dimensionless quantities:

$$\Lambda = \frac{\tau_s\, y}{\mu\, u} \qquad (3.2\text{-}13)$$

$$F = \frac{\rho'\, y^2}{\mu\, u} \qquad (3.2\text{-}14)$$

$$W = \frac{w\, y}{u} \qquad (3.2\text{-}15)$$

$$\varepsilon = \frac{\mu_{eff}}{\mu} \qquad (3.2\text{-}16)$$

$$Q = \frac{\nu}{\rho u y} \qquad (3.2\text{-}17)$$

$$S = \frac{\sigma J_{\phi,s}\, y}{\mu(\phi - \phi_s)} \qquad (3.2\text{-}18)$$

Further we shall also define the following dimensionless integrals.

$$I_{\tau,1} = \frac{1}{y} \int_0^y \frac{d\eta}{\varepsilon} \qquad (3.2\text{-}19)$$

$$I_{\tau,2} = \frac{1}{y^2} \int_0^y \int_0^\eta \frac{df\, d\eta}{\varepsilon} \qquad (3.2\text{-}20)$$

$$I_{\mu,1} = \frac{1}{y^2} \int_0^y \frac{\eta\, d\eta}{\varepsilon} \qquad (3.2\text{-}21)$$

$$I_{\mu,2} = \frac{1}{y^3} \int_0^y \int_0^\eta \frac{f\, df\, d\eta}{\varepsilon} \qquad (3.2\text{-}22)$$

$$I_\phi = \frac{1}{y}\int_0^y \frac{\sigma_{eff}\, d\eta}{\varepsilon} \qquad (3.2\text{-}23)$$

Finally, we name the point near the wall "P", and the one adjacent to it "N" (see fig 3.2-1), and define the following two quantities:

$$Z = 2\,\frac{u_N}{u_P}\,\frac{y_P}{y_N} \qquad (3.2\text{-}24)$$

$$\tau = \frac{y_P}{y_N - y_P} \qquad (3.2\text{-}25)$$

It may now be shown that eqn (3.2-2) can be replaced by the following finite-difference expression:

$$F = \frac{\omega_P \varepsilon_P}{\tau} - \frac{W_N \varepsilon_N Z}{2\tau} \quad * \qquad (3.2\text{-}26)$$

and equations (3.2-7), (3.2-8), (3.2-9) and (3.2-12) transform into:

$$-\varepsilon W = \Lambda + F \qquad (3.2\text{-}27)$$

$$1 = \Lambda I_{\tau,1} + F I_{r,1} \qquad (3.2\text{-}28)$$

$$Q = \Lambda I_{\tau,2} + F I_{r,2} \qquad (3.2\text{-}29)$$

$$S = I_\phi \qquad (3.2\text{-}30)$$

The wall boundary conditions

We are now in a position to specify the vorticity boundary condition. Indeed, we may specify it in more

---

* Strictly speaking eqn (3.2-26) is valid only in the Couette flow region, but even in other boundary layer flows it is approximately true, and may therefore be applied usually at the point "N".

than one way. First we may solve eqns (3.2-27), (3.2-28) and (3.2-29) for the three unknowns Λ, F, W, which are the non-dimensional forms of τ_S, p' and ω_ρ respectively. This method suffers, however, from the need to evaluate the four integrals, $I_{\tau,1}$, $I_{\tau,2}$, $I_{p,1}$ and $I_{p,2}$. This difficulty may be reduced, if we solve eqns (3.2-26), (3.2-27) and (3.2-28) instead. Then we need only the two integrals $I_{\tau,1}$ and $I_{p,1}$. The following expressions may be obtained:

$$W = -\frac{\gamma + (I_{p,1} - I_{\tau,1})\frac{W_N \varepsilon_N Z}{2}}{\varepsilon[I_{p,1} + I_{\tau,1}(\gamma - 1)]} \qquad (3.2\text{-}31)$$

$$\Lambda = \frac{\gamma - 1 + I_{p,1}\frac{W_N \varepsilon_N Z}{2}}{I_{p,1} + I_{\tau,1}(\gamma - 1)} \qquad (3.2\text{-}32)$$

$$F = \frac{1 - I_{\tau,1}\frac{W_N \varepsilon_N Z}{2}}{I_{p,1} + I_{\tau,1}(\gamma - 1)} \qquad (3.2\text{-}33)$$

where the non-subscripted quantities are at the point "P". This practice is possible only if eqn (3.2-2) is valid, at least approximately, at the point "N". It was used for all turbulent flows in the present paper.

For laminar flows a much simpler procedure is adopted: eqns (3.2-27) and (3.2-29) are solved, for s and F, taking W and Q from the finite difference solution. Then, when the proper substitutions are made, we get

$$\Lambda = \frac{Q + \varepsilon I_{p,2} W}{I_{\tau,2} - I_{p,2}} \qquad (3.2\text{-}34)$$

$$F = -\frac{Q + \varepsilon I_{\tau,2} W}{I_{\tau,2} - I_{\rho,2}} \qquad (3.2\text{-}35)$$

and obviously

$$\omega_s = -\frac{\tau_s}{\mu} = -\frac{s u}{y} \qquad (3.2\text{-}36)$$

Further, in laminar flow

$$\varepsilon = 1 \qquad (3.2\text{-}37)$$

$$I_{\tau,2} = 1/2 \qquad (3.2\text{-}38)$$

$$I_{\rho,2} = 1/6 \qquad (3.2\text{-}39)$$

and therefore

$$S = 3Q + \frac{3W}{2} \qquad (3.2\text{-}40)$$

The ϕ-flux at the wall may be easily evaluated from eqn (3.2-30).

Slip values

In all our finite-difference equations, a linear ϕ-profile is implied between adjacent nodes. This is not usually correct in turbulent flows, near walls. By forcing a linear profile on the virtually non-linear one, we introduce an error to our solution, which will be larger, the steeper the profile. Patankar and Spalding (1967) suggested a method to reduce such errors, by using in the finite-difference solution apparent wall values; these values were so chosen that the ϕ-gradient at P retains its true values, i.e.

$$\frac{\phi_P - \phi_s}{y_P} = \left(\frac{\partial \phi}{\partial y}\right)_P \qquad (3.2\text{-}41)$$

where ϕ_s is the apparent wall ϕ. Of course, we must specify the ϕ-gradient at "P", say by a Couette flow analysis. Patankar and Spalding called ϕ_s "the slip value of ϕ", because they applied eqn (3.2-41) to the velocity, and u_s may be regarded as a slip velocity on a no-slip boundary. In the present work slip values have been introduced for the temperature and turbulence energy. They have not been applied to the vorticity, because its near wall value was not computed by finite-differences, nor to the stream function, which is the best-behaved function near the wall.

3.3 Calculation of first derivatives

We have to compute first derivatives to evaluate the velocity components and the turbulence energy generation (as will be described in chapter 5). To find an accurate expression let us expand a function near the point P (fig 3.3-1). Thus

$$\phi_N = \phi_P + \left(\frac{\partial \phi}{\partial y}\right)_P (y_N - y_P) + \left(\frac{\partial^2 \phi}{\partial y^2}\right)_P \frac{(y_N - y_P)^2}{2} + O(\Delta y^3) \qquad (3.3\text{-}1)$$

$$\phi_S = \phi_P - \left(\frac{\partial \phi}{\partial y}\right)_P (y_P - y_S) + \left(\frac{\partial^2 \phi}{\partial y^2}\right)_P \frac{(y_P - y_S)^2}{2} + O(\Delta y^3) \qquad (3.3\text{-}2)$$

To get accuracy of order Δy^2, we multiply eqn (3.3-1) by $(y_P - y_S)^2$, eqn (3.3-2) by $(y_N - y_P)^2$, and subtract one

from the other. Finally we get, after rearrangement

$$\left(\frac{\partial \phi}{\partial y}\right)_P = \frac{(\phi_N - \phi_P)\frac{y_P - y_S}{y_N - y_P} + (\phi_P - \phi_S)\frac{y_N - y_P}{y_P - y_S}}{y_N - y_S} \qquad (3.3\text{-}3)$$

This equation will reduce to the familiar central difference equation, when the mesh is uniformly distributed.

3.4 The numerical procedure and the computer programme

The iterative scheme

In section (3.1) we have seen how the conservation equation for ϕ at a point P may be arranged as

$$\phi_P = \phi_P + \phi_S \text{ at neighbouring points} \qquad (3.4\text{-}1)$$

Obviously there are as many equations of this kind as unknown point-values of ϕ, so that we have a system of algebriac equations for which a solution will generally exist. Unfortunately there are always more than one ϕ, and they are coupled with one another by means of coefficients in the right-hand side of equation (3.4-1). This is the reason why iteration is likely to be always necessary; we compute the ϕ-values at all the mesh points, then compute the new coefficients in eqn (3.4-1), then compute new ϕ-values, and so on, until the difference between successive ϕ-values becomes small enough. We still have to decide, however, in which way to obtain the ϕ-distribution, once that the new coefficients in eqn (3.4-1) have been computed. We have in fact two

possible ways to achieve this:

(i) To obtain an approximation for the ϕ-distribution, by the use of eqn (3.4-1) at each mesh point successively, until all the points have been covered. To cut the computing time we would like to use new ϕ-values as soon as they become available (Gauss-Seidel technique). There is no need to iterate on ϕ, because anyhow we shall have to iterate on the coefficients of eqn (3.4-1). It cannot be proved at present that this procedure is convergent. Experience of many researchers has shown, however, that if equation (3.4-1) satisfies the stability criterion for linear equations, the above procedure will be convergent.

(ii) When the number of mesh points is not large, the exact ϕ-distribution may be obtained accurately, by applying Gauss's elimination, or a similar suitable technique. This method may cut the number of iterations very considerably, but it is suitable only for special cases. In the present work it has been used to obtain solutions for a one-dimensional turbulent Couette flow. For a one-dimensional flow, the elimination reduces to simple recurrence equations. Details of these equations are given in appendix A.3.

Termination of the computation

In the present work it was assumed that the difference between the computed and the exact solution can be represented by the difference of ϕ-values between successive iterations. Thus the computation was assumed to have converged to the exact solution if

$$\left| \frac{\phi_{p,n+1} - \phi_{p,n}}{\phi_{max,n}} \right| \leq c_c \qquad (3.4\text{-}2)$$

where subscript n denotes the n^{th} iteration, $\phi_{max;n}$ is the maximum value of ϕ in the whole field after the n^{th} iteration and c_c is a small constant. $\phi_{max,n}$ was chosen as scaling factor rather than $\phi_{p,n}$ in order to remove difficulties when $\phi_{p,n}$ becomes vanishingly small.

The computer programme

A copy of the computer programme used for the impinging jet computation is attached, in appendix A.4. A schematic flow diagram of this programme is shown in fig 3.4-1. The main symbols used in the programme are explained in section 9.2. The programme is written in FORTRAN IV and was run on the Imperial College IBM 7090, University College London IBM 360, and University of London Atlas computers. Minor modifications were required when transferring the programme from one computer to another. Very similar programmes have been discussed

in detail by Wolfshtein (1967) and Runchal and Wolfshtein (1967). Therefore it does not seem necessary to add any more details here.

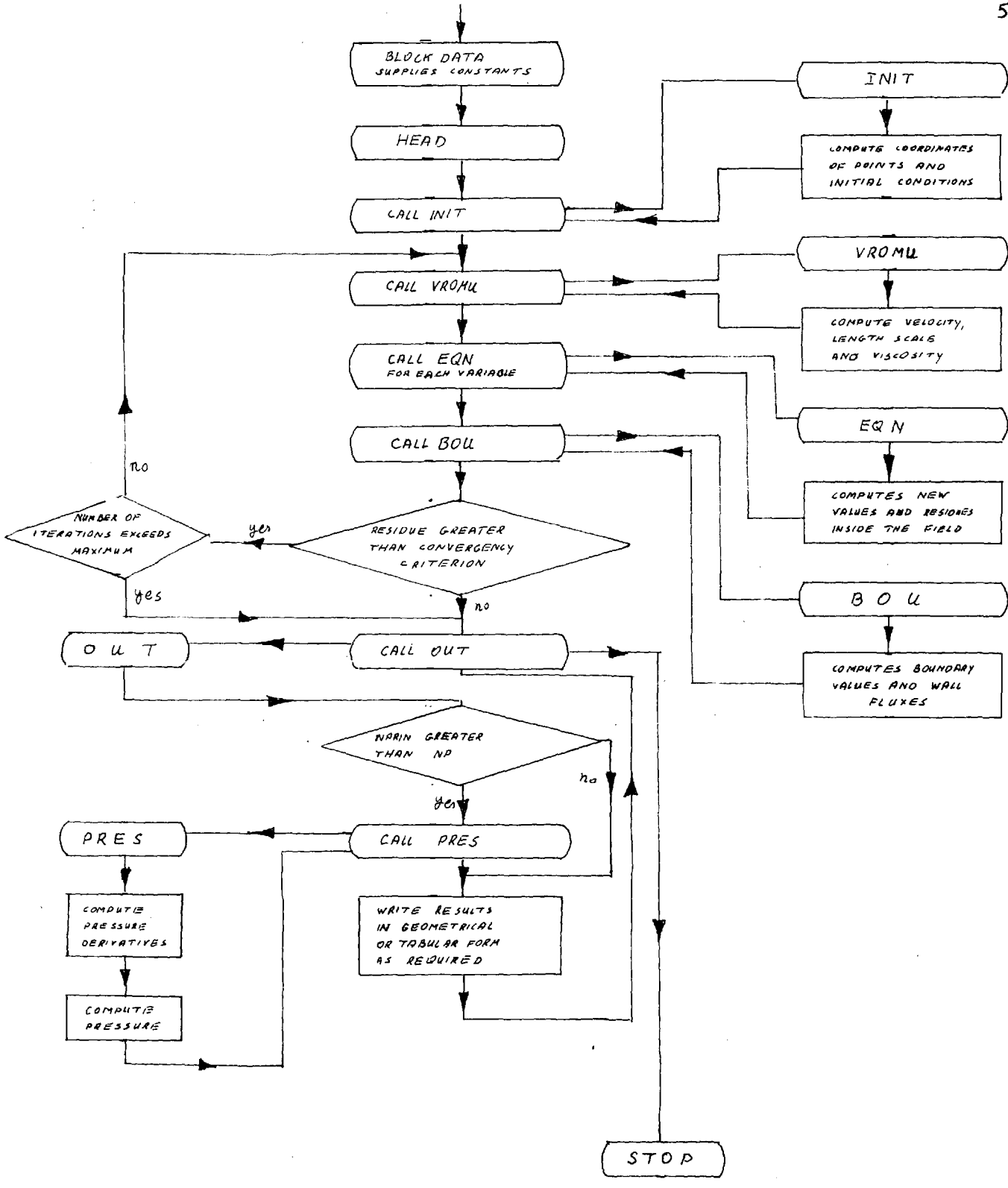

FIG 3.4-1 : THE COMPUTER PROGRAMME FLOW DIAGRAMME

4. Studies and discussion of accuracy, convergence and economy

In chapter 2 we outlined the set of differential equations, boundary conditions and auxiliary relations which we have to solve. In chapter 3 we replaced all the differential expressions with finite-difference ones and thus got a set of algebraic equations. An iterative procedure for the solution of these algebraic equations was suggested in chapter 3 as well. A proof of uniqueness and existence of a solution to the equations is beyond the scope of the present paper. We shall just assume, that a unique solution exists to the differential equations, and that another unique solution exists to the set of algebraic finite-difference equations. Now the first question which we have to answer is what is the difference between these two solutions? We shall refer to this as the problem of accuracy. Secondly we would like to know if our iterative procedure is converging to the exact solution of the algebraic finite difference equations? This will be termed the problem of convergence. Thirdly we wish to find out how many iterations, or how much time, are necessary to bring the iterated solution sufficiently near to the exact solution of the finite difference equations? This, of course, is the problem of economy.

Our present understanding of numerical methods is not sufficient to obtain a full theoretical answer to the above three questions. Therefore, we have to turn our attention to test solutions of some selected problems. In the present chapter, the three questions of accuracy, convergence, and economy, will be studied in the light of the results of such test solutions. The test cases will be (i) Couette flow with mass-injection through the wall, (ii) an impinging jet flow, and (iii) a uniform velocity flow, with zero diffusivity. Of these cases, the Couette flow needs fewer mesh points, and has an analytical solution. It has the further advantage of vorticity and stream-function profiles which may be made linear or non-linear, as necessary, by changing the blowing rate. Therefore, Couette flows will be studied first, and conclusions drawn from their solutions will then be checked in the impinging-jet case. The uniform-velocity zero-diffusivity problem will be used only in connection with the phenomenon of "false-diffusion", to be described in section 4.4.

4.1 Description of the test models

Laminar Couette flow with mass injection through the walls

The main features of this flow are its one-dimensionality, and the existence of analytical solutions. It was therefore used to check the influence of the mesh size and distribution on the accuracy and speed of convergence. The model is shown in fig (4.1-1). The flow is confined between, and induced by a pair of flat walls, the bottom one stationary, and the upper one moving at a velocity u_T. To this flow we inject through the walls a stream of the same fluid, with velocity v. The parameter for this problem is the blowing Reynolds number, defined in terms of the injection velocity and the distance between the two walls, or

$$M = \frac{\rho v h}{\mu} \qquad (4.1\text{-}1)$$

The exact solution of this problem is:

$$\frac{\omega}{\omega_T} = exp\left[M\left(\frac{y}{h} - 1\right)\right] \qquad (4.1\text{-}2)$$

$$\frac{\psi}{\psi_T} = \frac{exp\left(M\frac{y}{h}\right) - 1 - M\frac{y}{h}}{exp\,(M) \quad -1 - M} \qquad (4.1\text{-}3)$$

where the top wall vorticity and stream function are

$$\omega_T = -\frac{u_T}{h}\,\frac{exp\,(M)}{exp(M)-1} \qquad (4.1\text{-}4)$$

$$\psi_T = u_T h\left(\frac{1}{M} - \frac{1}{exp(M)-1}\right) \qquad (4.1\text{-}5)$$

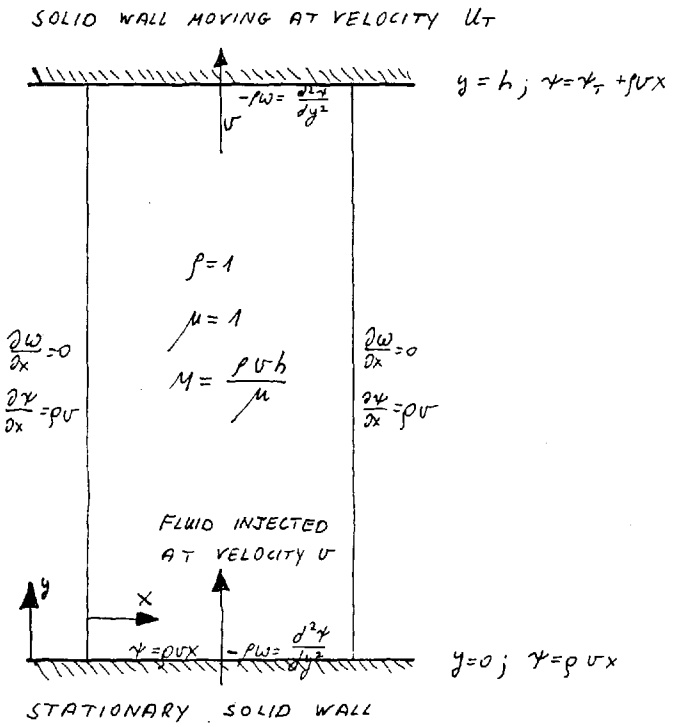

FIG 4.1-1: THE LAMINAR COUETTE FLOW, WITH MASS TRANSFER.

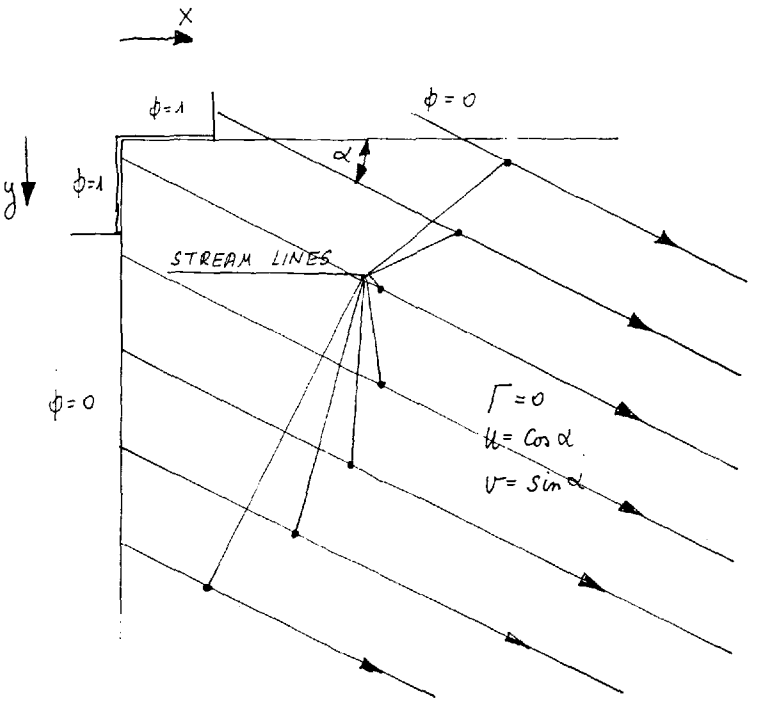

FIG 4.1-4: THE UNIFORM-VELOCITY ZERO DIFFUSION PROBLEM.

or, when $M = 0$

$$\omega = \omega_\tau = -\frac{U_\tau}{h} \tag{4.1-6}$$

$$\psi = \frac{U_\tau h}{2}\left(\frac{y}{h}\right)^2 \tag{4.1-7}$$

The exact vorticity and stream function profiles are shown in fig 4.1-2. During the computation the stream function at both walls was fixed at the exact values. The vorticity on the bottom wall was computed by eqn (3.2-40), and that on the top wall by a modified version of this equation, taking the wall velocity into account.

Impinging jet

The boundary of an impinging jet flow lies at infinity. There are two very distinct regions to such a flow: (i) the main jet flow, and (ii) the secondary entrainment flow. It has been shown by Runchal et al. (1967) that an arbitrary boundary may be located anywhere within the entrainment flow region, if sufficient fluid is allowed to pass through this bounary to supply all the necessary entrainment to the jet. At present we shall consider a square control volume, with one of its sides lying on the free-jet axis of symmetry, and another one on the solid wall (see fig 4.1-3).

The free jet, with a given velocity distribution, enters the square control volume in a direction normal to the solid wall. The half-width of the jet is half

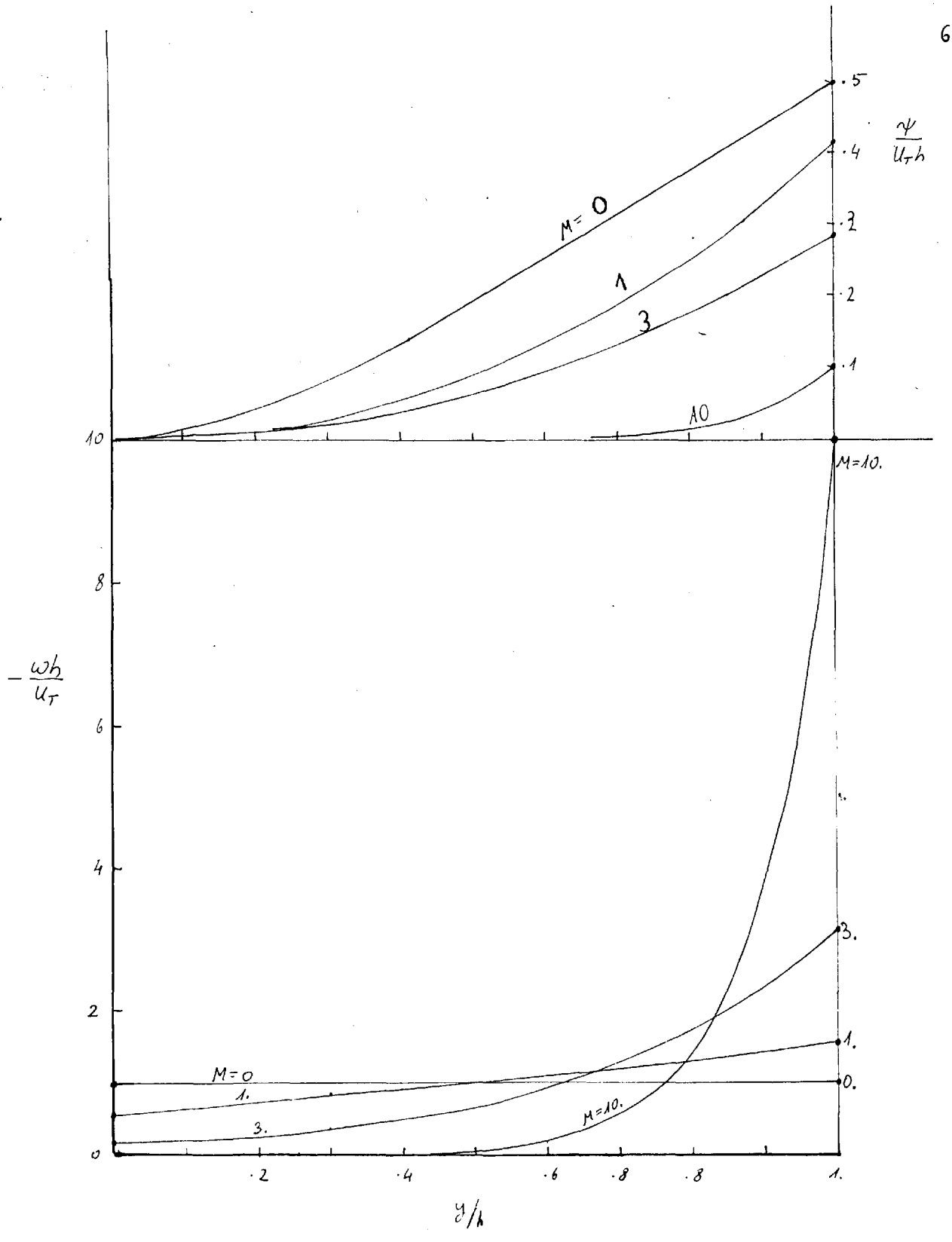

FIG 4.1-2: EXACT VORTICITY AND STREAM FUNCTION DISTRIBUTION, IN A LAMINAR COUETTE FLOW WITH INJECTION THROUGH THE WALLS.

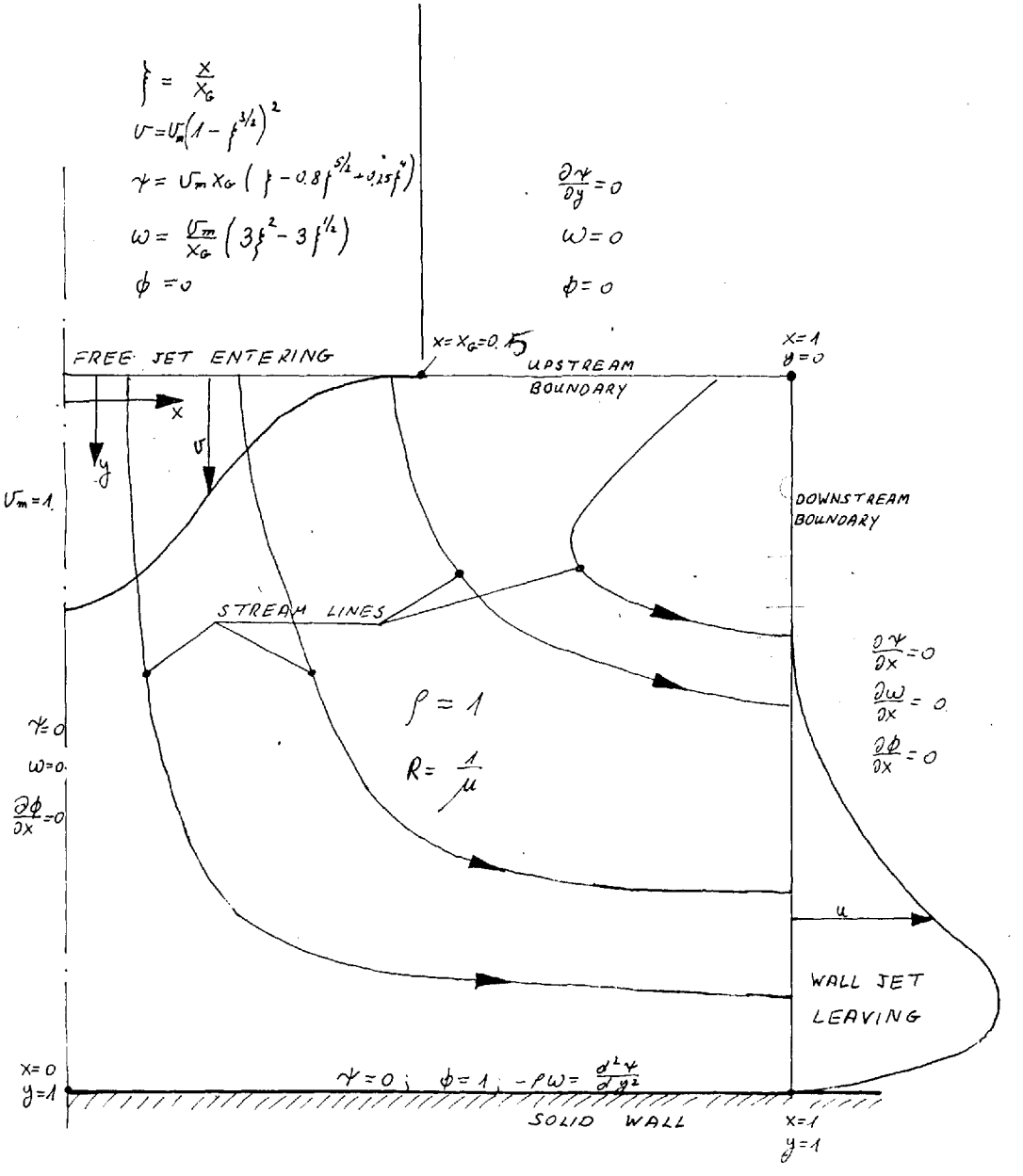

FIG 4.1-3: THE LAMINAR IMPINGING JET PROBLEM

that of the control volume, and the density is unity. Both laminar and turbulent cases will be considered.

We shall assume that the secondary, entrainment flow crosses the boundary at right angles to it and with a zero vorticity. On the downstream side, we shall assume that all the gradients parallel to the wall are zero.

The zero-diffusivity, uniform velocity flow

The third model to be used in the present chapter, is that of the diffusion of a conserved property source in a zero-diffusivity uniform-velocity field (see fig 4.1-4). The exact solution is, of course, that no diffusion occurs at all, and ϕ remains constant along any stream line. Indeed the problem is so simple, that one may wonder why it should be studied at all. We shall, however, see, in section 4.4, that just because of this simplicity, it is extremely useful in throwing some light on the difference between the respective solutions of the differential and difference equations.

4.2 The influence of the mesh size on accuracy

In this section we shall first compare the finite-difference and exact solutions of the Couette flow problem. In fig 4.2-1 predictions of the top wall vorticity

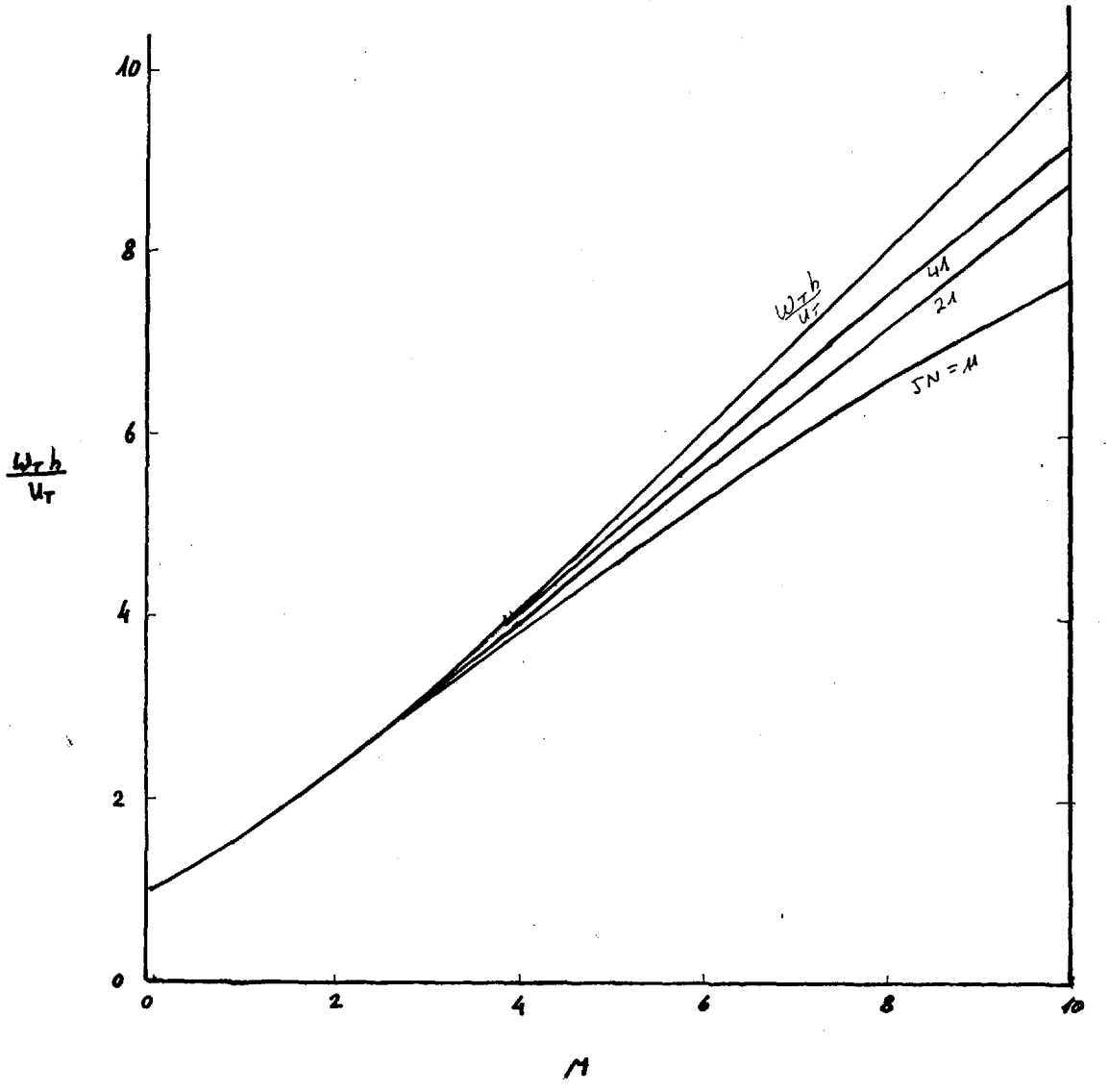

FIG 4.2-1: THE INFLUENCE OF THE MESH SIZE ON THE VORTICITY AT THE MOVING WALL IN A COUETTE FLOW WITH INJECTION. THE MESH IS UNIFORM.

are plotted versus the blowing Reynolds number M, for the three meshes of 3x11, 3x21 and 3x41 uniformly spaced mesh points. For M smaller than 3, even the coarser mesh is very satisfactory, but for larger M the finite difference solution deviates considerably from the exact one. In this region, refinement of the mesh increases the accuracy, but for M larger than 5, even the finest mesh used (3x41) was not sufficiently fine to yield a good agreement with the exact solution.

Next we shall try to assess, whether the finer meshes are giving better results inside the field. fig 4.2-2 shows the computed vorticity and stream function profile for $M = 10$, with the same three mesh sizes of 3x11, 3x21 and 3x41. It is quite clear that inside the field the vorticity distribution is hardly dependent on the mesh size; the only place where the mesh makes an important difference is on the top wall. But the stream function is sensitive to the mesh size, especially in the middle of the field; and even the solution with a 3x41 mesh is qualitatively wrong, although apparently better than the 3x11 mesh. Still, this is not likely to be connected with the bad top wall vorticity prediction: near this wall the stream function prediction is quite reasonable. Figure 4.2-2 reveals, however, the cause for the bad top wall vorticity prediction: the wall

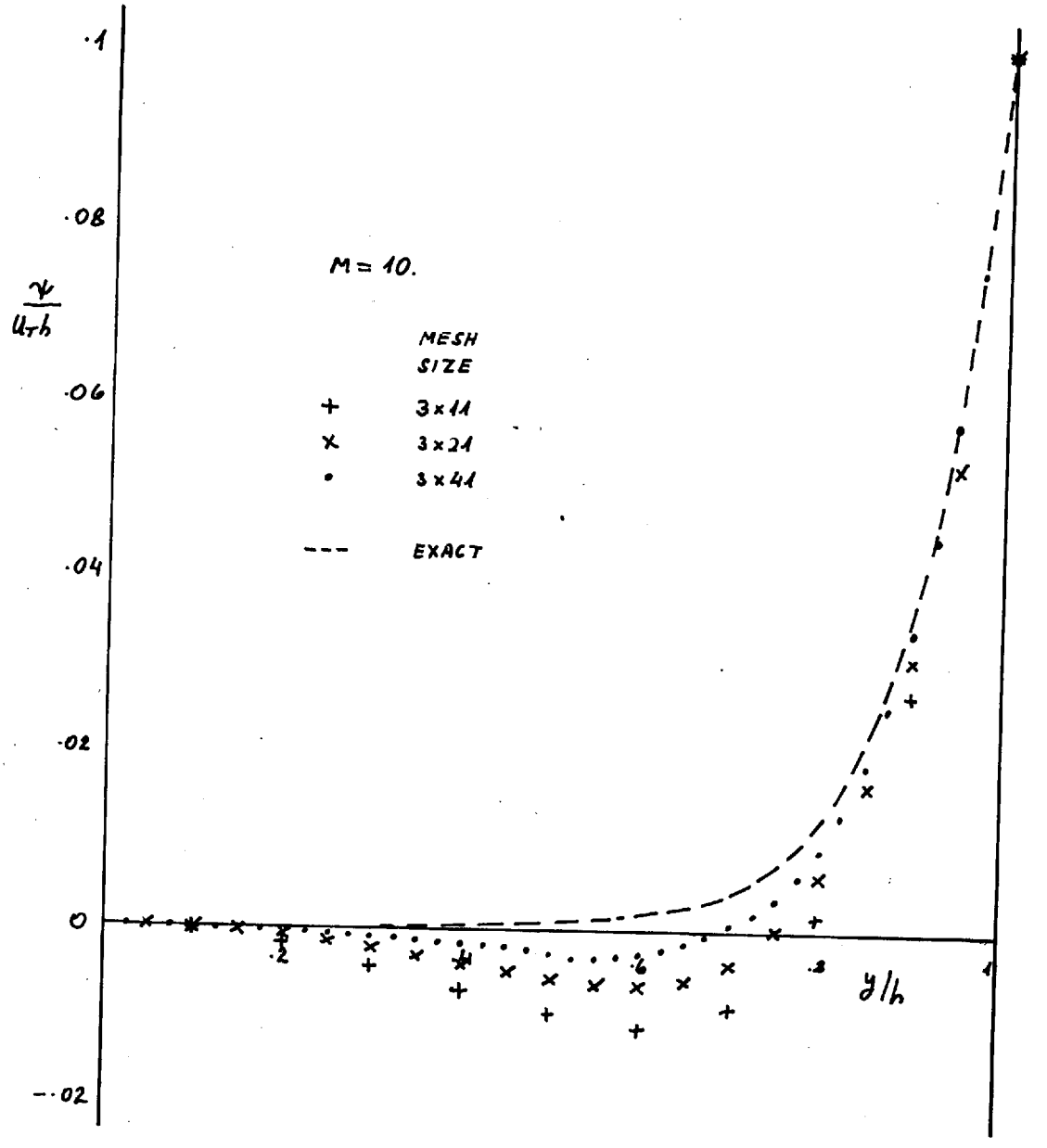

FIG 4.2-2 a: THE STREAM FUNCTION DISTRIBUTION IN A LAMINAR COUETTE FLOW WITH INJECTION. UNIFORM MESH. M=10.

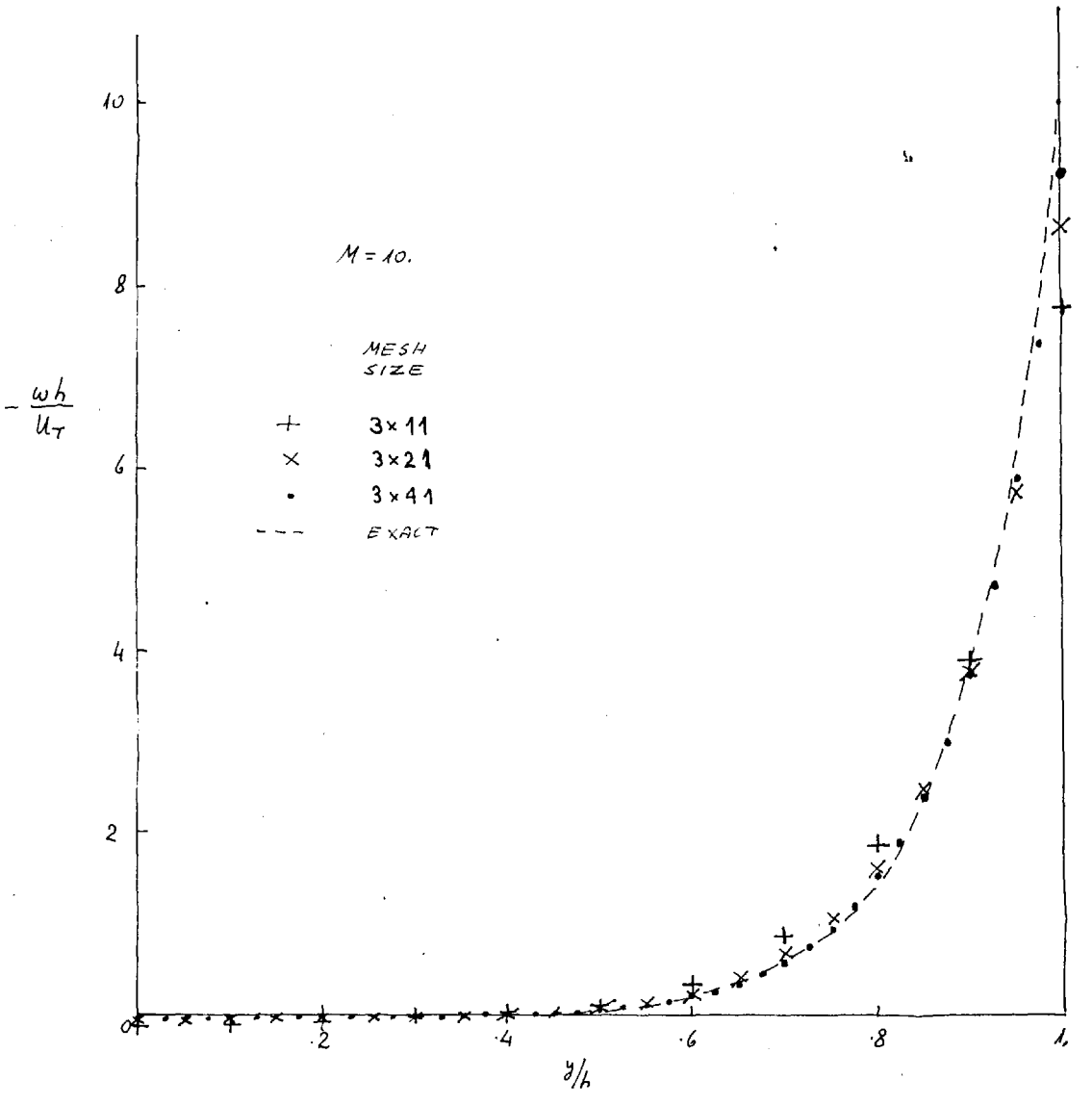

FIG 4.2-2 b: THE VORTICITY DISTRIBUTION IN A LAMINAR COUTTE FLOW WITH INJECTION. UNIFORM MESH. M=10.

boundary condition is based on a linear shear stress model, or in a laminar flow, a linear vorticity distribution; but the vorticity distribution near the top wall is linear only in the very close proximity to the wall. When a fine mesh is used, the point near the wall is in the linear vorticity region, and the wall-vorticity prediction is good. This conclusion is substantiated by fig 4.2-3, showing the vorticity profile at two sections of the impinging jet problem, for X = 0.3 and X = 0.8, where X is the distance along the wall. Here also, the wall vorticity prediction appears to be better when the near wall point is within the linear vorticity layer. But the vorticity away from the wall does not seem to be very sensitive to the mesh size. The overall picture is shown in fig 4.2-4, where the computed wall vorticity distributions obtained with the three meshes of 11x11, 21x21 and 41x41 are plotted.

The 11x11 mesh gives bad predictions everywhere, except for the downstream region, where the linear vorticity layer is quite thick. But the predictionsobtained with a 21x21 mesh are quitd near to those obtained with a 41x41 mesh, as is suggested by inspection of fig 4.2-3. The stream function discrepancy, shown in fig 4.2-2, cannot be explained in the same way. Perhaps it is connected to the strong non-linearity of the stream function distribution in the middle of the field,

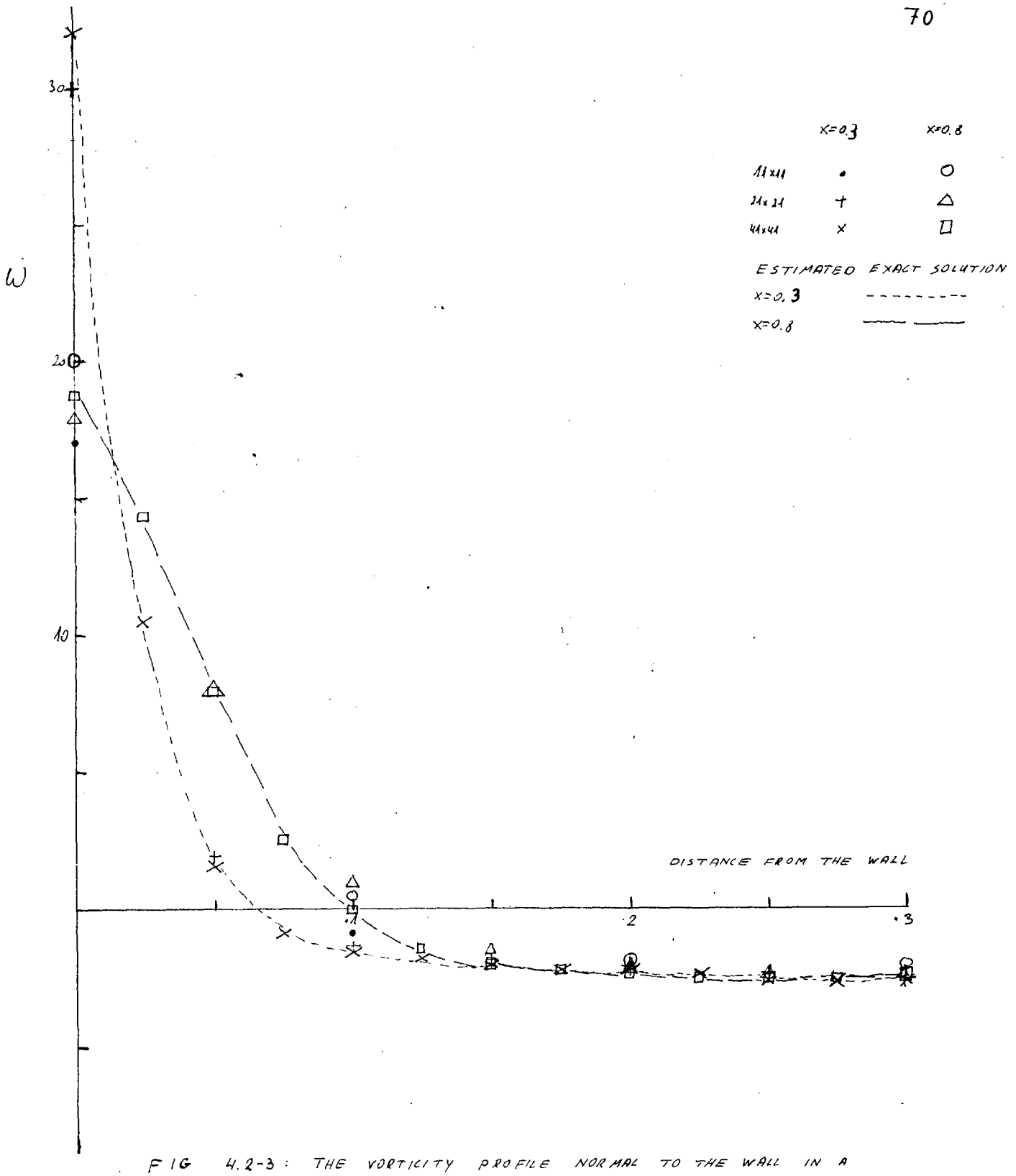

FIG 4.2-3 : THE VORTICITY PROFILE NORMAL TO THE WALL IN A LAMINAR IMPINGING JET, AT TWO STATIONS, FOR VARIOUS UNIFORM MESHES. R= 1000

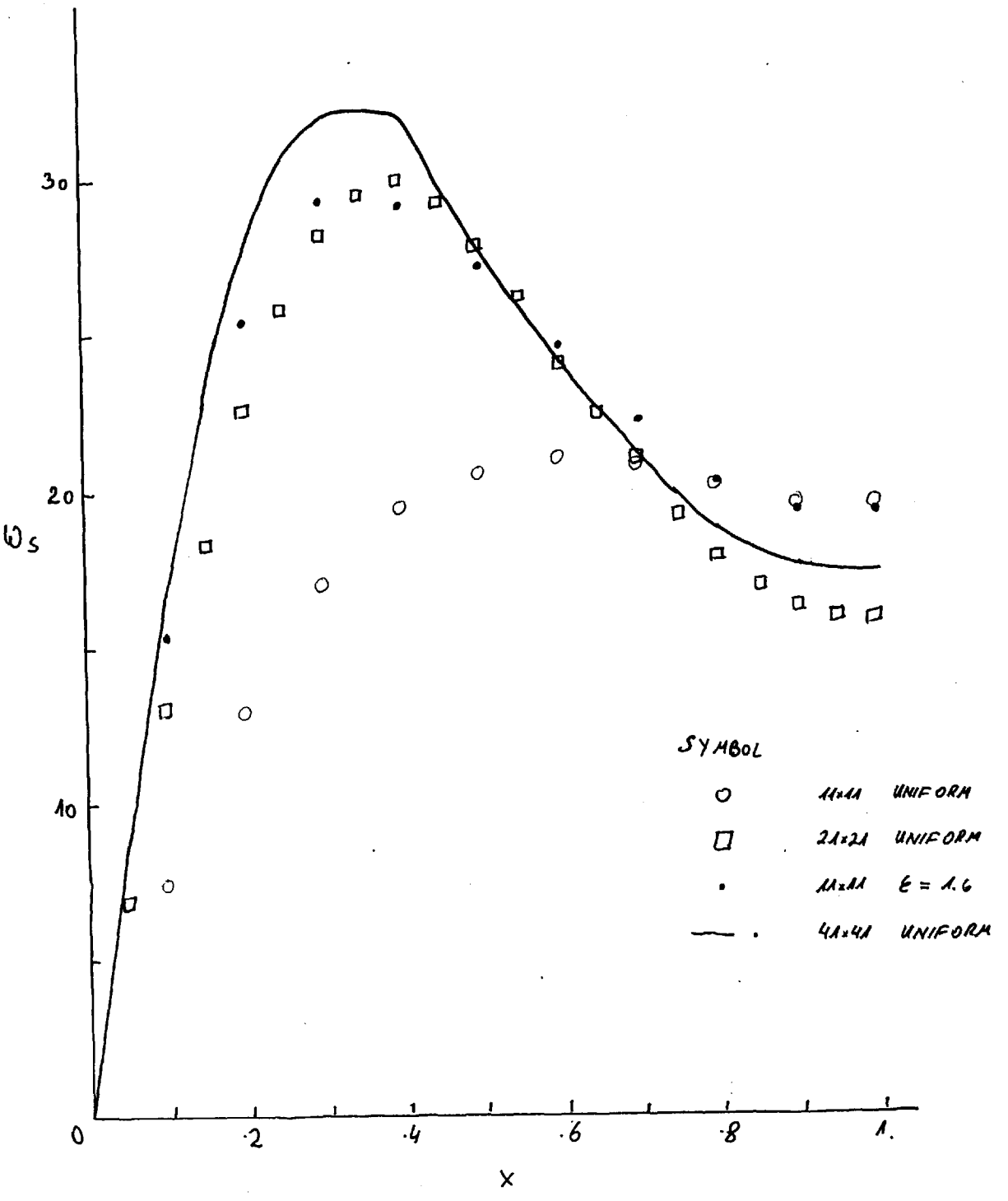

FIG 4.2-4 : THE WALL VORTICITY IN A LAMINAR IMPINGING JET FOR VARIOUS UNIFORM MESHES. R=1000.

but, admittedly, no satisfactory explanation is available at present. Interesting, though, is the fact that such a discrepancy does not appear in the solution for the impinging jet problem. In fig 4.2-5 the stream function distribution on the downstream boundary of the impinging jet is shown. Indeed, the difference between the meshes is very small. The same trend is shown also in fig 4.2-6, where the decay of the velocity normal to the wall on the jet axis is plotted.

Conclusions

In most cases, a refinement of the mesh is not likely to bring a considerable improvement of the solution inside the field. But, if the mesh point adjacent to the wall is outside the linear vorticity layer, a refinement of the mesh will improve the wall-vorticity prediction very considerably.

4.3 The influence of the mesh distribution on accuracy

The conclusions of the last section suggest the use of a variable mesh. It should be fine enough near the wall, as to ensure that the mesh penetrates into the linear vorticity region; but it may be much coarser away from the wall, where we have just seen that the use of fine meshes is not normally justified. To explore this possibility a mesh was devised, in which the mesh

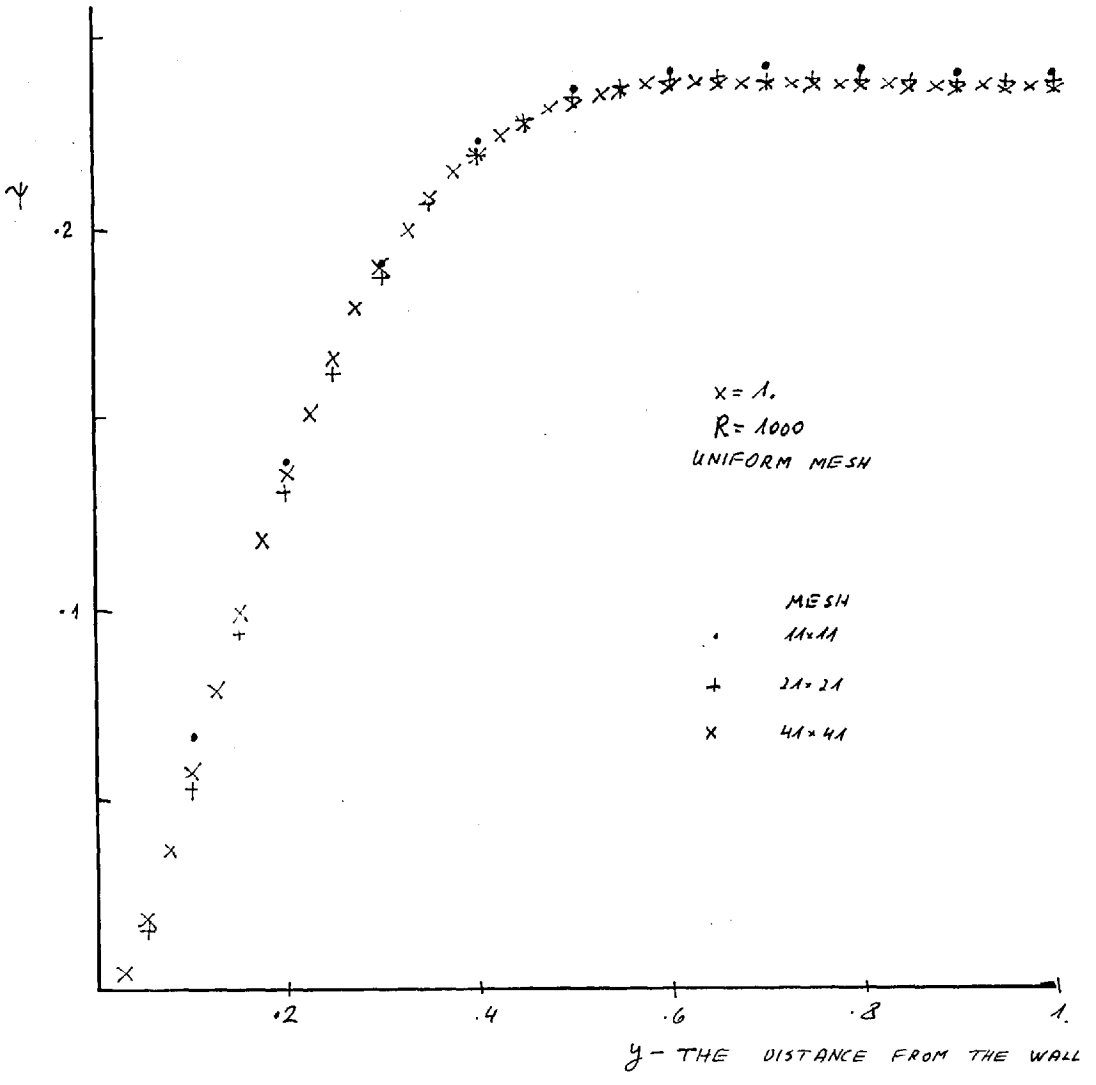

FIG 4.2-5: THE STREAM FUNCTION PROFILE AT THE DOWNSTREAM SIDE OF THE LAMINAR IMPINGING JET, FOR VARIOUS UNIFORM MESHES. R= 1000.

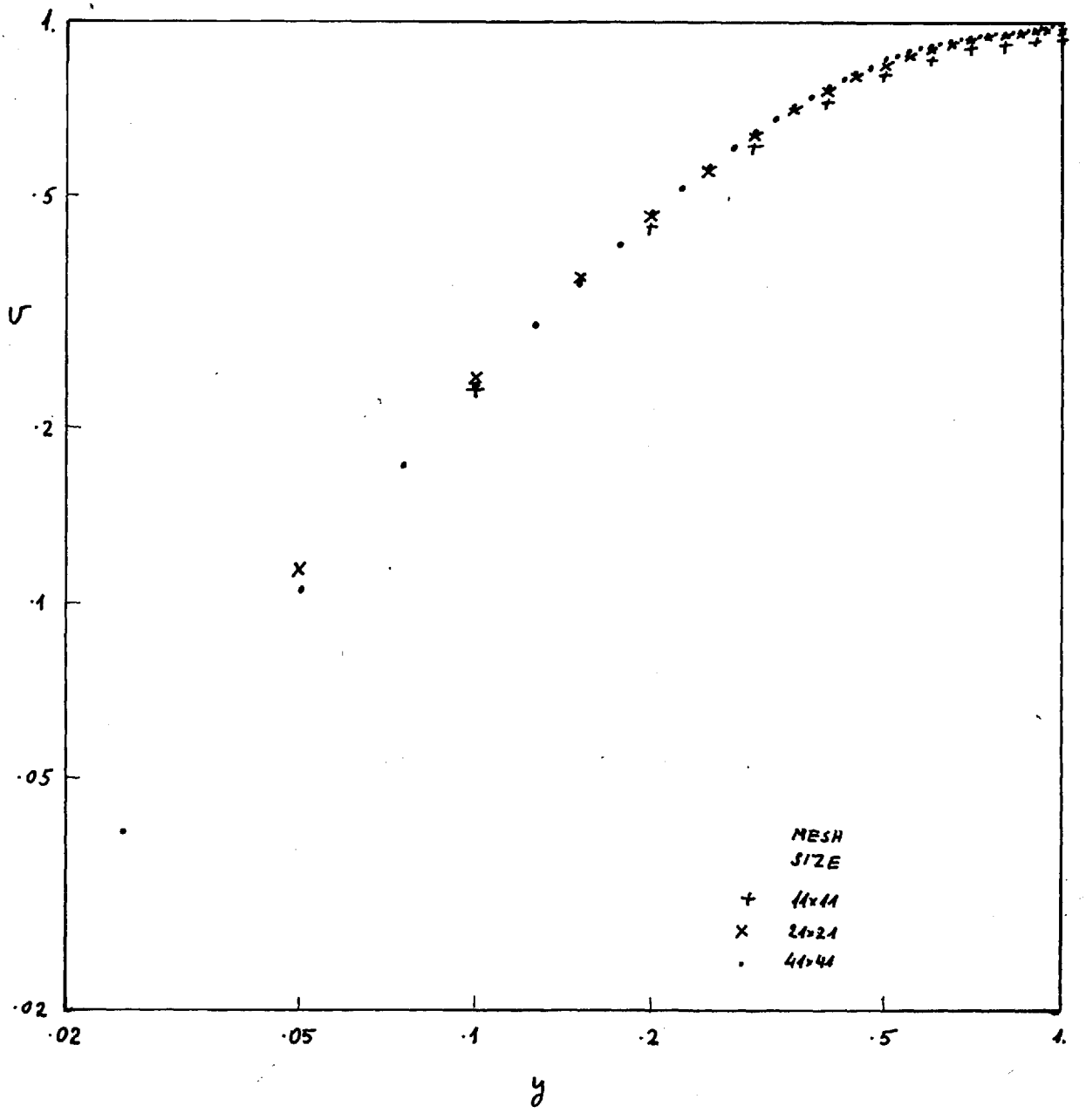

FIG 4.2-6 : THE DECAY OF THE NORMAL VELOCITY ON THE IMPINGING JET AXIS, IN LAMINAR FLOW, FOR VARIOUS UNIFORM MESHES. $R = 1000$.

size was growing in geometrical progression according to the following formula:

$$\frac{y_{n+1} - y_n}{y_n - y_{n-1}} = \varepsilon_y > 1 \qquad (4.3\text{-}1)$$

where y is the distance from the wall (the top wall in the Couette flow case), and ε_y is a constant varying from one run to another. The results are essentially supporting the conclusion of section 4.2, and need not be discussed in detail, and only three plots seem necessary. First, the top wall vorticity in the Couette flow is plotted in fig 4.3-1; then the solid wall vorticity in the impinging jet is plotted in fig 4.3-2; finally, the vorticity profiles at the two stations, X = 0.3 and X = 0.8, are plotted in fig 4.3-3. As expected the use of variable meshes enables us to approach the exact solution with meshes characterised by a small number of mesh points.

4.4 The false diffusion

One of the rare cases, when the vorticity equation can be exactly integrated, is that of the non-viscous flow, when we get

$$\omega = \text{const}$$

along any stream line. Therefore we expect that, in a high Reynolds number flow, the stream lines and the vorticity contours would run almost parallel. A solu-

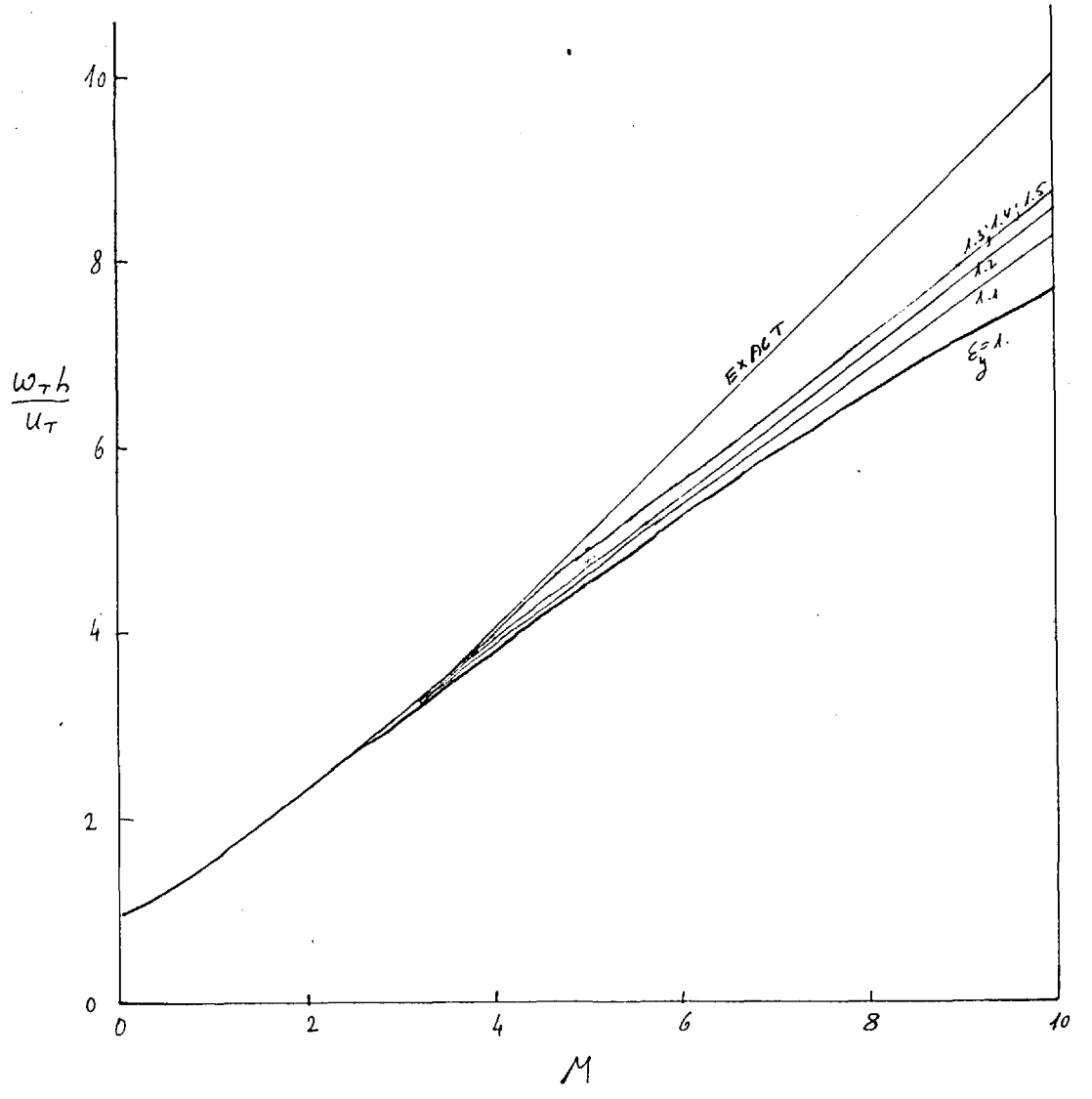

FIG 4.3-1: THE INFLUENCE OF THE MESH NON-UNIFORMITY PARAMETER ε_y ON THE VORTICITY AT THE MOVING WALL IN A COUETTE FLOW WITH INJECTION.

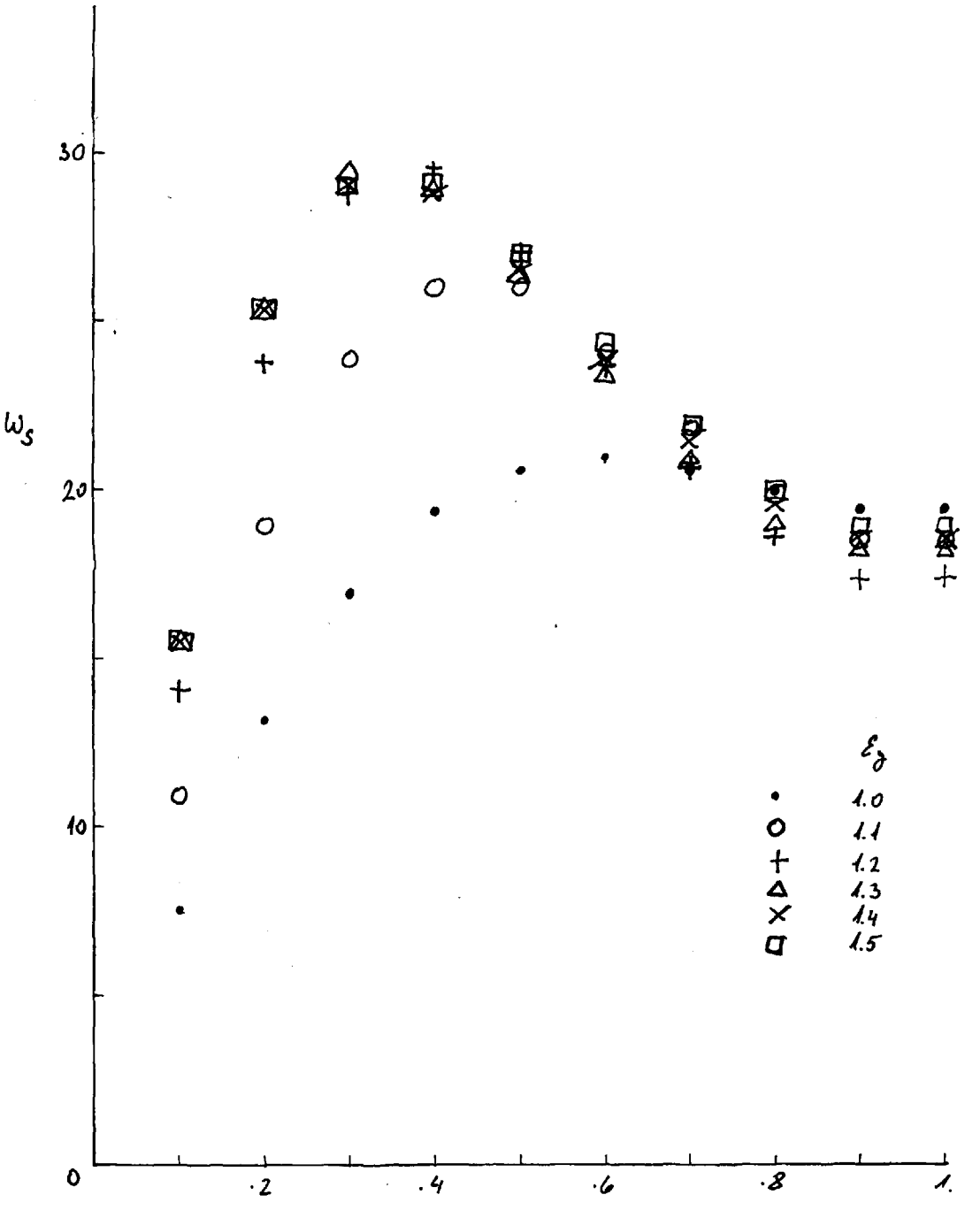

FIG 4.3-2 : THE WALL VORTICITY IN A LAMINAR IMPINGING JET FOR VARIOUS NON UNIFORMITY PARAMETERS ε_y. $R = 1000$.

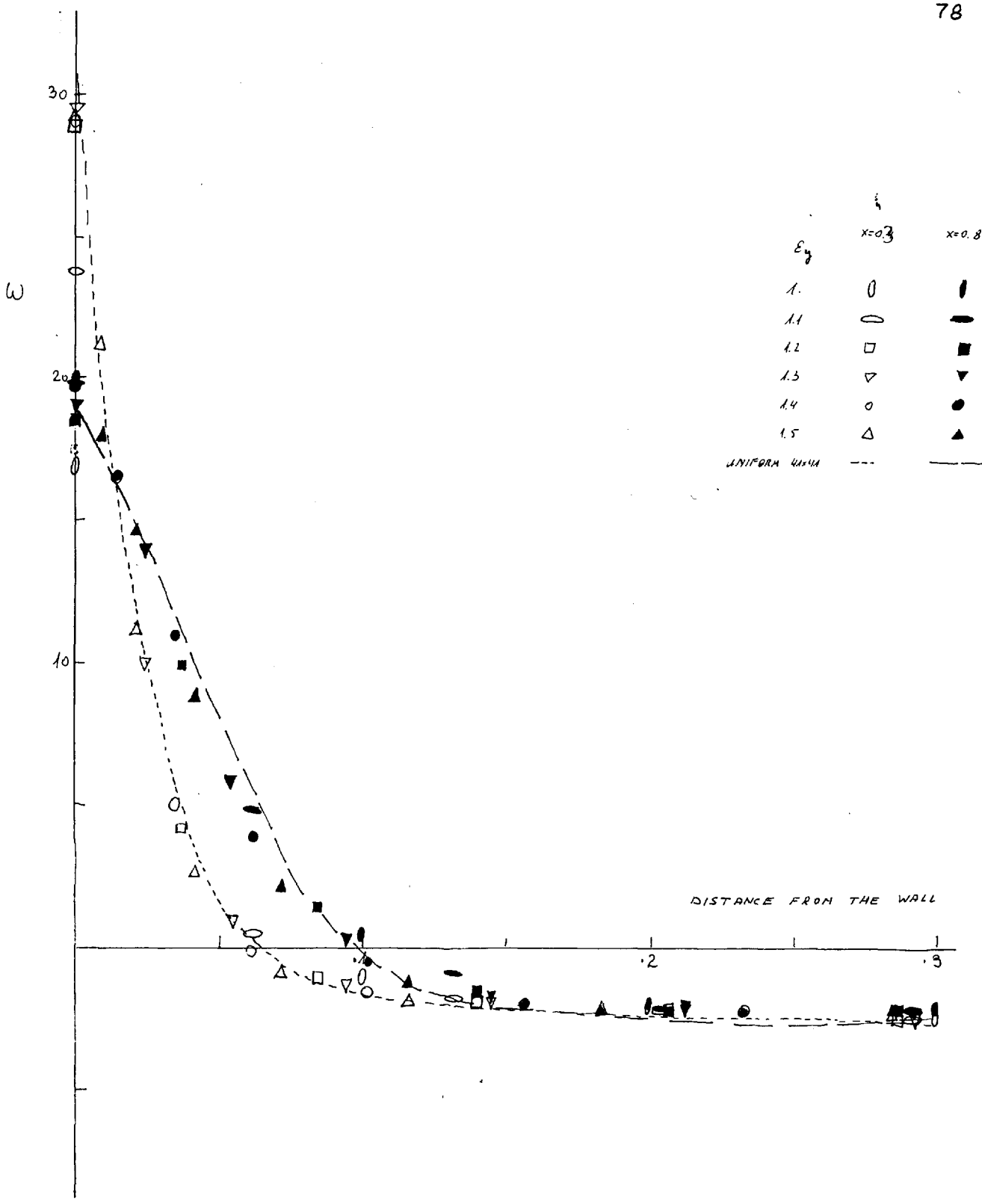

FIG 4.3-3: THE INFLUENCE OF THE MESH NON-UNIFORMITY PARAMETER ε_y ON THE VORTICITY PROFILE AT TWO STATIONS IN THE IMPINGING JET. R = 1000.

tion of the laminar impinging jet problem (as presented in section 4.1) for a Reynolds number of 10^6, is shown in fig 4.4-1 in the form of stream function and vorticity contours. Surprisingly, we notice that there is a region in the middle of the figure, where the vorticity varies along the stream lines. This region is seen to be distinguished in two ways from the rest of the flow:

(i) it contains a vorticity maximum (where the vorticity is not linear) and (ii) it is in the region where the stream lines have a 45 degrees inclination to the finite-difference mesh. In the rest of the present section we shall see that this departure from the exact solution of the differential equations, is inherent in our finite-difference method (and, indeed, in other ones as well) and may be described as a smearing effect, caused by the action of "false" viscosity. This false viscosity will be shown to be related to (i) and (ii) above.

Description of the smearing effect

"Smearing" of steep gradients as a result of one sided finite difference schemes has been mentioned in the literature (e.g. Alder et al., 1964, p. 335). It is usually connected with the first order derivatives, and is therefore mostly influential when the viscosity approaches zero. Also, from fig 4.4-1, it seems that this smearing is stronger when the stream lines are

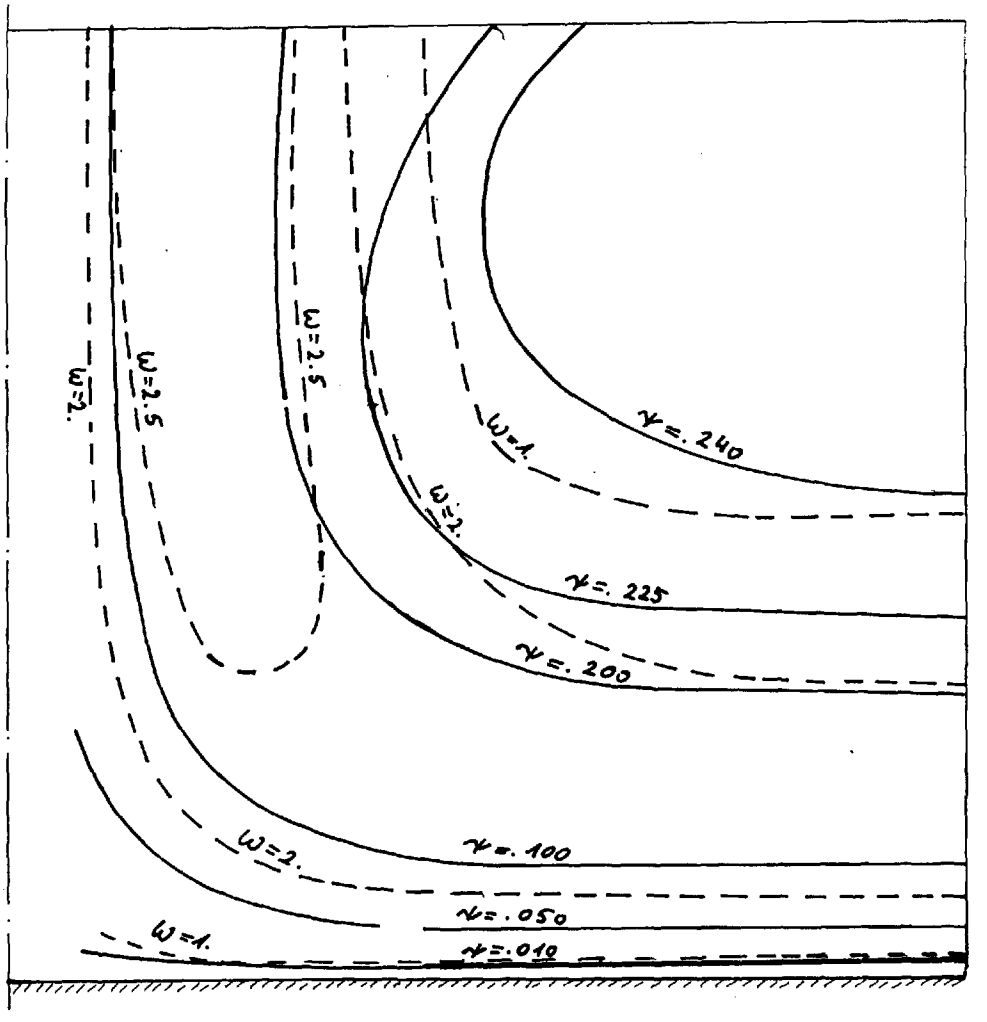

FIG 4.4-1: SMEARING OF A VORTICITY MAXIMUM IN A LAMINAR IMPINGING JET WITH A VANISHING VISCOSITY. $R=10^6$, AND THE MESH IS 11×11 NON-UNIFORM ONE. THE SOLID LINES REPRESENT STREAM LINES, AND THE DASHED LINES REPRESENT VORTICITY CONTOURS.

inclined towards the mesh lines. Thus, our first line of attack becomes clear: What will be the smearing effect in a uniform velocity non-diffusional flow, with stream-lines inclined towards the mesh? The case to be studied was described in section 4.1 and figure 4.1-4. A source of conserved property is placed in a uniform-velocity stream. The deviation from the exact solution (of constant ϕ along any stream line) may now be studied for various inclinations between the stream lines and the mesh. The results are shown in fig 4.4-2 in the form of the decay of ϕ along the stream line passing through the centre of the source. It isquite clear, that the smearing is dependent on the angle between the stream lines and the mesh lines. The maximum smearing occurs when $\alpha = 45^{o}$. When α decreases the smearing becomes smaller, until, when $\alpha = 0$, no smearing is present. By symmetry, the smearing decreases also when α increases, until it disappears completely, at $\alpha = 90^{o}$. This suggests that the smearing is a function of sin (2α). Indeed, if we multiply the ϕ-values by $\left[\sin (2\alpha)\right]^{+\frac{1}{2}}$ all the lines in fig 4.4-2 nearly reduce to a single line as shown in fig 4.4-3*.

---

* The power of sin (2α) was chosen as 0.5 in order that the influence of the angle α will be easily incorporated in eqn (4.4-7), to yield eqn (4.4-11).

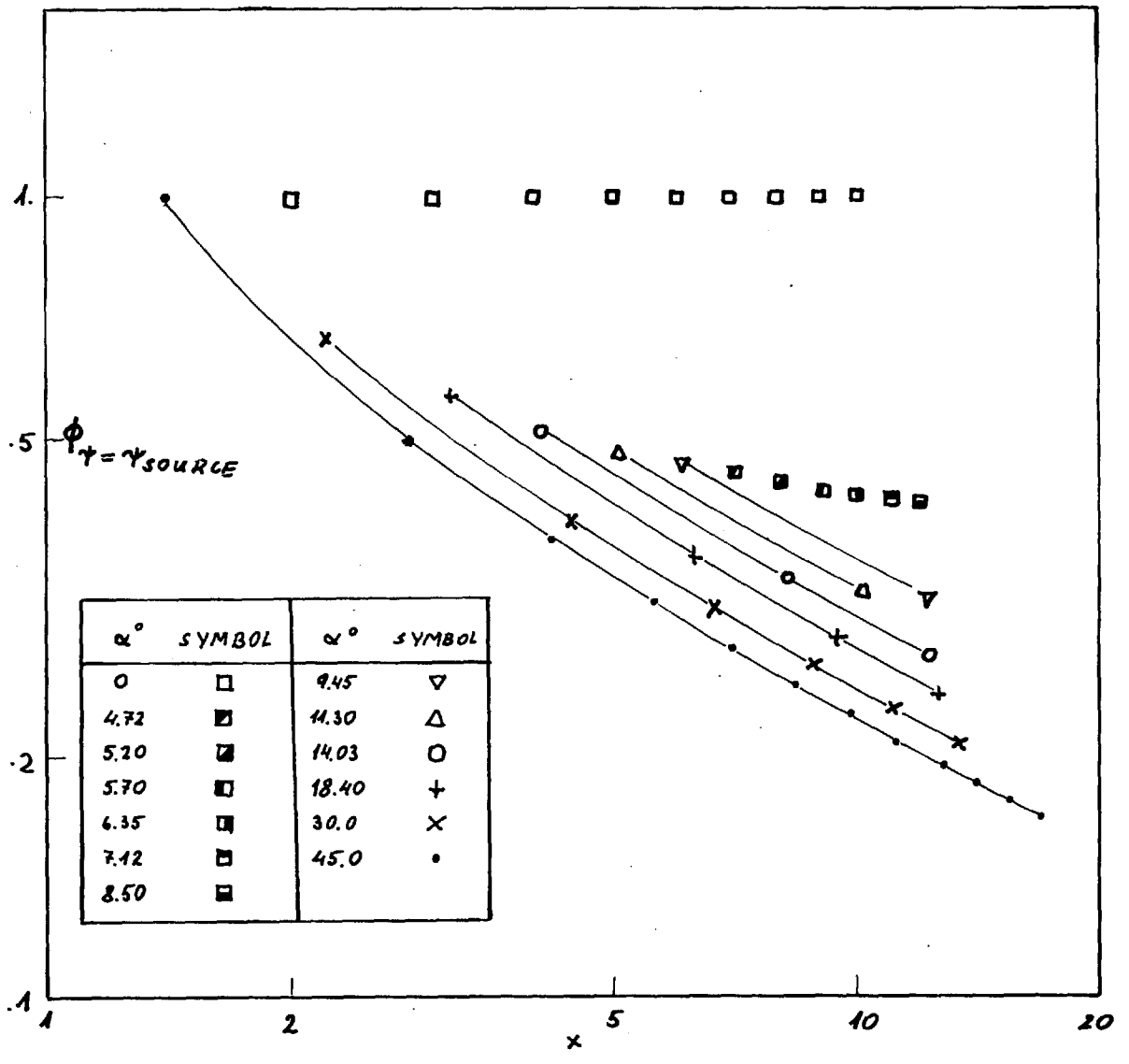

FIG 4.4-2 : THE DECAY OF THE CONSERVED PROPERTY ϕ ALONG THE STREAM LINE PASSING THROUGH THE SOURCE, FOR VARIOUS ANGLES α BETWEEN THE STREAM LINES AND THE MESH IN A UNIFORM-VELOCITY, NON-DIFFUSIONAL FLOW.

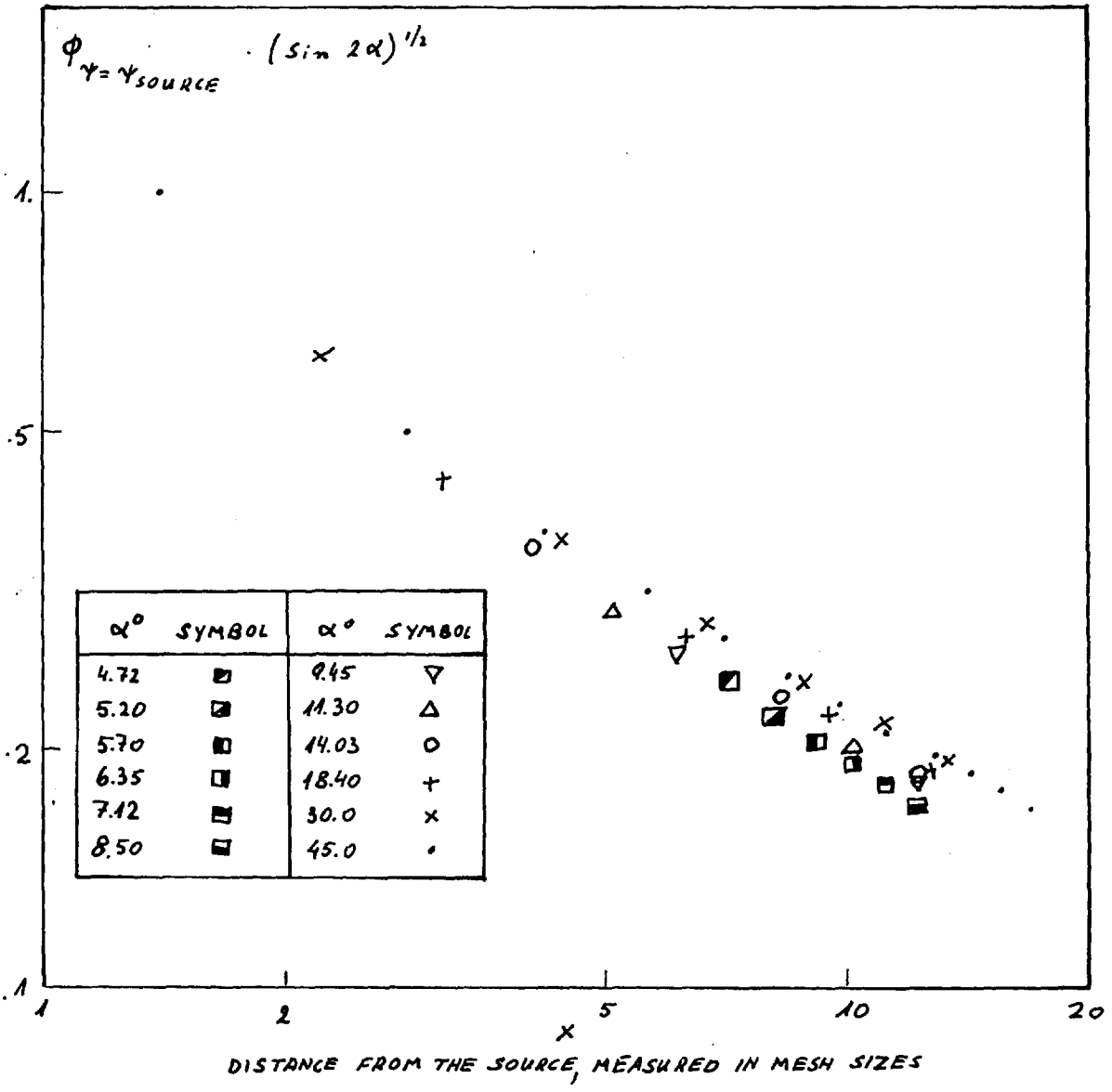

FIG 4.4-3 : REDUCED FORM OF THE ϕ-DECAY ALONG THE STREAM LINE PASSING THROUGH THE SOURCE.

Correlation of the smearing effect

In order to find out what the smearing looks like, it is advisable to carry out the integration further downstream from the source, so as to eliminate the local influence of the source and boundary. It will suffice to do this only for the case of maximum smearing, when the stream linss run at 45^{o} to the mesh. When such a computation is performed, the result is the formation of what we may conveniently call a ϕ-wake, which is shown in Fig 4.4-4. This is the region behind the source where the ϕ-discontinuity is smeared in a way very similar to that found in viscous free jets and wakes. Focusing our attention on the region far away from the source, the ϕ-profiles normal to the stream lines are plotted in fig 4.4-5. It is seen that they are similar when normalised by ϕ_{max} and $y_{\frac{1}{2}}$ (as defined in fig 4.4-4). Secondly we look at the decay of ϕ_{max} and the growth of $y_{\frac{1}{2}}$. They are both plotted in fig 4.4-6. Far away from the source, where the ϕ-profiles are similar, they can be correlated quite accurately, by

$$\frac{\phi_{max}}{\phi_o} = 0.68 \left(\frac{h}{x}\right)^{1/2} \qquad (4.4\text{-}1)$$

$$\frac{y_{1/2}}{h} = \left(\frac{x}{h}\right)^{1/2} \qquad (4.4\text{-}2)$$

where h is the mesh size, and ϕ_o is the ϕ-value at the source.

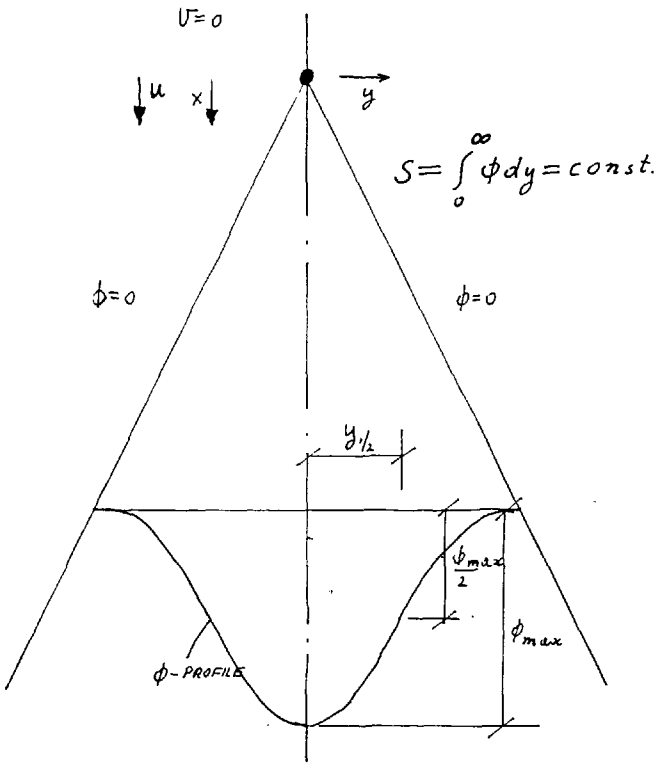

FIG 4.4-4: THE ϕ-WAKE

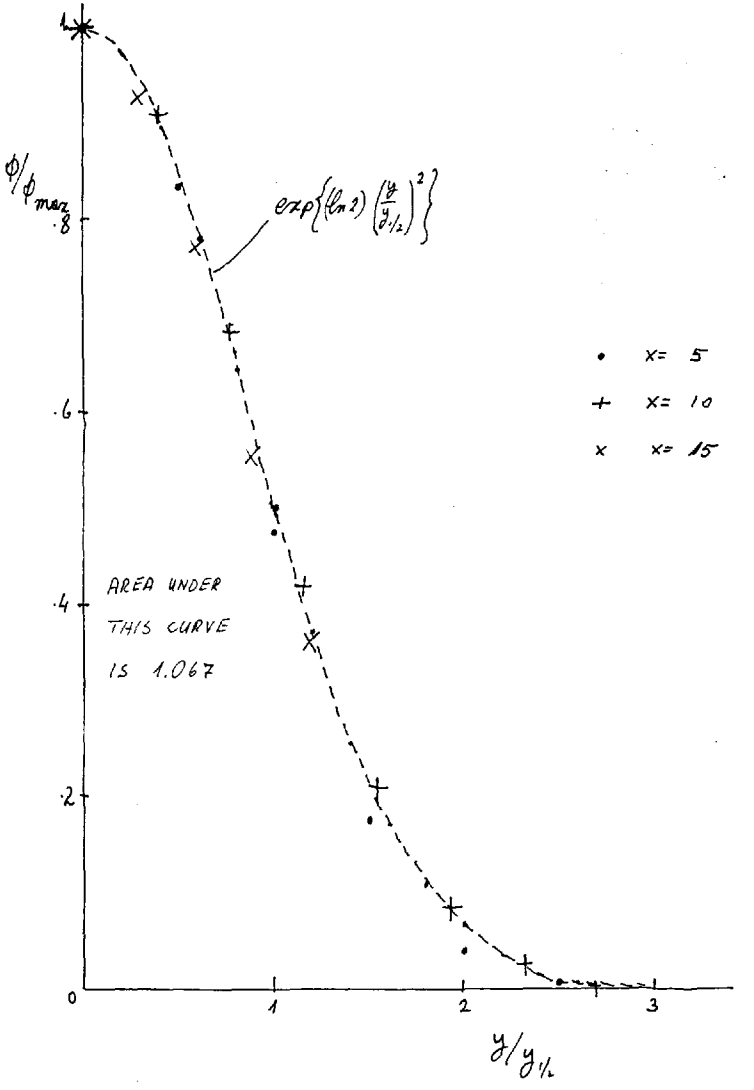

FIG 4.4-5: THE ϕ-PROFILE DOWNSTREAM OF A SOURCE IN A UNIFORM VELOCITY FIELD, WITH STREAM LINES INCLINED TO THE MESH AT 45°, AND ZERO DIFFUSION.

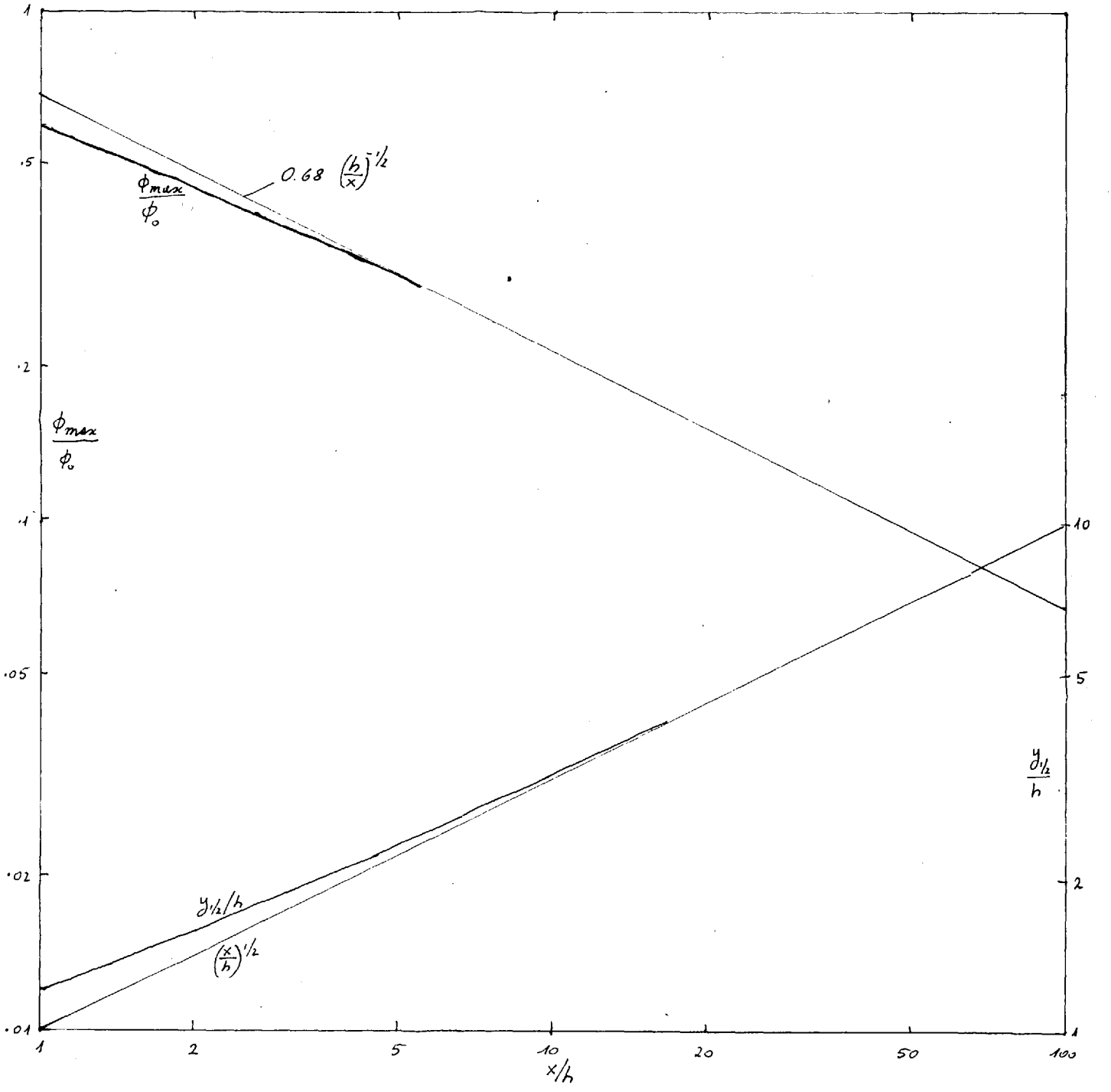

FIG 4.4-6 : THE ϕ_{max} – DECAY AND $y_{1/2}$ – GROWTH BEHIND A ϕ-SOURCE IN A UNIFORM VELOCITY FIELD WHEN THE STREAM LINES ARE INCLINED AT 45° TOWARDS THE MESH.

The "false diffusion" effect

Figures 4.4-5 and 4.4-6 show, quite convincingly, that the smearing of the source, described above, is very similar to the diffusion of a ϕ-source in a uniform-velocity, laminar flow field. Such a phenomenon is governed by the equation

$$u \frac{\partial \phi}{\partial x} = \Gamma \frac{\partial^2 \phi}{\partial y^2} \qquad (4.4\text{-}3)$$

where Γ is the laminar diffusion coefficient, and u is the constant velocity. The solution of this equation is

$$\phi = A\, x^{-1/2} \exp\left[-c^2 \frac{y^2}{4x}\right] \qquad (4.4\text{-}4)$$

where A is a constant, and

$$c^2 = \frac{u}{\Gamma} \qquad (4.4\text{-}5)$$

and the source strength is

$$S = 2A\left(\frac{\pi\Gamma}{u}\right)^{1/2} \qquad (4.4\text{-}6)$$

We shall now try to find out, which value we have to assign to the diffusivity Γ in order that equation (4.4.-4) will correspond to equations (4.4-1) and (4.4-2).
Now, eqn (4.4-4), together with (4.4-6) yields

$$\frac{\phi_{max}}{S/h} = \frac{1}{2}\left(\frac{uh}{\pi\Gamma}\right)^{1/2}\left(\frac{h}{x}\right)^{1/2} \qquad (4.4\text{-}7)$$

And comparison of the two expressions in eqns (4.4-7) and (4.4-1), immediately gives

$$\Gamma_{false} = 0.361\ u h \qquad (4.4\text{-}8)$$

$$S = 1.45\ \phi_0\ h \qquad (4.4\text{-}9)$$

where Γ_{false} is the diffusion coefficient which will cause a thermal wake similar to that represented by eqns (4.4-1) and (4.4-2). The source strength quoted in equation (4.4-9) is the same as the real strength of the source used in the computations, which was

$$S = 2 \times 1.067 \times 0.68\ \ \phi_0\ h \qquad (4.4\text{-}10)$$

Therefore we may conclude, that the effect of having the stream lines inclined at $\alpha = 45^{\circ}$ to the mesh, in a uniform velocity non-viscous field, is just the same as that which would result from the introduction of a "false-diffusion" as given by equation (4.4-8). When the angle α decreases the false diffusion decreases as well, and in view of the correlation shown in fig 4.4-3, it is clear that, finally, the false diffusion in a uniform velocity field may be well represented by

$$\Gamma_{false} = 0.36\ u\ h\ \sin(2\alpha) \qquad (4.4\text{-}11)$$

This false diffusion influences both the vorticity ω, and the conserved property ϕ.

Discussion

The results of the present section, as summarised in equation (4.4-11) set a limit to the accuracy which

we may hope to get from our finite-difference method. But we should examine whether this limit is too severe or not. To do this, let us write eqn (4.4-11) in the following form

$$\frac{\Gamma_{false}}{\Gamma_{eff}} = 0.36\ R_{eff}\ \sigma_{eff}\ \frac{h}{L}\ \sin(2\alpha) \qquad (4.4\text{-}12)$$

where

$$R_{eff} = \frac{u L}{\nu_{eff}} \qquad (4.4\text{-}13)$$

is the local effective Reynolds number,

$$\sigma_{eff} = \frac{\mu_{eff}}{\Gamma_{eff}} \qquad (4.4\text{-}14)$$

is the effective Prandtl number, and L is the length scale of the phenomenon.

Clearly an increase in either R_{eff} or σ_{eff} increases the ratio $\Gamma_{false}/\Gamma_{eff}$. This is very undesirable feature and, apparently, all we could do is to reduce h/L. There are however some factors which usually keep the level of false diffusion at an acceptable level:

(i) When either the diffusivity or the ϕ-gradients are small, the solution is not seriously dependent on the diffusivity (e.g. for a very low false viscosity, the flow becomes non-viscous, even if the false diffusion is much larger than the true one).

(ii) In turbulent flow σ_{eff} is likely to be near unity, and R_{eff} is likely to be kept at a fairly low level.

(iii) In any case, false diffusion plays a major role only when the stream lines run at 45 degrees incidence to the mesh.

Finally, we note that any non-symmetrical finite-difference scheme will be penalised by a false-diffusion effect. This seems to be the price which we have to pay for the much improved stability of such schemes.

4.5 Factors affecting convergence

No general theorems are currently available to prove that a given system of algebraic non-linear equations will converge, when iterated in any particular way. The present work does not make any contribution in this direction. It is, however, desirable to have a short discussion on convergence of the system of equations

$$\phi_i = \sum_{all\,j} a_{ij}\,\phi_j \qquad (4.5\text{-}1)$$

It has been shown by many (see for instance Golden, 1965, P.103) that if

$$a_{ij} = \text{const} \qquad (4.5\text{-}2)$$

equation (4.5-1) converges when

$$\sum_{all\,j} |a_{ij}| \leq 1 \qquad (4.5\text{-}3)$$

for all the values of i,

and for at least one i

$$\sum_{all\,j} |a_{ij}| < 1 \qquad (4.5\text{-}4)$$

Practice has shown that even when the $a_{i,j}$'s are functions of the ϕ's, equation (4.5-1) usually converges if conditions (4.5-3) and (4.5-4) are satisfied. In our case it is easily seen that equation (3.1-1) satisfies condition (4.5-3) in all the points inside the field, and that it satisfies condition (4.5-4) in all the points adjacent to the boundaries, apart from points near a solid wall. A comprehensive treatment of the subject is given by Barakat and Clark (1965).

In the points near the wall the various ϕ-equations are coupled in a more complex way than in the other points. Again the reasons are not completely clear, but it has been already claimed by Runchal et al. (1967), that divergence may develop near the wall. For suggestions on how to remove this divergence, the reader is referred to the above paper by Runchal et al.

4.6 Termination of computing, and computing time

In the present computations, a convergency parameter was used, as defined in eqn (3.4-2):

$$r_u = \frac{\phi_{p,n-1} - \phi_{p,n}}{\phi_{max,n}} \qquad (4.6\text{-}1)$$

After each iteration, the maximum absolute value of r_u for each variable was recorded. When the largest value of r_u became smaller than a pre-set small number c_c, the iteration was terminated.

The recorded τ_u values were also used to study the approach of the iterated solution to what was considered the exact solution. In practice it was found many times, that τ_u was fluctuating and changing signs, but the amplitude of the fluctuations, although small, did not vanish. In such situations, the solution could have been quite far from the exact one. In order to distinguish between such cases and real convergent solutions the convergency criterion had to be pushed down, to

$$c_c = 0.0001$$

This low value has caused, sometimes, long computing time, which was not matched by a considerable increase in the accuracy. The rate of convergence is shown in fig 4.6-1, where the maximum value of τ_u after each iteration is plotted versus the number of iterations N, for a case of a laminar impinging jet with fine mesh. The computing time for internal mesh points and two variables was about one minute.

In table 4.6-1 the number of iterations for various solutions is quoted. It appears that turbulent flow usually needs more iterations than a laminar one. Also, an increase in the number of mesh points is penalised by a further increase in the number of necessary iterations.

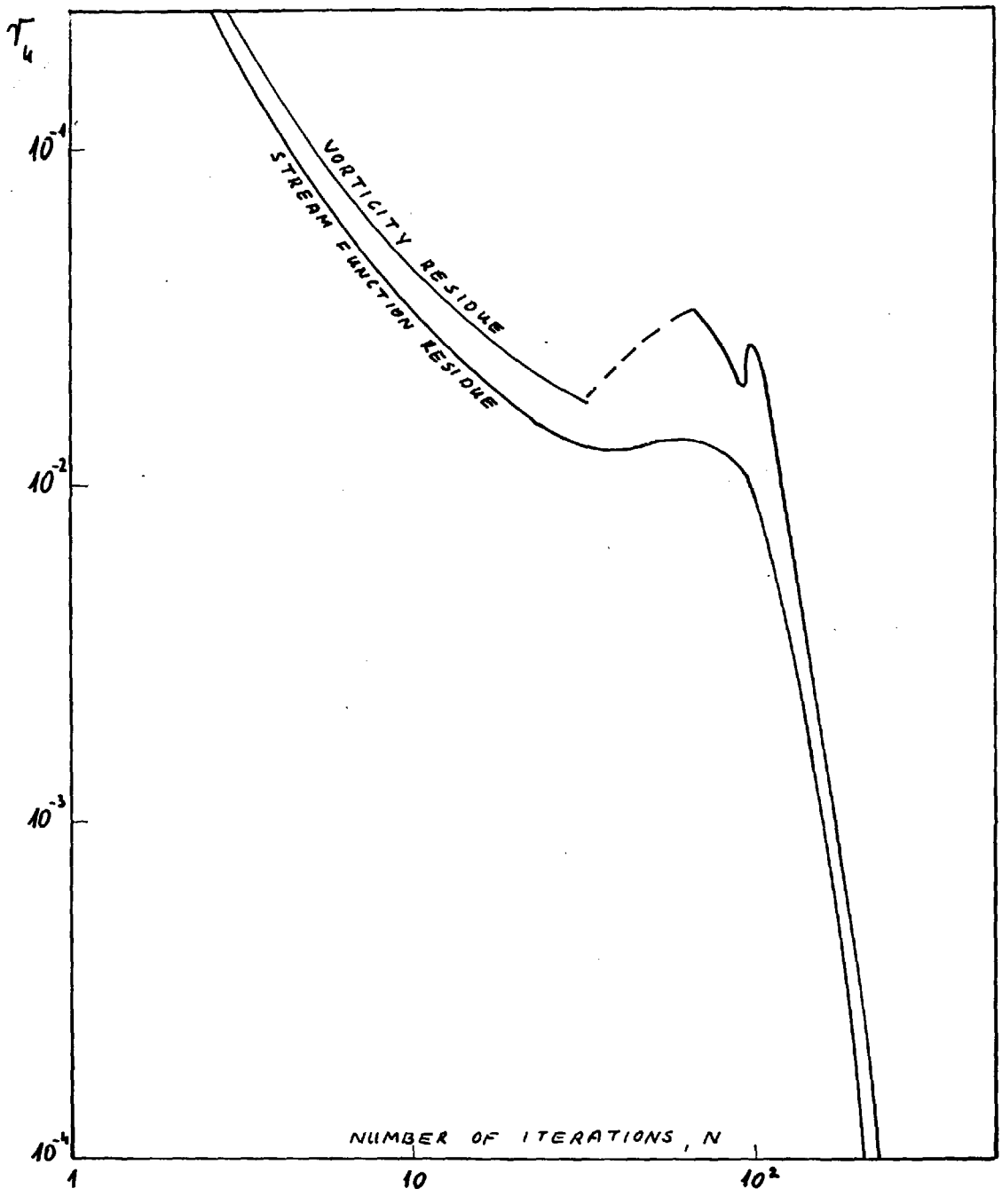

FIG 4.6-1: THE RATE OF CONVERGENCE FOR A LAMINAR IMPINGING JET AS DEFINED IN SECTION 4.1 . R = 1000. 21×21 UNIFORM MESH. THE DASHED LINE REPRESENTS NEGATIVE VALUES.

Table 4.6-1 : Number of iterations performed:

Case	Mesh	Number of internal mesh points	ε_y	Number of iterations
Couette flow M= 10	3x11	1x9	1	65
	3x21	1x19	1	216
	3x41	1x39	1	400*
Couette flow M= 10	3x11	1x9	1.1	62
			1.2	62
			1.3	53
			1.4	64
			1.5	72
Laminar impinging jet	11x11	9x9	1	50
	21x21	19x19	1	229
	41x41	39x39	1	624
	11x11	9x9	1.1	54
			1.2	51
			1.3	55
			1.4	59
			1.5	82
Turbulent impinging jet (as presented in chapter 7)	11x11	9x9	1	70
			1.1	61
			1.2	75
			1.3	80
			1.4	90
			1.5	101
			1.6	111

* In this case the maximum residue was still 0.006 after 400 iterations, but as the solution seemed to be correct, it was decided not to continue the iterations.

Closure to part II

Part II was devoted to the presentation of the mathematical problems involved in the solution of the incompressible, steady, two-dimensional, variable property flow. We have seen the set of differential equations, and the finite-difference method used to solve them. It was later demonstrated that convergent, accurate and economical solutions may be obtained by this method.

Part III : An application of the method to turbulent flows

In this part of the paper we shall examine and formulate the physical input necessary to solve problems of turbulent flow. Although the aim is to incorporate this physical input in the computational method, described in part II, most of the present part may stand by itself, and be used with other solution methods as well, as its development is fairly general. In chapter 5 we shall discuss a viscosity law, based on the Kolmogorov-Prandtl hypothesis; we shall present the turbulence energy equation, and determine the necessary empirical constants.

In chapter 6, we shall discuss the wall fluxes and develop a special practice for the treatment of thin boundary layers near walls. Finally, in chapter 7, solutions for the problem of a plane impinging jet will be presented. These will demonstrate the capability of the method, and will also throw light on some deficiencies of the physical input.

5. The turbulence energy, and the viscosity law

5.1 The general hypothesis on turbulence

In most previous theories of turbulence, it was assumed that the turbulence properties are dependent on the velocity field, and on some length scale only. Such theories are usually successful when equilibrium between generation and dissipation of turbulence is maintained. However, if turbulence is convected or diffused into the region under consideration, the velocity and the length scale are not sufficient to describe the level of turbulence. Such cases arise, for instance, when the turbulence in a boundary layer is augmented by a very high main-stream turbulence. Our present model, first suggested by Kolmogorov (1942) and Prandtl (1945), differs from other models by the assumption that the turbulence properties are dependent on the level of turbulence of the fluid and a length scale. The level of turbulence is characterised by the mean kinetic energy of the velocity fluctuations, k, which is defined as

$$k = \frac{1}{2}\left(\overline{u_1'^2} + \overline{u_2'^2} + \overline{u_3'^2}\right) \qquad (5.1\text{-}1)$$

where u_1', u_2' and u_3' are the fluctuating parts of the velocity components. The quantity k has been named the turbulent kinetic energy, or kinetic energy of turbulence. In the present thesis we shall use the term turbulence energy.

We have now to establish some way to compute the turbulence energy k and the length scale, ℓ. We need to find also the relation between the turbulent properties (as say μ_{turb}, Γ_{turb}) and k and ℓ. All this will be done in the following pages.

5.2 The turbulence energy equation

In the present section we shall be concerned with the derivation of a differential equation for the turbulence energy, k, and the necessary auxiliary relations. This will be done by algebraic manipulation of the equation of motion. Similar derivations have already been reported (e.g. Emmons, 1954), enabling the present one to be brief. To make the derivation shorter, we shall make use of index notation, where any index may be 1, 2 or 3. We shall also make use of the summation convention, by which, whenever an index appears twice in a term, it should be summed over all the three components, e.g.

$$\frac{\partial U_j}{\partial x_j} = \sum_{j=1,2,3} \frac{\partial U_j}{\partial x_j} = \frac{\partial U_1}{\partial x_1} + \frac{\partial U_2}{\partial x_2} + \frac{\partial U_3}{\partial x_3} \qquad (5.2\text{-}1)$$

In the above notation, the equations of continuity and motion for incompressible fluids, with uniform laminar viscosity, become

$$\frac{\partial U_j}{\partial x_j} = 0 \qquad (2.1\text{-}1)$$

$$\rho \frac{\partial u_i}{\partial t} + \rho u_j \frac{\partial u_i}{\partial x_j} + \frac{\partial p}{\partial x_i} = \mu \frac{\partial^2 u_i}{\partial x_j^2} + F \qquad (5.2\text{-}2)$$

where F is a body force, and p is the pressure.

We now make the assumption that in a turbulent flow all the quantities may be split into a time averaged part and a fluctuating part:

$$u_i = \bar{u}_i + u_i' \qquad (5.2\text{-}3)$$

$$p = \bar{p} + p' \qquad (5.2\text{-}4)$$

where the barred quantities are time averaged, the primed ones are the fluctuating components, and

$$\overline{u_i'} = \overline{p'} = 0 \qquad (5.2\text{-}5)$$

By time averaging eqn (2.1-1) and (5.2-2) we get

$$\frac{\partial \bar{u}_j}{\partial x_j} = 0 \qquad (5.2\text{-}6)$$

$$\rho \frac{\partial \bar{u}_i}{\partial t} + \rho \bar{u}_j \frac{\partial \bar{u}_i}{\partial x_j} + \frac{\partial \bar{p}}{\partial x_i} = \mu \frac{\partial^2 \bar{u}_i}{\partial x_j^2} + \rho \frac{\partial}{\partial x_j} \overline{u_i' u_j'} + F \qquad (5.2\text{-}7)$$

It may be shown after some lengthy algebra, that, if we multiply eqn (5.2-7) by $\bar{u}_i$ and subtract from the equation thus obtained the time average of the product of eqn (5.2-2) and u_i, we get eventually

$$\rho \frac{\partial k}{\partial t} + \rho \bar{u}_j \frac{\partial k}{\partial x_j} = -\rho \overline{u_i' u_j'} \frac{\partial \bar{u}_i}{\partial x_j} - \frac{\partial}{\partial x_j}\left(\rho \frac{\overline{u_j' u_i'^2}}{2} - \overline{u_j' p'}\right) + \mu \frac{\partial^2 k}{\partial x_j^2} - \mu \overline{\left(\frac{\partial u_i'}{\partial x_j}\right)^2} \qquad (5.2\text{-}8)$$

The physical meaning of the various terms in eqn (5.2-8) may be identified as follows:

$\rho \frac{\partial k}{\partial t}$ ≡ The non-steady growth of turbulence energy (this will be zero in the present thesis).

$\rho \bar{U}_j \frac{\partial k}{\partial x_j}$ ≡ Convection of turbulence energy by the mean motion.

$-\rho \overline{u_i' u_j'}$ ≡ The Reynolds stresses.

$-\rho \overline{u_i' u_j'} \frac{\partial \bar{U}_i}{\partial x_j}$ ≡ Production of turbulence energy.

$-\frac{\partial}{\partial x_j}\left(\rho \frac{\overline{u_j' u_i'^2}}{2} - \overline{u_j' p'}\right)$ ≡ Turbulent diffusion of turbulence energy.

$\mu \frac{\partial^2 k}{\partial x_j^2}$ ≡ Viscous diffusion of turbulence energy.

$-\mu \overline{\left(\frac{\partial u_i'}{\partial x_j}\right)^2}$ ≡ Viscous dissipation.

5.3 Elimination of the fluctuating quantities

Emmons (1954) has applied dimensional analysis to replace all the primed quantities in eqn (5.2-8) with simpler ones. His analysis is based on the assumption that all turbulent quantities are functions of k and ℓ only. It is not necessary to repeat all Emmons's arguments here. Whenever his expressions are used without much change, they will be just quoted without any elaboration.

The turbulent viscosity

In a laminar Newtonian flow the shear stress is given by

$$\tau_{ij} = \mu \left(\frac{\partial u_i}{\partial x_j} + \frac{\partial u_j}{\partial x_i}\right) \qquad (5.3\text{-}1)$$

An implication of eqn (5.3-1) is that the viscosity is a scalar. Now we shall assume that in a turbulent flow a scalar turbulent viscosity may be defined by the equation

$$-\rho\,\overline{u_i' u_j'} = \mu_{turb}\left(\frac{\partial \bar{u}_i}{\partial x_j} + \frac{\partial \bar{u}_j}{\partial x_i}\right) \qquad (5.3\text{-}2)$$

Dimensional considerations lead to the following form of the turbulent viscosity

$$\mu_{turb} = c_\mu\,\rho\,k^{1/2}\,\ell_\mu \qquad (5.3\text{-}3)$$

Where c_μ is a constant to be determined from experimental data and ℓ_μ is the turbulence length scale.

The turbulence energy diffusion

The turbulent diffusion of turbulence energy may be represented by

$$-\frac{\partial}{\partial x_j}\left(\rho\,\frac{\overline{u_j' u_i^2}}{2} - \overline{u_j' p'}\right) = \frac{\partial}{\partial x_j}\left(\frac{\mu_{turb}}{\sigma_{k,turb}}\,\frac{\partial k}{\partial x_j}\right) \qquad (5.3\text{-}4)$$

And if we add to this the viscous diffusion, we get (for a constant laminar viscosity):

$$\frac{\partial}{\partial x_j}\left[\left(\mu + \frac{\mu_{turb}}{\sigma_{k,turb}}\right)\frac{\partial k}{\partial x_j}\right] \qquad (5.3\text{-}5)$$

In fact we may now define an effective transfer coefficient for the turbulence energy diffusion, which will be very similar to that of any other conserved property:

$$\Gamma_{k,eff} = \frac{\mu}{\sigma_k} + \frac{\mu_{turb}}{\sigma_{k,turb}} \qquad (5.3\text{-}6)$$

with

$$\sigma_k = 1 \qquad (5.3\text{-}7)$$

and $\sigma_{k,turb}$ is a constant to be deduced from experimental data. We shall later see that $\sigma_{k,turb}$ is quite different in magntidue from $\sigma_{\phi,turb}$.

Dissipation

We shall represent the viscous dissipation by

$$\mu \overline{\left(\frac{\partial u_i'}{\partial x_j}\right)^2} = c_D \frac{\rho k^{3/2}}{\ell_D} \qquad (5.3\text{-}8)$$

Again c_D is a constant to be determined from experimental data. It will be noted also, that a new length scale ℓ_D has been introduced. It will be later shown that if c_D is chosen appropriately ℓ_D can be put equal to ℓ_μ everywhere, apart from the region very near to the wall, where the viscous stresses are large in comparison to the Reynolds stresses. A distribution different from the ℓ_μ distribution was suggested by Glushko (1965). During the present investigation it was found that a good fit with Couette flow data, for the transition from the laminar sub-layer to the fully turbulent region, could not be obtained without the introduction of ℓ_D. The actual ℓ_D distribution will be discussed in the next section, together with that for ℓ_μ.

The turbulence energy equation

We may now substitute all the above expressions in eqn (5.2-8), to get:

$$\rho \frac{\partial k}{\partial t} + \rho \bar{u}_j \frac{\partial k}{\partial x_j} = \frac{\partial}{\partial x_j}\left(\Gamma_{k,eff} \frac{\partial k}{\partial x_j}\right) + \mu_{turb}\left(\frac{\partial \bar{u}_i}{\partial x_j} + \frac{\partial \bar{u}_j}{\partial x_i}\right)\frac{\partial \bar{u}_i}{\partial x_j} - C_o \frac{\rho k^{3/2}}{\ell_o} \qquad (5.3\text{-}9)$$

where μ_{turb} and $\Gamma_{k,eff}$ are defined in eqns (5.3-3) and (5.3-6).

5.4 The length scale

In the last two sections we have developed an equation for the turbulence energy. It would be advisable to have a similar equation for the length scales ℓ_μ and ℓ_D. However, it is not possible, at the present stage, to report advances in this direction. Instead, we shall have to rely on other sources of information. The most important of them is the similarity with the Prandtl mixing length to which our length scales should reduce in certain circumstances. Thus, in such cases, we expect the length scales to be proportional to the distance from the wall near solid walls, and to be proportional to the width of a jet, in jet flow.

It has been shown by Glushko (1965) and van Driest (1956) that, very near to the wall, the length scale decreases much faster than the distance from the wall, y. Glushko suggested to use very near to the wall

$$\frac{\ell}{y} = a R \qquad (5.4\text{-}1)$$

where a is a constant which has a different value for ℓ_μ than for ℓ_D, and

$$R = \frac{k^{1/2} y \rho}{\mu} \qquad (5.4\text{-}2)$$

It has been widely accepted that, when R is very large

$$\frac{\ell_\mu}{y} = \frac{\ell_0}{y} = \text{const} \qquad (5.4\text{-}3)$$

which prevails in the fully turbulent region. The constant in the right-hand side of eqn (5.4-3) is usually put equal to unity, by a suitable choice of the constants c_μ and c_0.

The van Driest hypothesis is connected with the Prandtl mixing length hypothesis. Following Patankar (1967), it may be written as:

$$\frac{\ell}{y} = 1 - \exp\left(-\frac{y\sqrt{\tau\rho}}{A\mu}\right) \qquad (5.4\text{-}4)$$

Where A is a constant. The expression $y\sqrt{\tau\rho}/\mu$ represents the non-dimensional distance from the wall when the mixing-length hypothesis is used. But when the turbulence energy hypothesis is used, the distance from the wall is usually represented by R as given in eqn (5.4-2). Indeed, these two expressions are proportional to one another in a constant-shear non-diffusional Couette flow. Thus we may deduce, for the length scale near

walls

$$\frac{\ell_\mu}{y} = 1 - \exp\left(-A_\mu \frac{k^{1/2} y \rho}{\mu}\right) \qquad (5.4\text{-}5)$$

$$\frac{\ell_D}{y} = 1 - \exp\left(-A_D \frac{k^{1/2} y \rho}{\mu}\right) \qquad (5.4\text{-}6)$$

where A_μ and A_D are constants, to be fitted to experimental data. ℓ_μ and ℓ_D designate length scales for viscosity and dissipation respectively, as they are used in equation (5.3-3) and (5.3-8); y is the distance from the wall. We shall arrange that for large y both ℓ_μ and ℓ_D are equal to y.

It will be shown in the next section that for good agreement with experimental results, we have to take:

$$A_\mu = 0.016 \qquad (5.4\text{-}7)$$

$$A_D = 0.263 \qquad (5.4\text{-}8)$$

A comparison of the resulting length scales distributions with those recommended by Glushko is shown in fig 5.4-1. Also shown in this figure are the implications of a recent suggestion for the length scales made by Spalding (1967).

Discussion of the length scale distribution near walls

Three suggestions for length scale distribution near walls have been reported above. All of them suggest that far away from the wall, one can take

$$\ell_\mu = \ell_D = y \qquad (5.4\text{-}9)$$

which has been well confirmed by work on the Prandtl mixing-length hypothesis. Very near to the wall, an expansion of

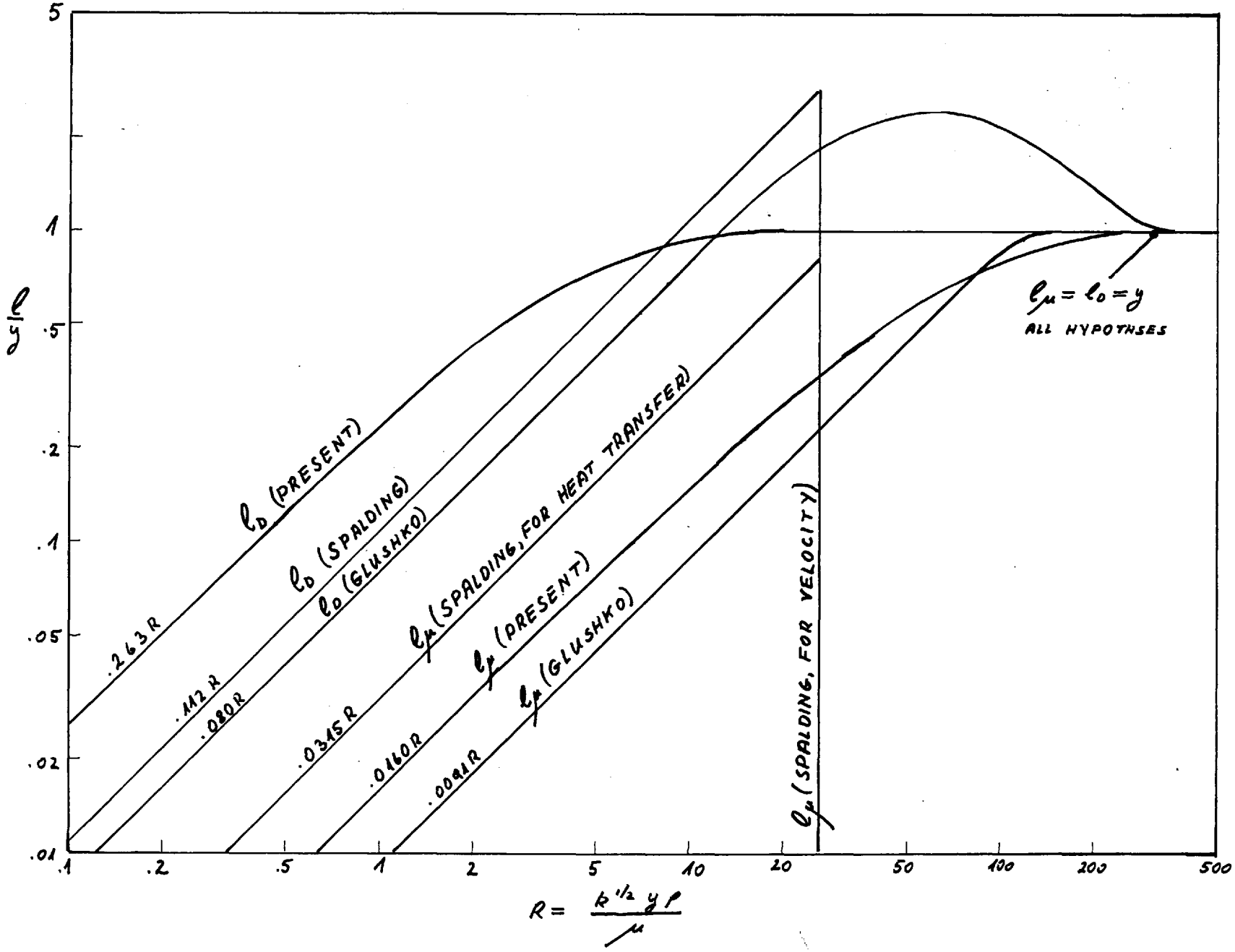

FIG 5.4-1 : COMPARISON OF LENGTH SCALE DISTRIBUTIONS.

equations (5.4-5) and (5.4-6) leads to:

$$\frac{\ell_\mu}{y} = A_\mu \frac{k^{1/2} y \rho}{\mu} \qquad (5.4\text{-}10)$$

$$\frac{\ell_o}{y} = A_o \frac{k^{1/2} y \rho}{\mu} \qquad (5.4\text{-}11)$$

These expressions are in agreement with the other two proposals and with the meagre experimental evidence on the flow in the laminar sub-layer.

The present approach is to join eqn (5.4-9) with (5.4-10) or (5.4-11) together by an exponential expression. This practice finds some support in the van Driest hypothesis, which has been used very successfully by Patankar (1967) together with the Prandtl mixing-length. It also results in a fairly good agreement with measured velocity profile in a constant-shear non-diffusional Couette flow, as will be demonstrated in the next section. It has the disadvantage , that it does not yield to analytical integration when substituted in the equations but this is not a real difficulty for the numerical analyst. More serious is the fact that we do not have sufficient measurements to correlate and confirm the exponential form of the length scale distribution. Therefore we must accept eqns (5.4-5) and (5.4-6) as tentative, until direct measurements of the shear stress and turbulent properties are available all the way through, from the sub-layer to the fully turbulent region in a variety of conditions.

5.5 The turbulent exchange coefficient

We shall suppose, following Spalding (1967c), that

$$\Gamma_{\phi,eff} = \frac{\mu_{eff}}{\sigma_{\phi,eff}} = \frac{\mu}{\sigma_\phi} + \frac{\mu_{turb}}{\sigma_{\phi,turb}} \qquad (5.5\text{-}1)$$

This expression reduces to the proper asymptotic forms at the two extremes of fully turbulent or fully laminar flow. $\sigma_{\phi,turb}$ is constant in the fully turbulent region. We do not know much about its behaviour in the transition region and the viscous sub-layer. Therefore, we shall follow Spalding, and assume that

$$\sigma_{\phi,turb} = const \qquad (5.5\text{-}2)$$

across the whole flow.

Eqn (5.5-1) may be rearranged as

$$\frac{\sigma_{\phi,eff}}{\sigma_\phi} = \frac{1 + \varepsilon_{turb}}{1 + \varepsilon_{turb}\,\frac{\sigma_\phi}{\sigma_{\phi,turb}}} \qquad (5.5\text{-}3)$$

where

$$\varepsilon_{turb} = \frac{\mu_{turb}}{\mu} \qquad (5.5\text{-}4)$$

5.6 Determination of the constants

In the earlier parts of chapter 5 we have enlisted various expressions for turbulent viscosity, turbulence energy and the length scales. Six unspecified constants have been used in these expressions, namely:

C_μ in eqn (5.3-3)

$\sigma_{k,turb}$ in eqn (5.3-4)

c_0 in eqn (5.3-8)

A_μ in eqn (5.4-5)

A_0 in eqn (5.4-6)

$\sigma_{\phi,turb}$ in eqn (5.5-1)

In the present section we shall see how these constants may be evaluated from experimental data.

We shall obtain all the constants from correlations of measurements in one-dimensional (Couette) flow, for two reasons. Firstly, the experimental data for such situations are by far more numerous and reliable than for almost any other type of flow; secondly, we may obtain analytical solutions for some cases of one-dimensional flow, as will be illustrated in the forecoming pages. Such analytical solutions considerably reduce the work involved in the fitting of the constants. These two reasons seem sufficient to justify the restriction of the present chapter to Couette flows only.

Empirical relations

The one-dimensional flows, for which we have appropriate correlations of experimental date, are:

(i) The logarithmic law of the wall for a constant-shear non-diffusional Couette flow, in which

$$\kappa \frac{u}{\sqrt{\tau_s/\rho}} = \ln\left(E \frac{y\sqrt{\tau_s \rho}}{\mu}\right) \qquad (5.6\text{-}1)$$

where κ and E are empirical constants (Schlichting, 1960)

(ii) The velocity distribution in the linear-shear Couette flow in which

$$u = \frac{2}{K_o}\sqrt{\frac{dp}{dx}\frac{y}{\rho}} + \text{const} \qquad (5.6\text{-}2)$$

where K_o is an empirical constant (Townsend, 1961).

(iii) The turbulent-viscosity law in the laminar-sublayer of a constant shear, non-diffusional Couette flow, in which

$$\frac{\mu_{turb}}{\mu} = a\left(\frac{y\sqrt{\tau_s \rho}}{\mu}\right)^{\alpha} \qquad (5.6\text{-}3)$$

where a and α are empirical constants (Spalding and Jayatillaka, 1964).

(iv) The empirical P-function, describing the resistance to heat transfer of a constant-shear non-diffusional Couette flow. (Spalding and Jayatillaka, 1964) It will be noted that the P-function is different from eqn (5.6-3) only when the Prandtl number is low.

The one-dimensional turbulence energy equation

In a steady, one-dimensional flow eqn (5.3-9) reduces to:

$$0 = \frac{d}{dy}\left(\Gamma_{k,eff}\frac{dk}{dy}\right) + \mu_{turb}\left(\frac{\tau}{\mu_{eff}}\right)^2 - C_D\frac{\rho k^{3/2}}{\ell_D} \qquad (5.6\text{-}4)$$

This equation has to be solved together with the viscosity hypothesis, eqn (5.3-3), and the length-scale hypothesis, eqns (5.4-5) and (5.4-6) or their asymptotic forms, eqn (5.4-9), (5.4-10) and (5.4-11).

The constant-shear, non-diffusional layer, for $y \to \infty$

When $y \to \infty$

$$\mu_{eff} \approx \mu_{turb} = C_\mu \rho k^{1/2} \ell_\mu >> \mu \qquad (5.6\text{-}5)$$

$$\Gamma_{k,eff} = \frac{\mu_{turb}}{\sigma_{k,turb}} \qquad (5.6\text{-}6)$$

$$\ell_\mu = \ell_D = y \qquad (5.4\text{-}9)$$

$$\tau = \tau_s \qquad (5.6\text{-}7)$$

Also, in a non-diffusional Couette flow

$$k = \text{const.} \qquad (5.6\text{-}8)$$

Under these conditions, eqn (5.6-4) reduces to:

$$\frac{\tau_s^2}{C_\mu \rho k^{1/2} y} = \frac{C_D \rho k^{3/2}}{y} \qquad (5.6\text{-}9)$$

and

$$k = \frac{\tau_s/\rho}{\sqrt{C_\mu C_D}} \qquad (5.6\text{-}10)$$

We may now integrate

$$\mu_{eff} \frac{du}{dy} = \tau_s \tag{5.6-11}$$

to get the velocity

$$\frac{C_\mu^{3/4}}{C_D^{1/4}} \frac{u}{\sqrt{\tau_s/\rho}} = \ln\left(E \frac{y\sqrt{\tau_s \rho}}{\mu}\right) \tag{5.6-12}$$

where E is an arbitrary integration constant.

The linear shear layer, for y→∞

Here, as in the previous case, eqn (5.6-5), (5.6-6) and (5.4-9) hold; but the shear stress is given by

$$\tau = p' y \tag{5.6-13}$$

where

$$p' = \frac{1}{\rho} \frac{dp}{dx} \tag{5.6-14}$$

In these conditions eqn (5.6-4) reduces to

$$\frac{d}{dy}\left(C_\mu \rho k^{1/2} \frac{dk}{dy}\right) + \frac{(p'y)^2}{C_\mu \rho k^{1/2} y} - \frac{C_D \rho k^{3/2}}{y} = 0 \tag{5.6-15}$$

Spalding (1967a) showed that the solution to eqn (5.6-15) is

$$k = \frac{p' y}{\sqrt{C_\mu \left(C_D - \frac{3 C_\mu}{2 b_{k,turb}}\right)}} \tag{5.6-16}$$

and the resulting velocity profile is

$$u = 2\sqrt{p'y} \frac{\left(C_D - \frac{3 C_\mu}{2 b_{k,turb}}\right)^{1/4}}{C_\mu^{3/4}} + const \tag{5.6-17}$$

The constant shear layer, $y \to 0$

In this case we get

$$\mu_{eff} \approx \mu >> \mu_{turb} \tag{5.6-18}$$

$$\Gamma_{k,eff} \approx \mu \tag{5.6-19}$$

$$\ell_\mu = A_\mu \frac{k^{1/2} y \rho}{\mu} y \tag{5.4-10}$$

$$\ell_0 = A_0 \frac{k^{1/2} y \rho}{\mu} y \tag{5.4-11}$$

$$\tau = \tau_s \tag{5.6-7}$$

and eqn (5.6-4) reduces to:

$$\frac{d}{dy}\left(\mu \frac{dk}{dy}\right) = \frac{C_D \rho k^{3/2} \mu}{A_0 k^{1/2} \rho y^2} \tag{5.6-20}$$

with the solution:

$$k = A' y^{B'} \tag{5.6-21}$$

where

$$B'(B'-1) = \frac{C_D}{A_D} \tag{5.6-22}$$

and A' is an arbitrary constant.* However, it will be easier for further use if we rearrange eqn (5.6-21) in a non-dimensional form

$$\frac{k \rho}{\tau_s} = A \left(\frac{y k^{1/2} \rho}{\mu}\right)^B \tag{5.6-23}$$

---

* The other integration constant is put zero, as k = 0 at y = 0.

Eqn (5.6-22) will now change to:

$$\frac{2B(3B-2)}{(2-B)^2} = \frac{C_D}{A_D} \qquad (5.6\text{-}24)$$

The turbulent viscosity may be computed through eqns (5.3-3) and (5.4-10) to get

$$\frac{\mu_{turb}}{\mu} = C_\mu A_\mu A^{\frac{2}{2-B}} \left(\frac{\sqrt{\tau_s \rho}\, y}{\mu}\right)^{\frac{4}{2-B}} \qquad (5.6\text{-}25)$$

Values of the constants

We have now obtained all the possible analytical solutions of eqn (5.6-4). Next we have to compare these solutions with the experimental evidence, listedain the beginning of the present section.

From eqn (5.6-1) and (5.6-12) we get

$$\kappa = \frac{C_\mu^{3/4}}{C_D^{1/4}} \qquad (5.6\text{-}26)$$

From eqns (5.6-3), (5.6-24) and (5.6-25) we get:

$$1.5(\alpha-2)(\alpha-3) = \frac{C_D}{A_D} \qquad (5.6\text{-}27)$$

And from eqn (5.6-2) and (5.6-17) we get

$$\frac{1}{K_0} = \frac{\left(C_D - \frac{3}{2}\frac{C_\mu}{\sigma_{k,turb}}\right)^{1/4}}{C_\mu^{3/4}} \qquad (5.6\text{-}28)$$

A simple rearrangement of eqns (5.6-26), (5.6-27) and (5.6-28) leads to:

$$\sigma_{k,turb} = \frac{1.5}{C_\mu^2\left(\frac{1}{\kappa^4} - \frac{1}{K_0^4}\right)} \qquad (5.6\text{-}29)$$

$$c_0 = \frac{c_\mu^3}{\kappa^4} \tag{5.6-30}$$

$$A_0 = \frac{c_0}{1.5(\alpha-2)(\alpha-3)} \tag{5.6-31}$$

We have thus managed to eliminate three of the unknown constants. Further, there is no reason to change $\sigma_{\phi,turb}$ from the value of 0.9 which was recommended by Spalding and Jayatillaka (1964), and supported by Patankar (1967). So we have to fit c_μ and A_μ only. These two constants were so chosen, as to give a good agreement with the $u_+(y_+)$ function and the $P(\sigma/\sigma_{turb})$ function for a constant-shear, non-diffusional Couette flow. The procedure is quite straightforward; it is as follows:

(i) c_μ and A_μ are tentatively prescribed.

(ii) Eqn (5.6-4) is numerically solved, for constant shear stress $\tau = \tau_s$, with the boundary conditions:

$$k = 0 \quad \text{at} \quad y = 0$$
$$k = k_G = \frac{\tau_s}{\rho\sqrt{c_0 c_\mu}} \quad \text{at } y = y_G \tag{5.6-32}$$

(iii) The turbulent viscosity is computed, by eqn (5.3-3).

(iv) The following necessary functions may now be computed numerically

$$y_+ = \frac{y\sqrt{\tau_s \rho}}{\mu} \tag{5.6-33}$$

$$u_+ = \frac{u}{\sqrt{\tau_s/\rho}} = \int_0^{y_+} \frac{\mu}{\mu_{eff}}\, dy_+ \tag{5.6-34}$$

$$\phi_+ = \frac{\phi\sqrt{\tau_s \rho}}{J_s} = \int_0^{y_+} \frac{\mu}{\frac{\mu}{\sigma} + \frac{\mu_{turb}}{\sigma_{turb}}}\, dy_+ \tag{5.6-35}$$

(5.6-36)

(v) All the previous steps should be repeated for different values of A_μ and c_μ until the computed $u_+(y_+)$ and $P(\sigma/\sigma_{turb})$ give a satisfactory agreement with empirical correlations.

It will be noted that until this very moment we have been discussing "empirical constants and correlations" without referring to any particular numerical values. Now the time has come to make numerical specifications. Some of the values which we shall use are fairly well established, others are not. So we can specify our constants (A_μ, c_μ etc.) only tentatively, pending accumulation of more experimental information. The values used in the present thesis are:

κ = 0.4 (recommended by Schlichting, 1960);

E = 9. (recommended by Schlichting, 1960);

K_o = 0.48 (recommended by Townsend, 1961);

α = 4 (resulting from Spalding and Jayatillaka's P-function for high Prandtl numbers, 1964);

and, of course, the P-function itself, and the turbulent Prandtl number $\sigma_{\phi,turb} = 0.9$.

The P-function was preferred to a $t_+(y_+)$ profile, because it is based on a large number of observations,

and for a very wide range of Prandtl numbers.

The resulting constants are:

$$\begin{aligned} A_\mu &= 0.016 \\ A_0 &= 0.263 \\ c_\mu &= 0.22 \\ c_0 &= 0.416 \\ \sigma_{k,turb} &= 1.53 \end{aligned} \qquad (5.6\text{-}37)$$

The resultant $u_+(y_+)$ and $P(\sigma/\sigma_{turb})$ functions are compared with Schlichting's and Spalding and Jayatillaka's functions in figures 5.6-1 and 5.6-2 respectively. The agreement is good. We must, however, note a difference between the present set of constants and those suggested by Spalding (1967c, p. 1.134). Spalding chose the constant value of the turbulence energy in a constant-shear non-diffusional Couette flow to be about $5\frac{\tau_s}{\rho}$. However, if we substitute the above constants in eqn (5.6-10) we get:

$$\frac{k\rho}{\tau_s} = \frac{1}{\sqrt{0.22 \times 0.416}} = 3.3 \qquad (5.6\text{-}38)$$

Some attempts were made to increase the value of $(c_0 c_\mu)^{-\frac{1}{2}}$ by suitable changes of c_0 and c_μ. These attempts always caused some deviation from either Spalding and Jayatillaka's P-function or Schlichting's $u_+(y_+)$ relation.

The experimental evidence currently available is not sufficient to establish the value of $\frac{k\rho}{\tau_s}$ in the constant-shear layer accurately.

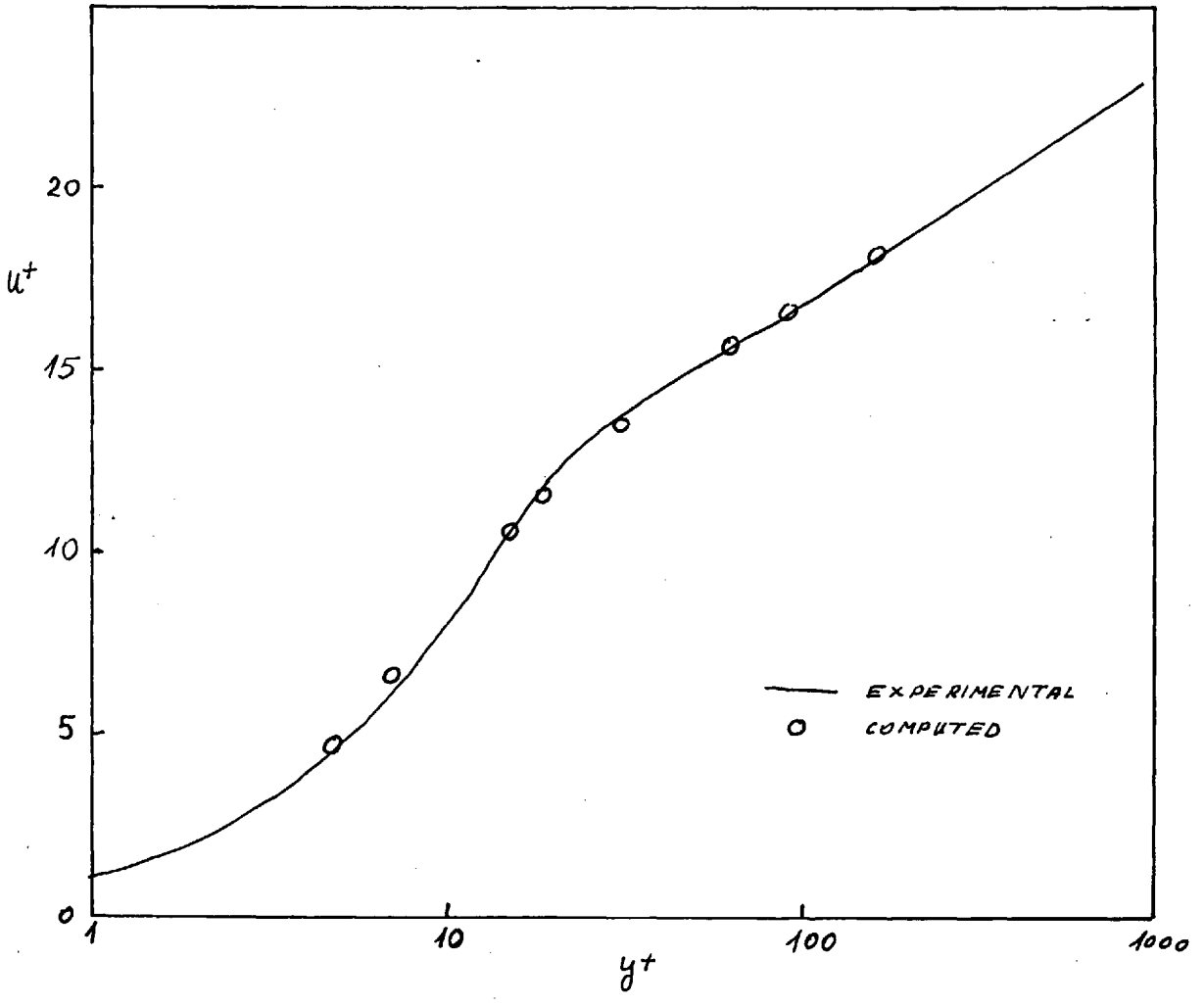

FIG 5.6-1: COMPUTED AND MEASURED VELOCITY PROFILE IN A CONSTANT-SHEAR NO-DIFFUSION COUETTE FLOW. DATA REPORTED BY SCHLICHTING (1960).

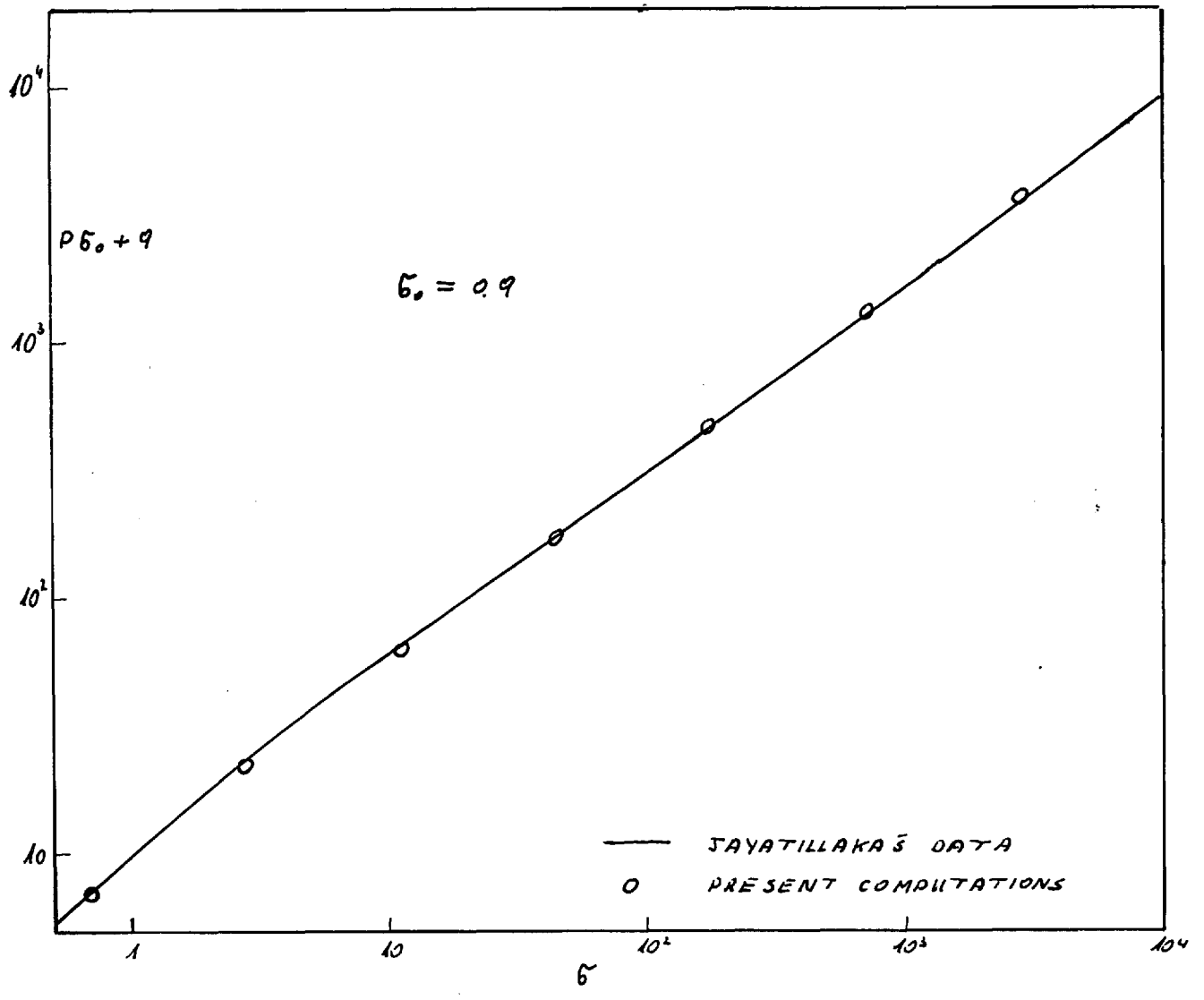

FIG 5.6-2 : COMPARISON OF THE P-FUNCTION IN A CONSTANT SHEAR NON-DIFFUSIONAL COUETTE FLOW WITH SPALDING AND JAYATILLAKA'S RECOMMENDATIONS (1964).

6. Wall functions

6.1 What wall functions are

We have been looking in chapter 5 into a particular model of turbulence, which appears to be powerful enough to satisfy our present needs. Apparently we may proceed straight ahead to the solution of the finite-difference equations. Unfortunately, we may get accurate solutions by our finite-difference method, only when the variation of all the quantities concerned between adjacent mesh points is nearly linear. Therefore in regions of high-gradients, as, say, a boundary-layer near a wall, we must specify a very fine mesh. Fine meshes are, in general, a legitmate part of the finite-difference method, but they tend to be very costly in computer time. This is the main reason which leads us to seek an alternative method to the finite-difference one in thin boundary-layers. Such a method should, in principle, yield some algebraic relations between quantities in the outer part of the boundary-layer and the wall fluxes, without integration of the equations governing the flow inside the boundary-layer. These relations are called wall functions.

The wall functions have already been employed, for very similar reasons, to boundary-layer work, by Patankar and Spalding (1967). Their work was, however, restricted to the Prandtl mixing-length hypothesis. Our present need

is for wall functions which will make use of the Kolmogorov-Prandtl hypothesis, and which will apply to cases of augmented turbulence.

We still have to face the fact that the wall functions must be simplified correlations of theoretical solutions; there is hardly a chance of getting a general exact solution of the boundary-layer equation in a simple algebraic form. Even when we agree to the use of correlations, we soon find that we may obtain them only for very simple boundary-layers; in fact the solutions used in the present paper (as well as in Patankar and Spalding's work) are for one-dimensional boundary-layers, or, as they are often called, Couette flows. This fact should not, however, deter us from the use of these wall functions. All boundary layers have some similarity to Couette flow, and the nearer to the wall that we are, the stronger this similarity is. Practice has shown that the region where the flow is one-dimensional is, in many cases, much thicker than that in which it is linear (in the laminar sublayer). So we have much to gain by the use of wall functions, even in their present simple form.

We shall restrict ourselves to flow on smooth surfaces, not having large rates of mass transfer. Pressure gradient effects will be only slightly described.

6.2 Definition of terms

In the present work we aim at highly turbulent flows, where the shear stress as well as the velocity may become vanishingly small. Therefore we have to define all our non-dimensional groups in such a way that no troubles will occur when they become excessively large or small. But, on the other hand, we wish to get groups which will make sense also in more normal situations. The most suitable groups, are then

$$R = \frac{k^{1/2} y \rho}{\mu} \qquad (5.4\text{-}2)$$

$$K = \frac{k \rho}{\tau_s} \qquad (6.2\text{-}1)$$

$$S = \frac{\tau_s y}{\mu u} \qquad (3.2\text{-}13)$$

$$S = \frac{\sigma J_s y}{\mu \phi} \qquad (3.2\text{-}18)$$

where y is the distance from the wall, and ϕ is the temperature (or conserved property) difference between the point in question and the wall.*

6.3 Solutions for particular cases

The usefulness of the above expression will be demonstrated by considering their values in some particular cases of flows without pressure-gradient:

---

* Interested readers should note that these definitions are different from those used by Spalding (1967c) in a similar treatment.

(i) When y = 0 (or in laminar flows)

$$R = K = 0 \tag{6.3-1}$$

$$s = S = 1 \tag{6.3-2}$$

(ii) In the constant shear, non-diffusional layer, when y becomes very large, we have, from eqn (5.6-10)

$$K = \frac{1}{\sqrt{C_\mu C_D}} \tag{6.3-3}$$

If we make use of eqn (6.3-3) we may now rearrange eqn (5.4-2) to get

$$R = \frac{y\sqrt{\tau_s \rho}}{\mu (C_\mu C_D)^{1/4}} = \frac{y_+}{(C_\mu C_D)^{1/4}} \tag{6.3-4}$$

Similarly, we may rearrange eqn (3.2-13) using eqns (6.3-4), (5.6-1) and (5.6-26). We get then

$$S = \frac{C_\mu R}{\ln(E C_\mu^{1/4} C_D^{1/4} R)} \tag{6.3-5}$$

and by the use of the equations for heat transfer in Couette flow, suggested by Spalding and Jayatillaka, we may rearrange eqn (3.2-18), to get

$$S = \frac{\sigma/\sigma_{turb}}{\frac{1}{S} + \frac{P}{R(C_\mu C_D)^{1/4}}} \tag{6.3-6}$$

(iii) In the zero shear layer, K will become infinite, but $\underline{R}$, $\underline{S}$ and $\underline{s}$ will remain finite. Spalding (1967a) has shown that in this case

$$k = a\, y^m \tag{6.3-7}$$

where

$$m = \sqrt{\frac{2 C_0 \sigma_{k,turb}}{3 C_\mu}} \tag{6.3-8}$$

The definitions (5.4-2) and (6.2-1) may now be used together with eqn (6.3-7), to yield

$$K \propto R^{\frac{2m}{2-m}} \tag{6.3-9}$$

In a vanishing-shear layer both τ_S and u are vanishingly small. Still, the limit of τ_S/u must then have a finite constant value. Therefore we may deduce from the definition of s, eqn (3.2-13), that

$$s \propto y \tag{6.3-10}$$

which by use of eqns (6.3-7) and (6.3-9), is the same as

$$s \propto R^{\frac{2}{2-m}} \tag{6.3-11}$$

For S we shall use the relation

$$\phi = \frac{\tau_s \sigma_k}{\tau_s} (U + p') \tag{6.3-12}$$

where

$$p' = \int_0^y \left(\frac{\sigma_{eff}}{\sigma_{turb}} - 1 \right) du = const \tag{6.3-13}$$

and this, when combined with the definitions (3.2-18) and (3.2-13) yields

$$S = \frac{s u}{U + p'} \propto s \tag{6.3-14}$$

When actual numbers are subsituted, we get:

$$\begin{aligned} m &= 1.39 \\ K &\propto R^{0.82} \\ s \propto S &\propto R^{0.59} \end{aligned} \tag{6.3-15}$$

6.4 Integration of the turbulence energy equation (uniform shear)

In section 6.3 we have obtained solutions of the turbulence energy equation for the following asymptotic cases of a uniform-shear Couette flow: (i) laminar flow; (ii) fully turbulent, non-diffusional flow; (iii) fully turbulent flow with a very large diffusion of turbulence energy from the outer edge of the layer (the no-shear layer). Now we have to fill in the gap left between these solutions by numerical integration of eqn (5.6-4). There is no need to describe the method of integration, which is essentially the same as that described in the end of section 5.6. The results are plotted in figures 6.4-1, 6.4-2 and 6.4-3 in the form of $k(R)$, $s(R)$ and $S(R)$ (for $\sigma = 0.7$) functions respectively. Similar $S(R)$ functions have to be computed for different values of σ. All these figures show two main characteristics:

(i) When the turbulence level inside the layer is augmented by diffusion of turbulence from the main stream, k, s and S satisfy eqns (6.3-9), (6.3-10) and (6.3-11) respectively, and thus behave in a fashion similar to the no-shear layer. The proportionality constants in the above equations are functions of the turbulence augmentation.

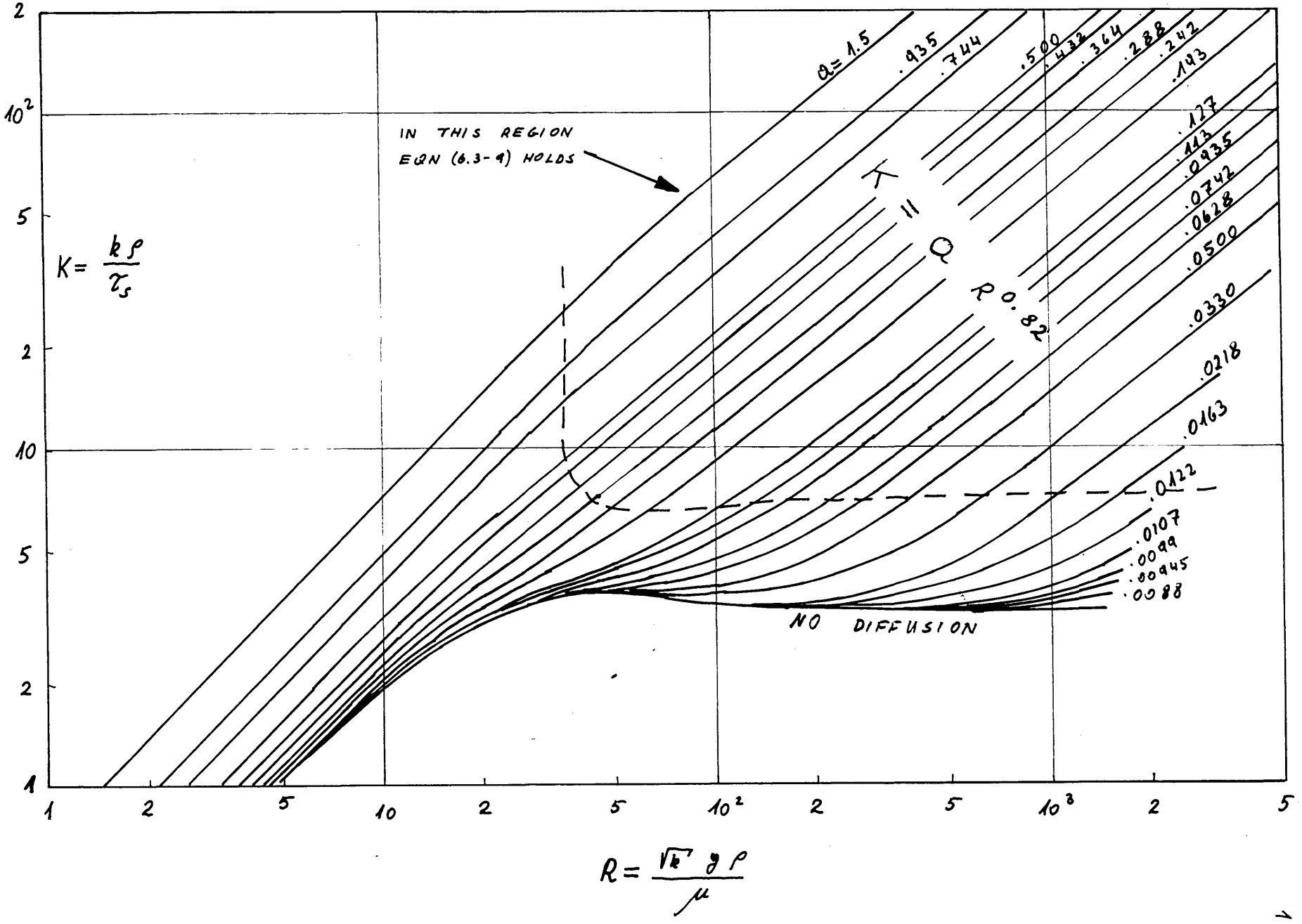

FIG 6.4-1: $K \sim R$ RELATION IN A CONSTANT SHEAR COUETTE FLOW.

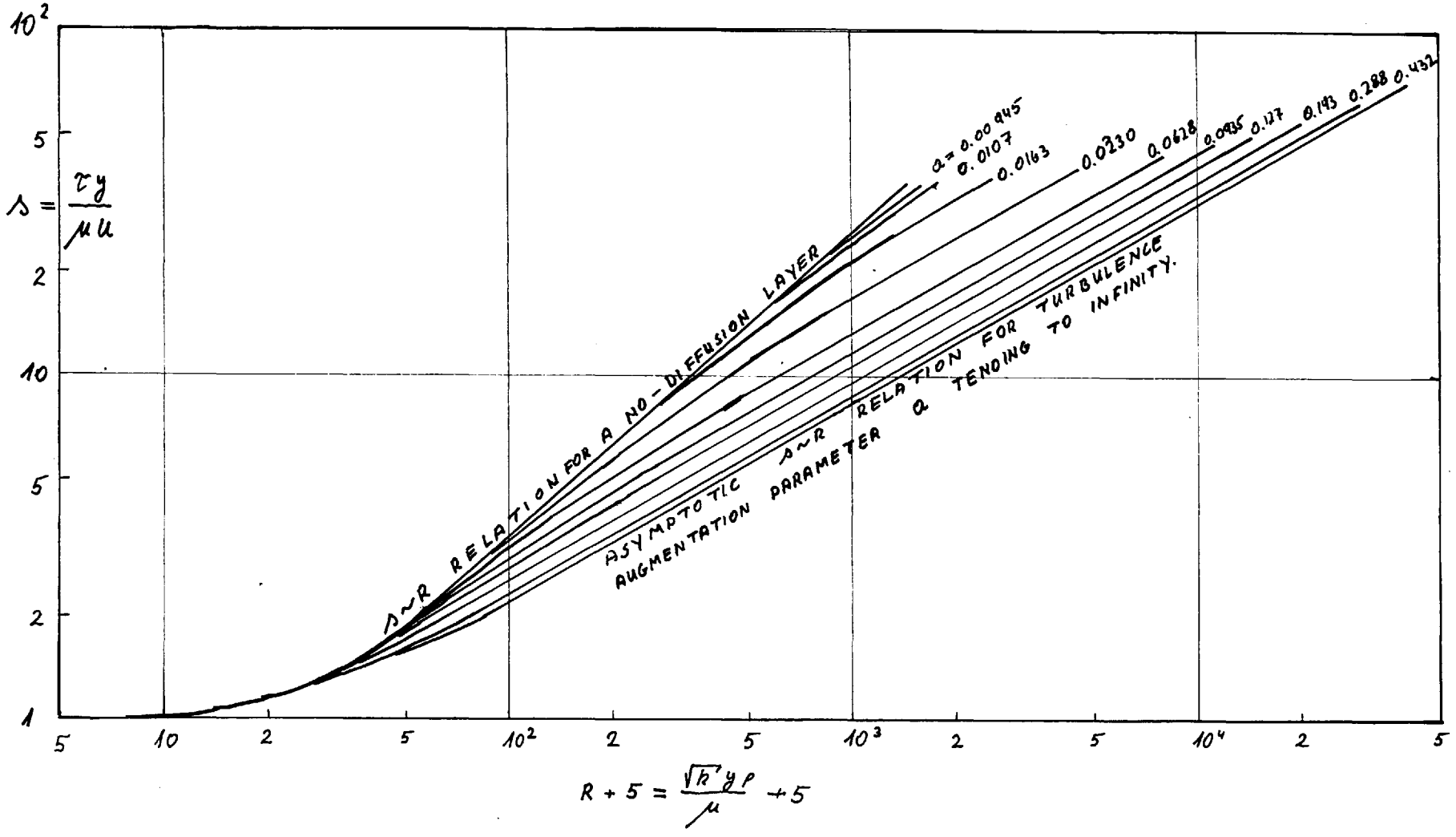

FIG 6.4-2: $\Lambda \sim R$ RELATION IN A CONSTANT-SHEAR COUETTE FLOW.

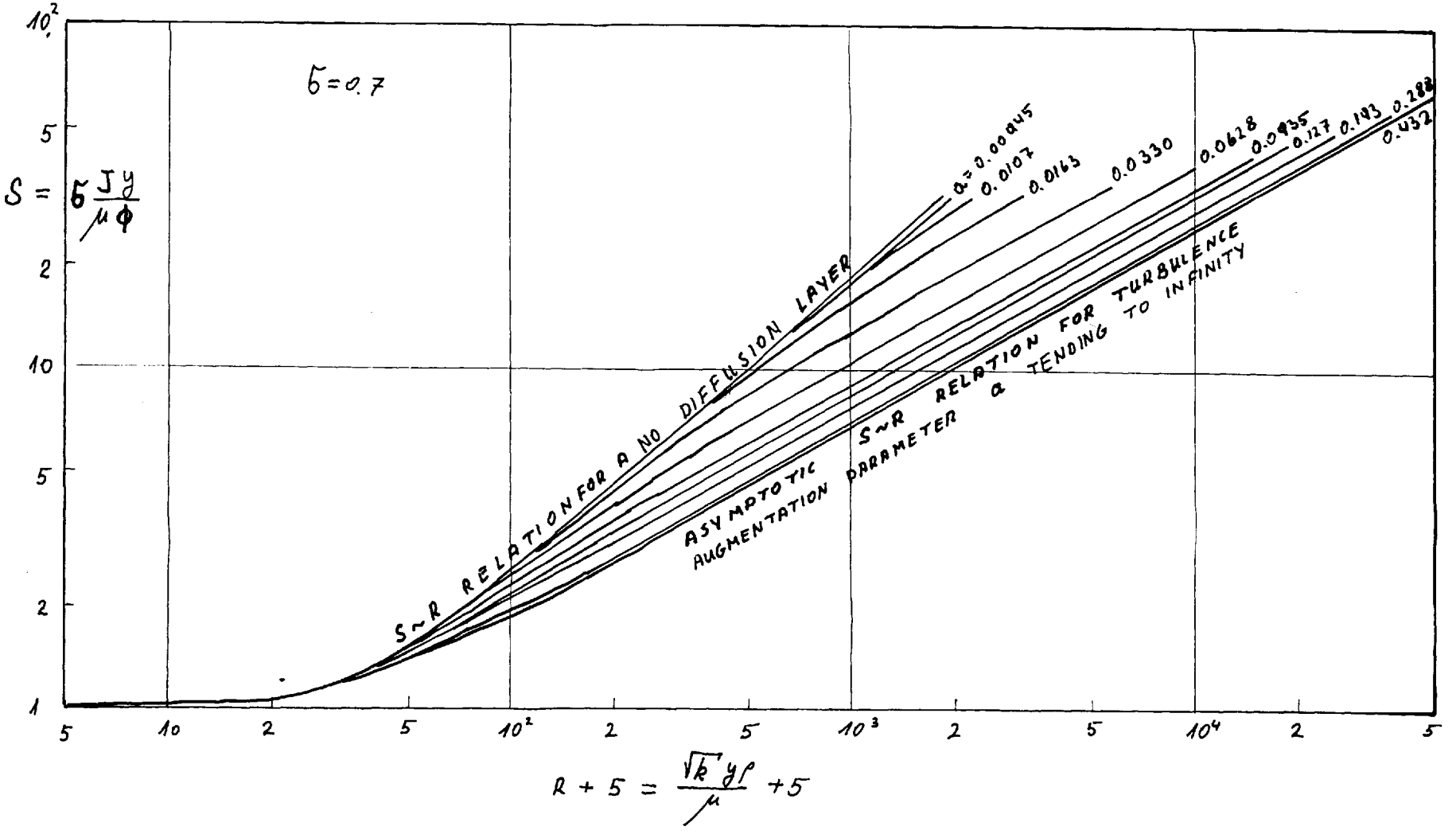

FIG 6.4-3 : S~R RELATION IN A CONSTANT-SHEAR COUETTE FLOW.

(ii) When R remains constant, s and S decrease if the turbulence energy is augmented, until they reach a minimum value. When the turbulence is further increased, s and S will not decrease any more.

In this situation, it seems natural to characterise the state of augmentation of the layer, by the proportionality constants in eqn (6.3-9) calculated as

$$a = \frac{K}{R^{\frac{2m}{2+m}}} \qquad (6.4\text{-}1)$$

in that part of the layer which behaves as a no-shear layer. The quantity a was used, in fact, as a parameter in figures 6.4-1, 6.4-2 and 6.4-3. The asymptotic solutions obtained analytically in section 6.3 are shown to be accurately obtained by the numerical integration as well, thus serving as a check on the accuracy.

6.5 The s(R,a) correlation

a/

We are now in a position to obtain our first wall function: the s(R,a) function. This may be done by fitting straight lines to fig 6.4-2. The resulting function is plotted in fig 6.5-1, and may be represented by the following formulae:

at $R \leq 19.8$: $S = 1$ (6.5-1)

at $R > 19.8$; $a = 0$: $S = 0.0565(R+5)^{0.895}$ (6.5-2)

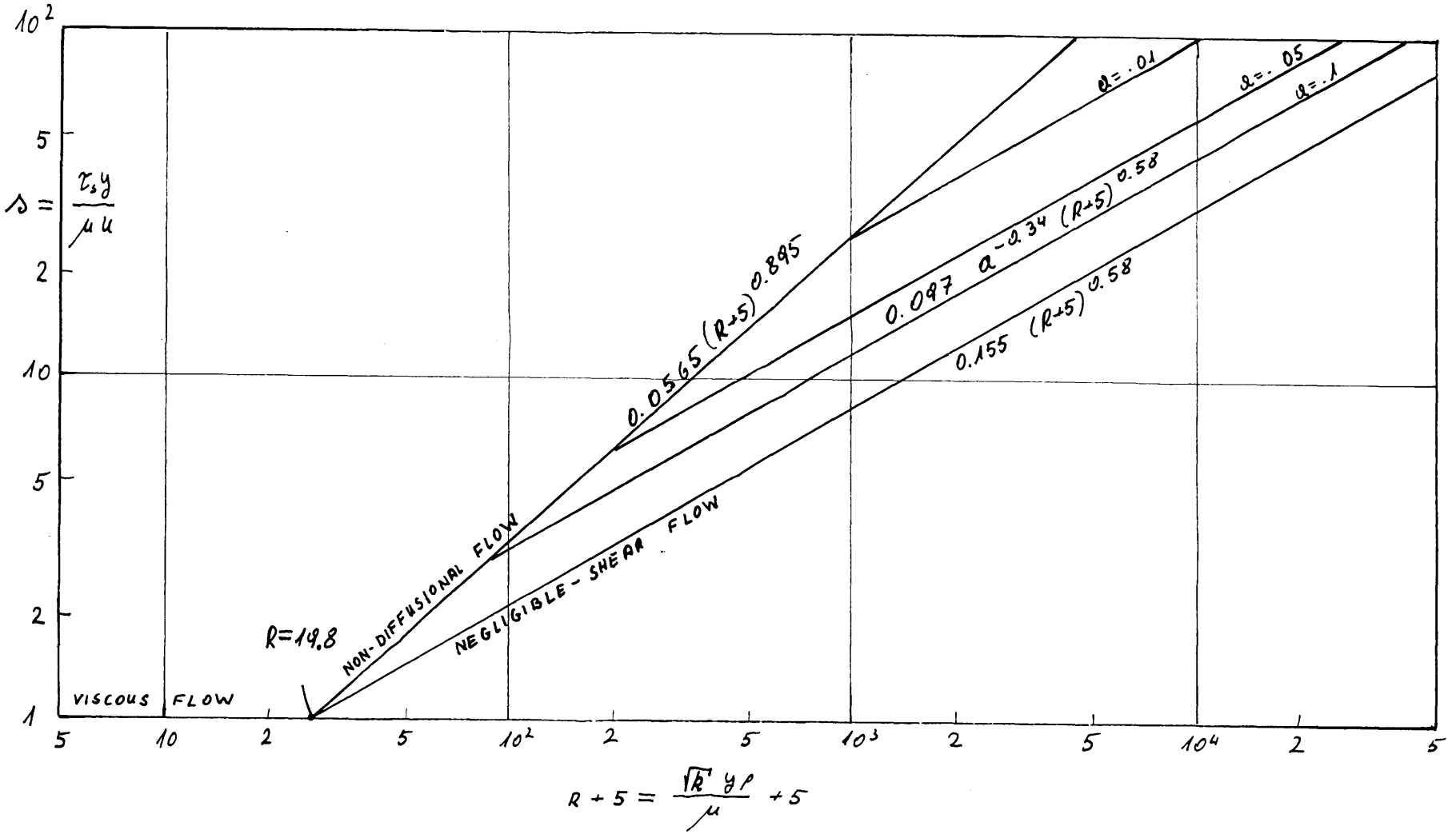

FIG 6.5-1: $S \sim R$ CORRELATION IN A CONSTANT-SHEAR COUETTE FLOW.

at $R > 19.8$; $0.252 > a > 0$: $S = 0.097\, a^{-0.34}(R+5)^{0.58}$ (6.5-3)

at $R > 19.8$; $a \geq 0.252$: $S = 0.155\,(R-5)^{0.58}$ (6.5-4)

a, the augmentation parameter, is required only when $R > 19.8$; and in these circumstances, we see in fig 6.4-1 that it is quite safe to compute it from:

$$a = \frac{k}{R^{0.82}} \tag{6.4-1}$$

6.6 The correlation for S

It is quite easy to obtain a correlation for S, in a very similar way to the one for s. Such a correlation is shown in fact in fig. 6.6-1, for $\sigma = 0.7$, and is summarised by the following relations:

at $R \leq 25$: $S = 1$ (6.6-1)

at $R > 25$; $a = 0$: $S = 0.0475\,(R+5)^{0.895}$ (6.6-2)

at $R > 25$; $0.278 > a > 0$; $S = 0.09\, a^{-0.34}\,(R+5)^{0.58}$ (6.6-3)

at $R > 25$; $a \geq 0.278$: $S = 0.139\,(R+5)^{0.58}$ (6.6-4)

This correlation is valid, however, only for one particular Prandtl number. We shall therefore try to obtain a more general one. Spalding (1967c) has integrated the turbulence energy equation for a Couette flow. He used a discontinuous length scale distribution, and therefore

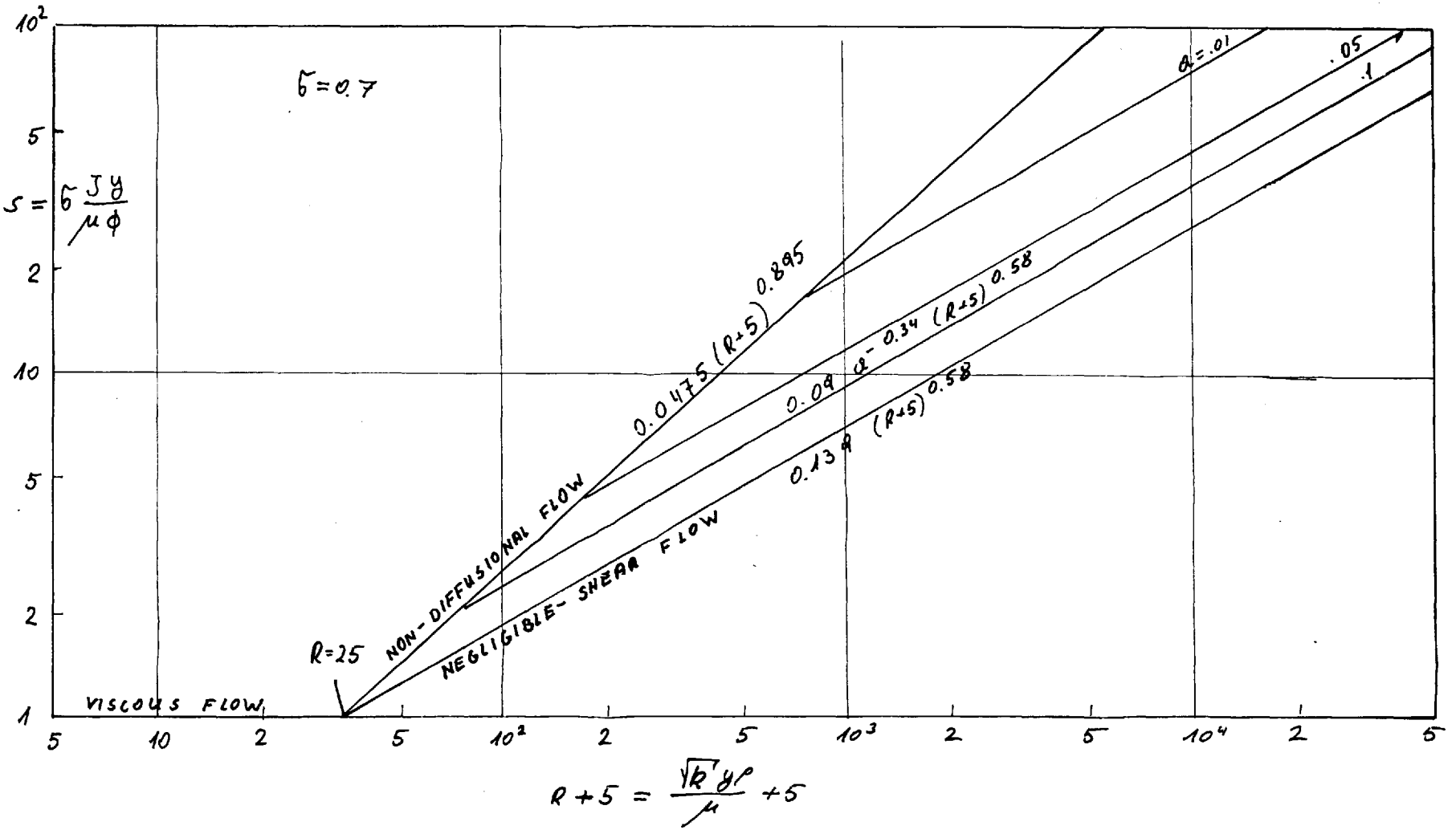

FIG 6.6-1 : A POSSIBLE S~R CORRELATION FOR A CONSTANT-SHEAR COUETT FLOW AND $\sigma = 0.7$.

was able to get approximate analytical solutions to a large number of problems. We shall now try to deduce from his solutions the general shape of an S(s,K,σ) function. If we substitute the present notation in Spalding's formulae, we get, for the constant-shear layer,

$$\frac{1}{s} - \frac{\sigma}{\sigma_{turb} S} = -R^{\alpha} g\left(\frac{\sigma}{\sigma_{turb}}\right) \qquad (6.6\text{-}5)$$

where $\alpha = -1$ in a non-diffusional layer, and $\alpha = -2/(m+2)$ in a no-shear layer (m is defined in equation (6.3-8). Spalding also investigated cases where $-1 < \alpha < -2/(m+2)$ but as these cases are excluded from the present correlation they need not be considered here. Now, it is clear that $g(\sigma/\sigma_{turb})$ should have some connection to the P-function recommended by Spalding and Jayatillaka (1964). Let us assume a linear relation between the two functions

$$g = c \cdot P \qquad (6.6\text{-}6)$$

where c is a constant (or rather a function of the augmentation parameter, a). The best values for c may be shown to be:

$$\begin{aligned} c &= 1.8 \quad \text{for a non-diffusional layer} \\ c &= 0.45 \quad \text{for a no-shear layer} \end{aligned} \qquad (6.6\text{-}7)$$

and so, from eqn (6.6-5)

$$\frac{1}{S} = \frac{\sigma_{turb}}{\sigma s} + \frac{\sigma_{turb}}{\sigma} c R^{\alpha} P \qquad (6.6\text{-}8)$$

where

$$\begin{aligned} \alpha &= -1 \quad \text{for a non-diffusional layer} \\ \alpha &= -0.59 \quad \text{for a no-shear layer} \end{aligned}$$

and

$$P = 9.24\left[\left(\frac{\delta}{\delta_{turb}}\right)^{0.75} - 1\right]\left[1 + 0.28\exp(-0.07\frac{\delta}{\delta_{turb}})\right] \qquad (6.6\text{-}9)$$

as recommended by Spalding and Jayatillaka.

We note that in the present correlations, the fluid should be in either a non-diffusional or a no-shear state; therefore two values only for α and c are sufficient.

There is still one point to note: when y is very small, eqn (6.6-8) may be misleading, because the P-function is meaningful only for points far away from the wall. We must, in such cases, make sure that S never drops below unity, the value which is appropriate to a laminar flow.

6.7 The pressure-gradient influence

We have hitherto neglected the pressure-gradient influence on s. Theoretically, a correction must be applied. Spalding (1967c) obtained an approximate expression for this correction. His expression may be rearranged as

$$\frac{s}{s_o} = 1 - \frac{F}{R} f\{R, K\} \qquad (6.7\text{-}1)$$

where s_o is the value of s corresponding to the same R and K, but with the pressure-gradient neglected, and

$$F = \frac{\frac{dp}{dx}\, y^2}{\mu\, u} \qquad (3.2\text{-}14)$$

To obtain f we must solve the equation

$$\mu_{eff}\frac{du}{dy} = \tau_s + p' y \qquad (6.7\text{-}2)$$

and it may be easily shown that

$$f = \frac{k^{1/2}\rho}{y}\int_0^y \frac{\eta\, dn}{\mu_{eff}} = \frac{K}{R}\int_0^R \frac{R'\, d\left(\frac{R'}{k^{1/2}}\right)}{k^{1/2}\left(1+c_\mu R\frac{l}{y}\right)} \qquad (6.7\text{-}3)$$

There is no particular difficulty in computing f when the μ_{eff} distribution is known. We shall however adopt a slightly different approach. First, we note that in a laminar flow

$$f = \frac{R}{2} \qquad (6.7\text{-}4)$$

Also for very large R,

$$\mu_{eff} = c_\mu \rho k^{1/2} y \qquad (6.7\text{-}5)$$

and

$$K = a R^{\alpha} \qquad (6.7\text{-}6)$$

and then we may get by integration of eqn (6.7-3)

$$f = \frac{2-\alpha}{c_\mu(2-2\alpha)} + const \qquad (6.7\text{-}7)$$

so that for a large R, f is not dependent on R.

On the basis of the above considerations and some numerical computations, an $f \sim R$ relation was complied, as shown in figure 6.7-1. In this figure, a of equation (6.4-1) is the parameter. The correlation may be summarised by

$$at \quad R \geq 20\, a^{\sigma} : \quad f = 0\, a^{\sigma} \qquad (6.7\text{-}8)$$

$$at \quad R < 20\, a^{\sigma} : \quad f = \frac{R}{2} \qquad (6.7\text{-}9)$$

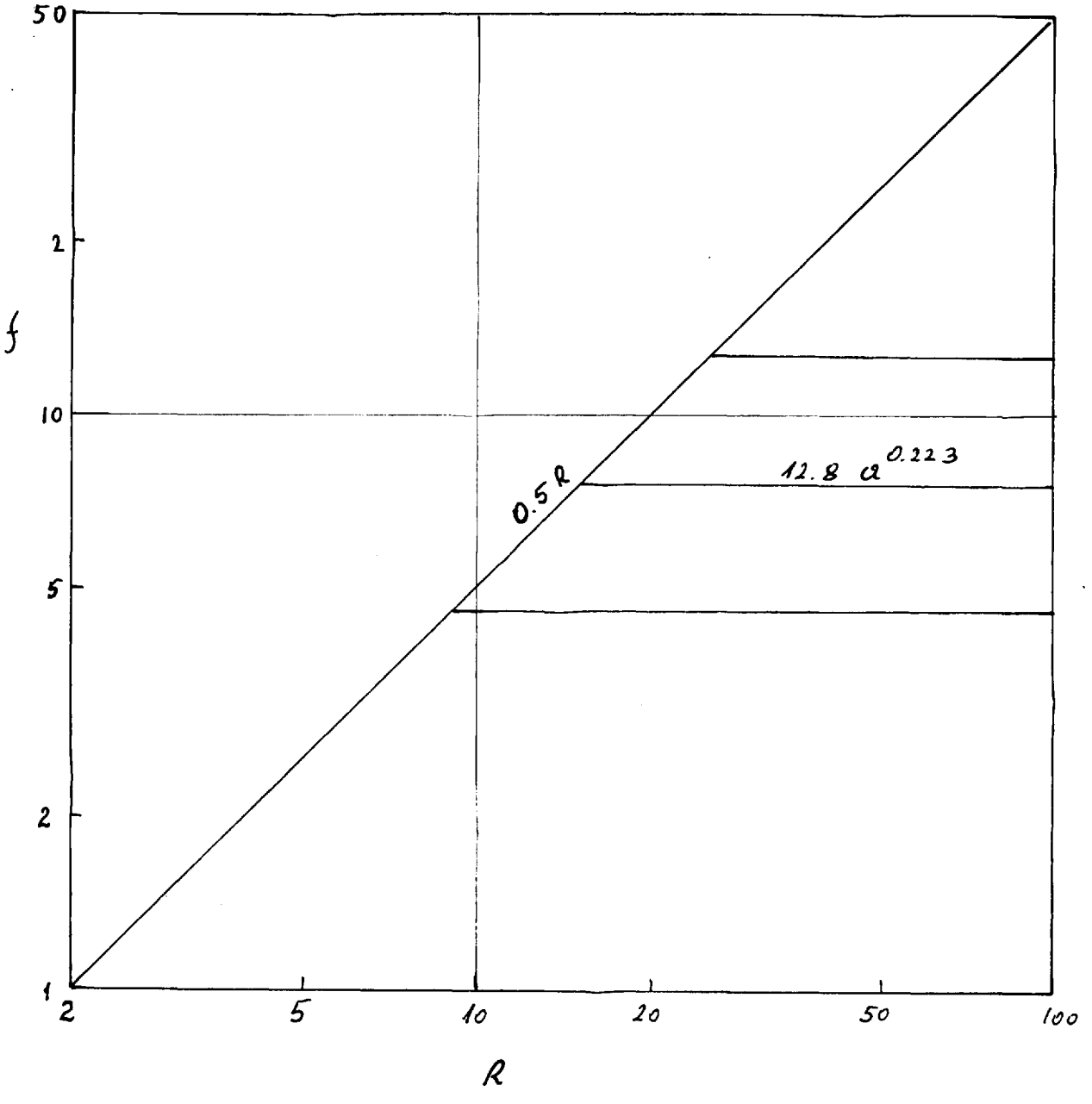

FIG 6.7-1 : THE $f \sim R$ CORRELATION.

where

$$D = 12.8$$
$$\delta = 0.223 \qquad (6.7\text{-}10)$$

We shall now examine when s may become considerably different from s_o. In the laminar sublayer we may transform eqn (6.7-9) to

$$\frac{\Lambda}{\Lambda_o} = 1 - \frac{F}{2} \qquad (6.7\text{-}11)$$

so that if F is not larger than say 0.1 the correction will be smaller than 5%. There is very little likelihood of F to be larger than 0.1 inside the thin laminar sublayer.

In the turbulent case it is more difficult to define the pressure-gradient influence. But we may note that only for large F and small R is the pressure-gradient influence going to be considerable. It was due to these reasons that the above corrections were not applied to the impinging jet computations, which will be reported in chapter 7. If, however, the pressure-gradient influence has to be accounted for, the following correlation is found to give good results for small and medium pressure gradient:

$$\frac{\Lambda}{\Lambda_o} = 1 - \frac{F - .072}{R + 40} f \qquad (6.7\text{-}4)$$

The correlation is compared with the exact solution in fig 6.7-2, for values of p' varying between -0.5 and +100.

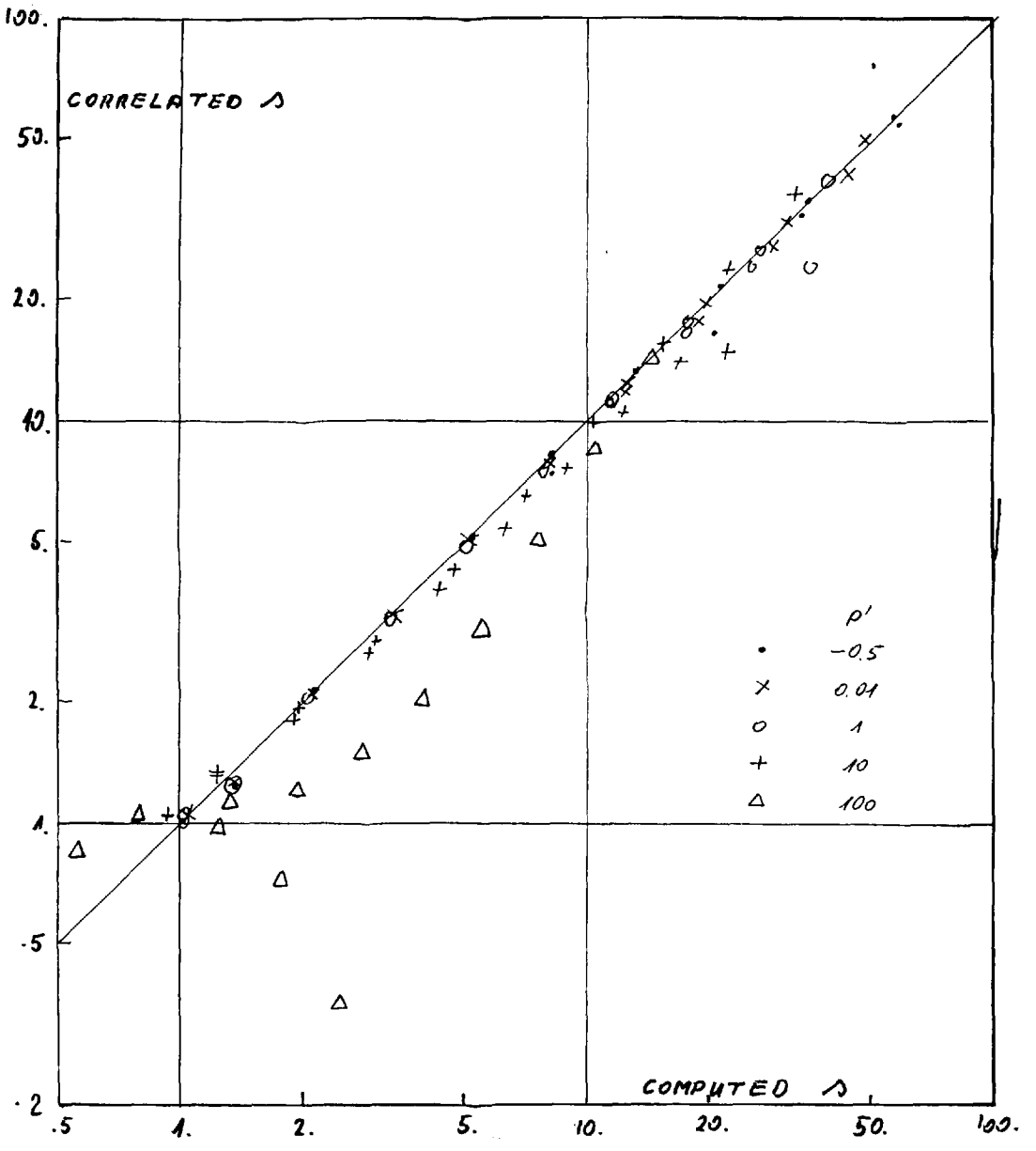

FIG 6.7-2 : COMPARISON OF COMPUTED AND CORRELATED Λ - VALUES FOR COUETTE FLOW WITH PRESSURE GRADIENT.

No serious disagreement between the computed and correlated s values is present for $p' < 100$.

7. Studies of the turbulent impinging jet

Until now, we have been concerned with generalities. First, in part II, a method was devised to solve the general equations. Later in chapter 5, a turbulent viscosity hypothesis was developed, and, in chapter 6, a special procedure for the treatment of the boundary conditions near walls was devised. Now the time has come to obtain solutions for the impinging jet problem. In studying such solutions our purpose is two-fold. First we wish to present a theory which can agree with as much as possible of our existing experimental knowledge, and which enables predictions to be made. Secondly, we have to explore the limitations of the theory, and its failures to agree with measurements. Knowledge of such failures is essential when we plan our future research.

In view of the above discussion the present chapter will be constructed as follows. First in section 7.1 the turbulent impinging jet problem will be mathematically presented. Then in section 7.2 we shall study the gross features of the flow, such as contours of properties, and pressure and velocity profiles. In section 7.3 we shall look at the wall fluxes in detail. It is in this section, that some failures of the computational scheme will be displayed, and their possible cause suggested. The whole chapter will be summarised and discussed, then,

in section 7.4. However, final recommendations on further research will be deferred until part IV.

7.1 Description of the impinging jet system

The plane impinging jet is shown in fig 7.1-1. The turbulent viscosity is computed by the equations described in chapter 5 from the turbulence energy. The boundary conditions are very much the same as those described in section 4.1. Wall functions are used to evaluate the skin friction and wall heat flux. Details of the wall boundary conditions are given in section 3.2. We still have, however, to consider the boundary conditions at the entrance of the free-jet to the control volume in the "F" state (see fig 7.1-1). We shall assume that the nozzle-to-plate distance h_c is larger than the length of the potential core of the free jet. We shall use the relations recommended by Schauer and Eustis (1963)

$$\frac{U_{max,F}}{U_c} = \frac{2.35}{\sqrt{y_F/d_c}} \qquad (7.1\text{-}1)$$

$$\frac{x_G}{y_F} = 0.11 \qquad (7.1\text{-}2)$$

where y_F is the distance from the nozzle to the near boundary of the control volume.

The stream function and vorticity in the "F" state (see fig 7.1-1) are given, as in section 4.1, by

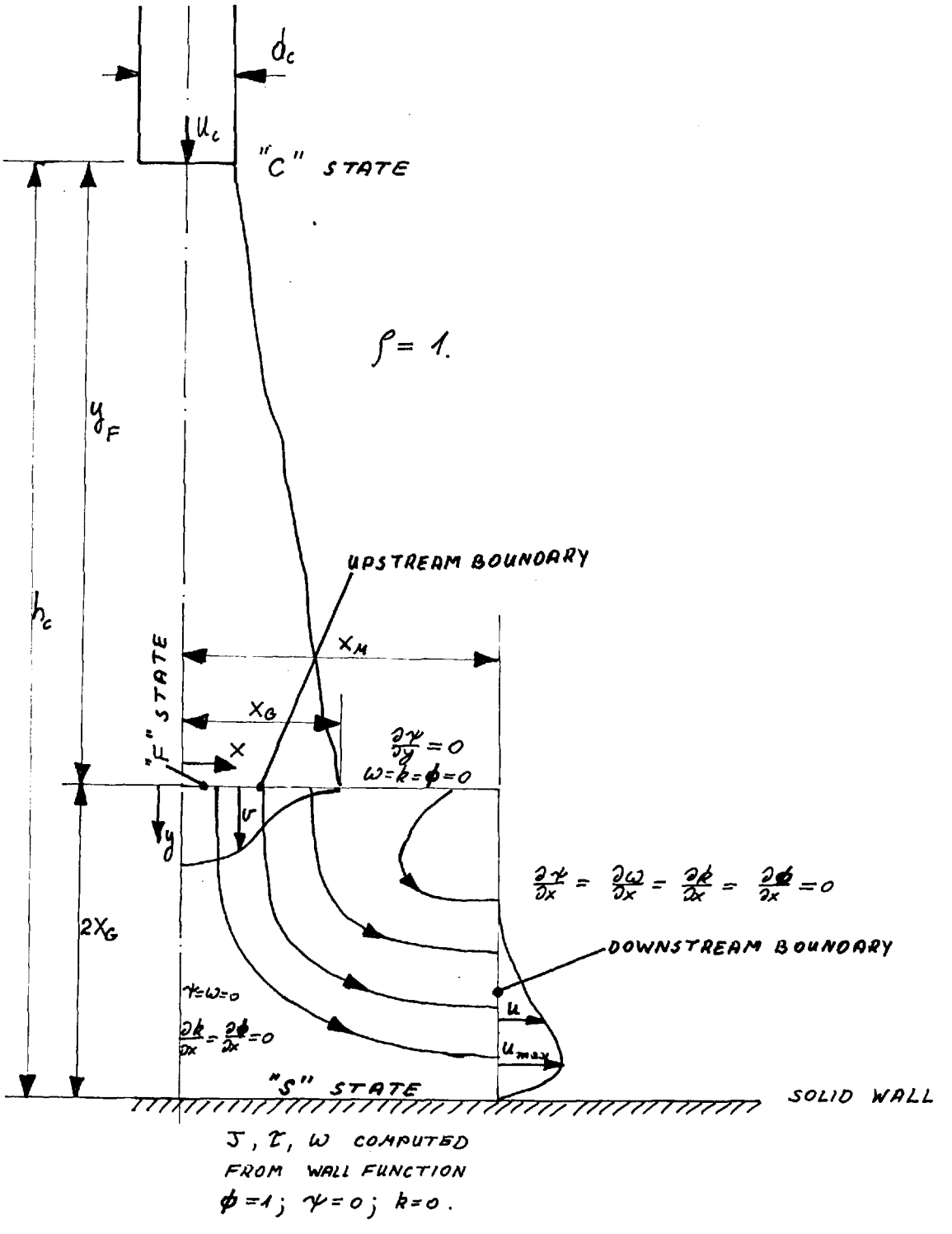

FIG 7.1-1: THE TURBULENT IMPINGING JET

$$\omega_F = 3 \frac{U_{max,F}}{x_G} \left[\left(\frac{x}{x_G}\right)^2 - \left(\frac{x}{x_G}\right)^{1/2} \right] \qquad (7.1\text{-}3)$$

and

$$\psi_F = U_{max,F}\, x_G \left[\frac{x}{x_G} - \frac{4}{5} \left(\frac{x}{x_5}\right)^{5/2} + \frac{1}{4} \left(\frac{x}{x_G}\right)^4 \right] \qquad (7.1\text{-}4)$$

We also deduce from Heskested's measurements (1956) that

$$k_F \approx 0.04 \left(U_{max,F}\right)^2 \qquad (7.1\text{-}5)$$

The meshes used will be non-uniform ones. The non-uniformity will be specified, in the x direction, by requiring that

$$\mathcal{E}_x = \frac{x_{i+1} - x_i}{x_i - x_{i-1}} \qquad (7.1\text{-}6)$$

and in the y direction

$$\mathcal{E}_y = \frac{y_j - y_{j-1}}{y_{j-1} - y_j} \qquad (4.3\text{-}1)$$

where both ε_x and ε_y will be taken as constants, greater than unity. Therefore the mesh is finer near the jet axis and near the wall.

The turbulent length scale will be taken as

$$\ell = 0.2\, x_6 \qquad (7.1\text{-}7)$$

everywhere; but near the wall equations (5.4-5) and (5.4-6) will be used, whenever they yield a smaller length scale than the one computed by eqn (7.1-7).

7.2 General description of the impinging jet flow

In this section we are concerned with the gross features of the flow. It will be shown that the general pattern of the flow is obtained in a satisfactory way; on the other hand, we shall not concern ourselves in this section with the boundary-layer near the wall, or the fluxes of momentum and energy from the wall. Thus we shall study contours of various quantities, as well as profiles of some of them.

7.2.1 Contours

We first look on contours of the main variables: the vorticity, stream function, turbulence energy, temperature, dynamic pressure, and static pressure. They are presented in figures 7.2-1 a - f, for the case of

$$\frac{h_c}{d_c} = 8$$

$$Re_c = \frac{U_c d_c \rho}{\mu} = 11\,000 \qquad (7.2\text{-}1)$$

$$\sigma = 0.71$$

and a normal level of turbulence in the free jet, as given by eqn (7.1-5). The mesh is a 14x16 one, with the non-uniformity parameter $\varepsilon_y = 1.3$.

Some conclusions may be drawn from these contours, as follows:

(i) A thin boundary-layer appears near the wall,

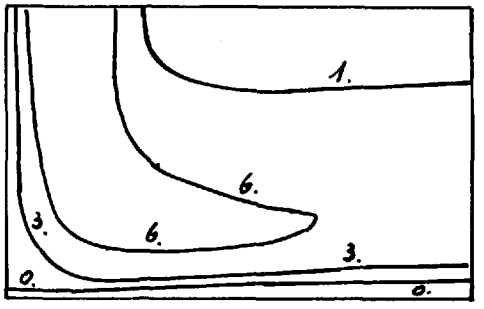

a: VORTICITY

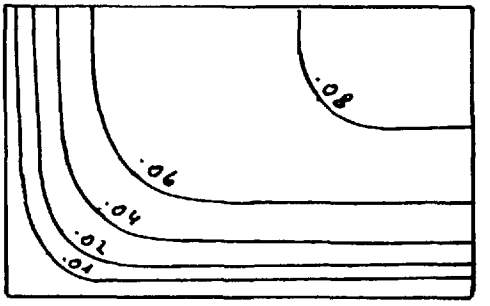

b: STREAM FUNCTION

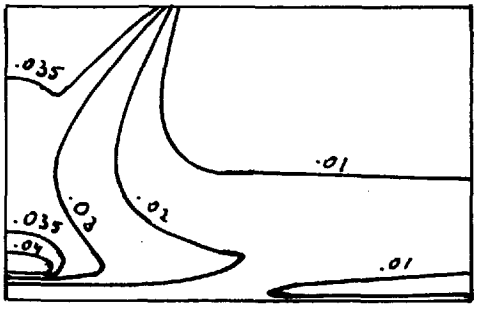

c: TURBULENCE ENERGY

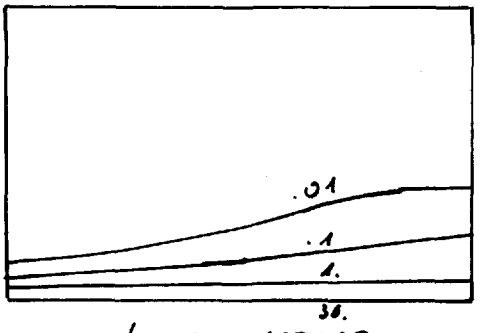

d: TEMPERATURE

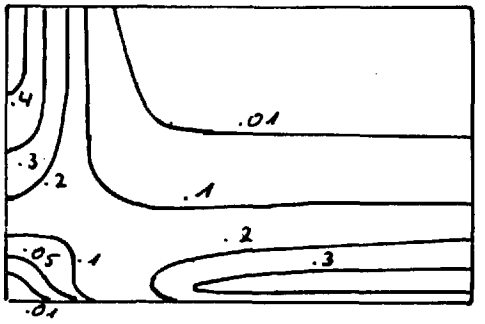

e: DYNAMIC PRESSURE

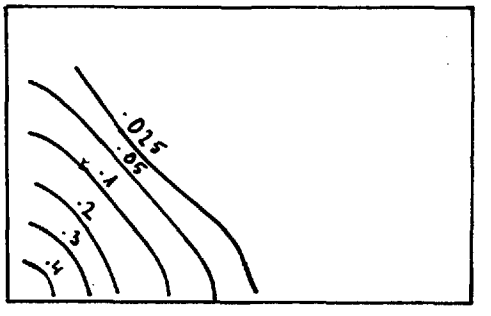

f: STATIC PRESSURE

FIG 7.2-1: CONTOUR PLOTS OF A TURBULENT IMPINGING JET ; $h_n/d_c = 8$; $Re_c = 11\,000$; $\bar{b} = 0.7$.

where the stream lines are nearly parallel to the wall, and the vorticity and turbulence become very large. The pressure drop across the boundary-layer is negligible.

(ii) Although a uniform turbulence energy distribution was prescribed in the free jet, on the boundary of the control volume, a maximum of the turbulence energy appears in the jet inside the field. This maximum is located about half-way between the centre and the outer edge of the jet. From this maximum k drops only slightly towards the centre, but very considerably towards the outer edge. However, when the solid surface is approached the k-maximum is shifted to the centre of the jet.

(iii) The boundary condition on the downstream side of the jet flow, specifies that there are no gradients parallel to the wall. This does not seem to distort the results appreciably.

Confirmation of the results

No detailed measurements of these contours in plane impinging jets are currently available. But contours of stream function, and static and dynamic pressure measured by Poland (1967) in axially-symmetrical impinging jets are very similar in shape to those displayed in figure 7.2-1, b, e, f.

7.2.2 Velocity and pressure profiles

We were not able to confirm the computed contours, as no experimental evidence was available. We can, however, confirm some velocity and pressure profiles by comparing them with Schauer and Eustis's measurements (1963). The system under consideration is the same as the one presented in section 7.1, but we now choose

$$h_c/d_c = 40 \qquad Re_c = 43000 \tag{7.2-2}$$

in order to agree with Schauer and Eustis's experimental set up. The mesh is a 14x12 one, non-uniformly spaced, with $\varepsilon_y = 1.5$.

The maximum velocity growth

First we consider the growth of the maximum velocity parallel to the wall. In fig 7.2-2 measured values designated by (x) are compared with the computed values designated by (o). The computed values have the right shape, but they are consistently lower than the measured ones. To find the reasons for this two other runs were made: In the first run, designated by (+) the wall was considered as a slip-boundary (physically this is similar to the impingement of two jets on one another). The results of this run were still lower than the measured ones. Then, in the second run, designated (Δ), laminar flow with a

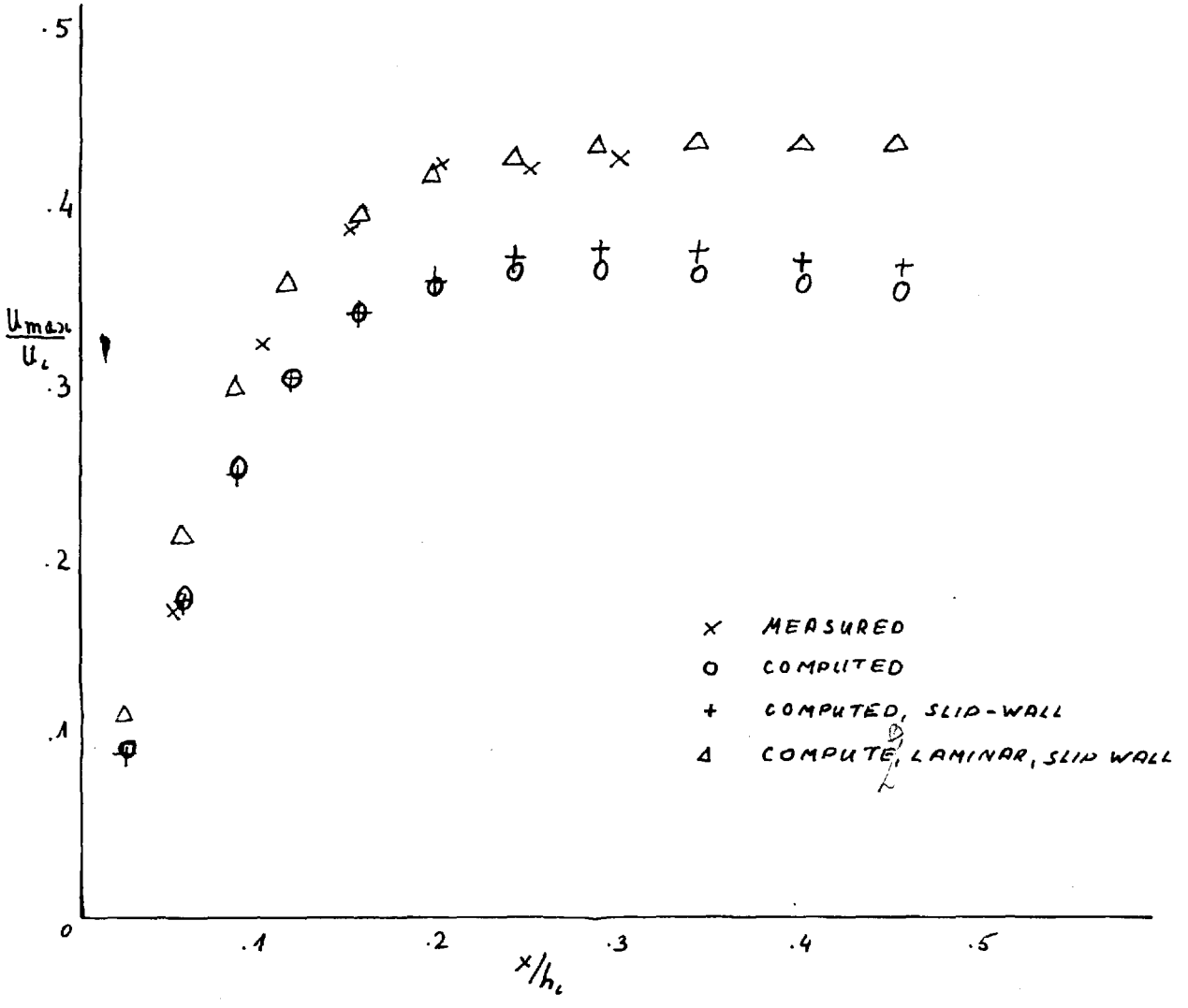

FIG 7.2-2 : MAXIMUM VELOCITY GROWTH IN THE IMPINGEMENT REGION. $Re_e = 43\,000$. $h_e/d_e = 40$. DATA OF SCHAUER AND EUSTIS.

slip-wall was considered. This improved the agreement with the experimental results very considerably. Thus these tests suggest that the turbulent viscosity hypothesis is the source of the discrepancy between the measured and computed maximum velocities. We cannot, however, definitely attribute the whole discrepancy between the measured and computed velocities to the viscosity hypothesis. Schauer and Eustis did not report the velocities in the free jet. Thus the use of wrong values of the velocity and stream-function in the free jet entering the control volume may be the cause for the low maximum velocity.

The wall static pressure

The static pressure distribution on the wall was measured by Schauer and Eustis, whose results are compared with the computed ones in fig 7.2-3. The agreement may be considered acceptable, in view of the discussion of possible reasons for disagreement between experiment and theory, in section 7.2.2.

The axis-velocity decay

This quantity has not been measured by Schauer and Eustis. However, we may expect that it is not very different from the exact solution for a stagnation flow (Schlichting, 1960). Thus we anticipate that the axis

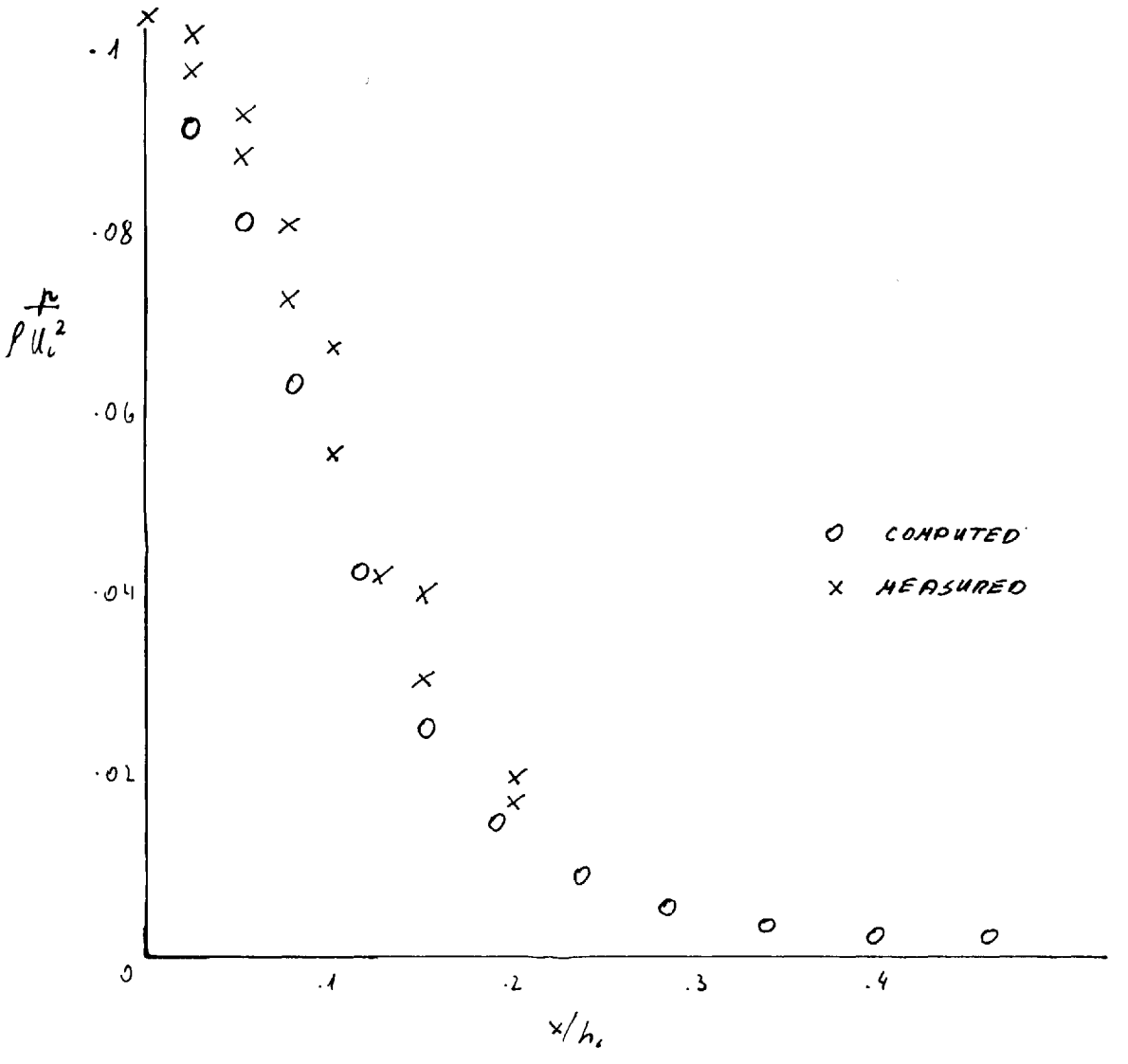

FIG 7.2-3 : THE STATIC PRESSURE DISTRIBUTION ON THE WALL. $Re_i \cong 43\,000$. $h_i/d_i = 40$. DATA OF SCHAUER AND EUSTIS (1963).

velocity, away from the wall, will obey

$$v = A\,y \qquad (7.2\text{-}3)$$

where A is a constant and y is the distance from the wall. Very near to the wall, the laminar stagnation flow solution reduces to

$$v = B\,y^2 \qquad (7.2\text{-}4)$$

where B is a constant.

The computed results are plotted in fig 7.2-4. The linear $v \sim y$ relation is very evident. The quadratic relation is not as clear, almost certainly because the mesh employed was not sufficiently fine near the wall.

The wall-jet velocity profile

The profile of the velocity component parallel to the wall on the downstream boundary is shown in fig 7.2-5. No velocity profiles normal to the wall have been reported as near to the impingement point as to enable a direct comparison with the present computation. Still, the computed velocity profile looks very feasible.

7.2.3 The turbulence energy on the jet axis

The present section, in contrast to 7.2.1 and 7.2.2, is not concerned with comparison with experiments. Indeed, the main object of this section is to make a preliminary exploration of the development of turbulence in

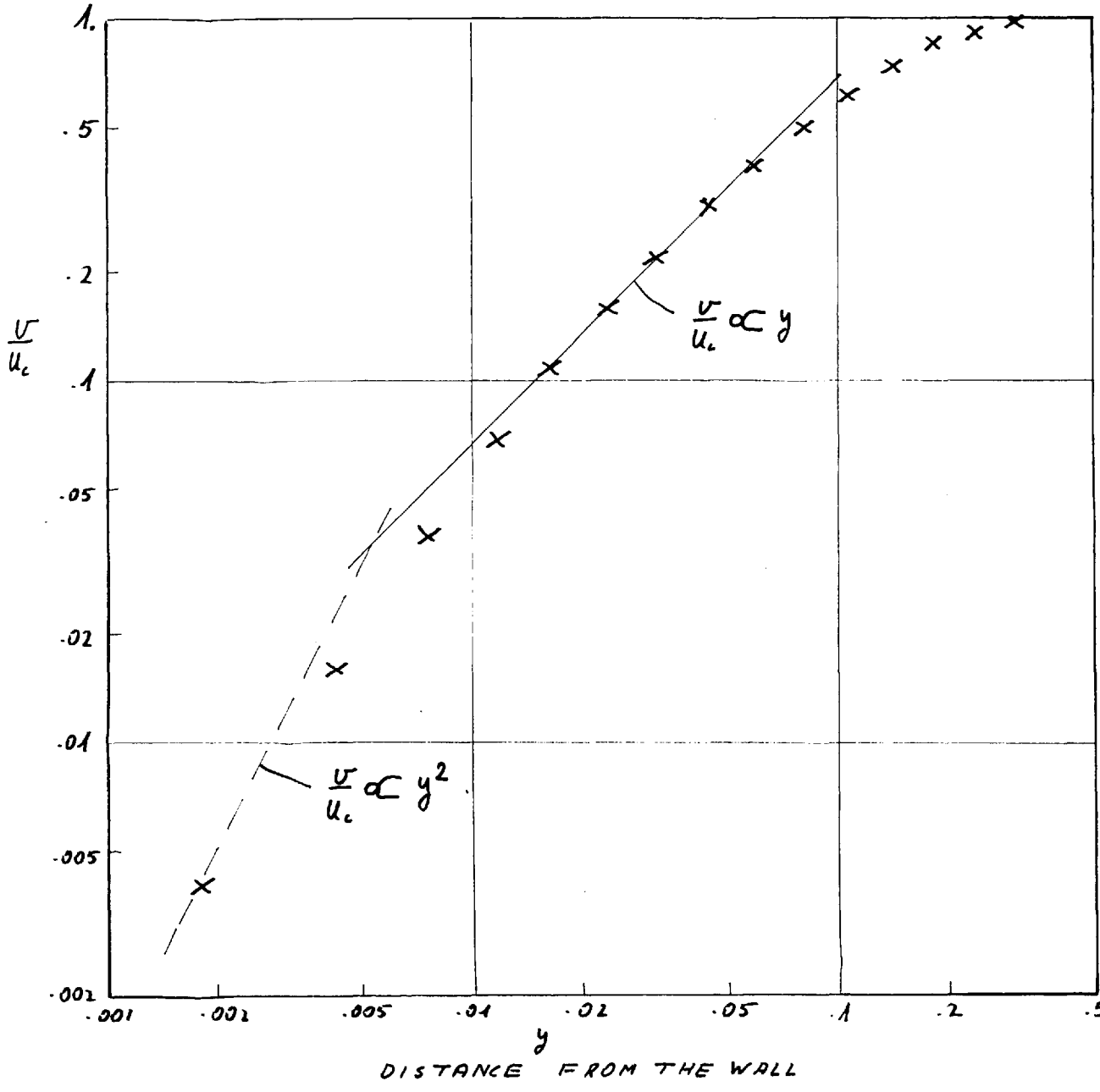

FIG 7.2-4: COMPUTED AXIS-VELOCITY DECAY IN THE IMPINGEMENT REGION. $Re_o = 950$. $h_c/b_c = 8$

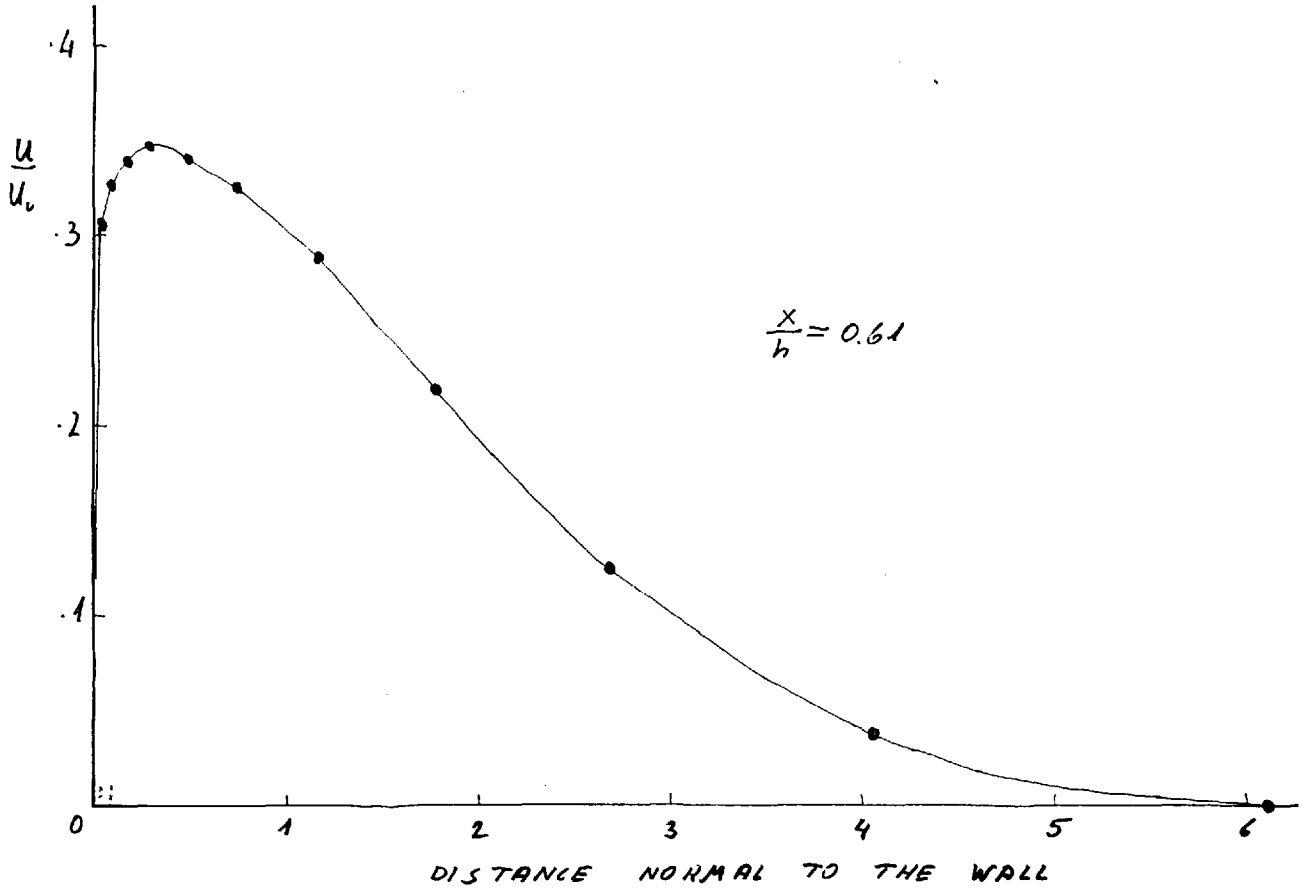

FIG 7.2-5 : COMPUTED VELOCITY PROFILES ON THE DOWNSTREAM BOUNDARY OF THE CONTROL VOLUME Re_c = 43 000 . h_c / d_c = 40.

the impingement region. Apart from the general advantages of increased insight and the description of the directions for further research, we shall refer to these results also in section 7.3. For these computations, again, the impinging jet system described in section 7.1 was used. Computations were obtained for various Reynolds numbers, and for $h_c/d_c = 8$. Various mesh distributions were used, as it was found necessary to refine the mesh near the wall for higher Reynolds numbers. The turbulence energy on the jet axis is plotted in fig 7.2-6, where y is the distance from the wall. Also, in fig 7.2-7 the turbulence energy profiles in the x-direction are plotted for $Re_c = 11000$, and different distances from the wall.

When we wish to interpret these figures we must first recall that, in the present hypothesis, the generation of turbulence energy is proportional to:

$$k^{1/2}\left[2\left(\frac{\partial u}{\partial x}\right)^2 + 2\left(\frac{\partial v}{\partial y}\right)^2 + \left(\frac{\partial u}{\partial y} + \frac{\partial v}{\partial x}\right)^2\right] \qquad (7.2\text{-}5)$$

Obviously, this term does not vanish on the jet axis. Even in a free jet, when $\partial v/\partial y$ is not very large, the axis turbulence generation is enough to raise the turbulence level on the axis considerably. Nevertheless the maximum turbulence is found halfway from the centre towards the jet edge, where $\partial v/\partial x$ attains its maximum value, as shown

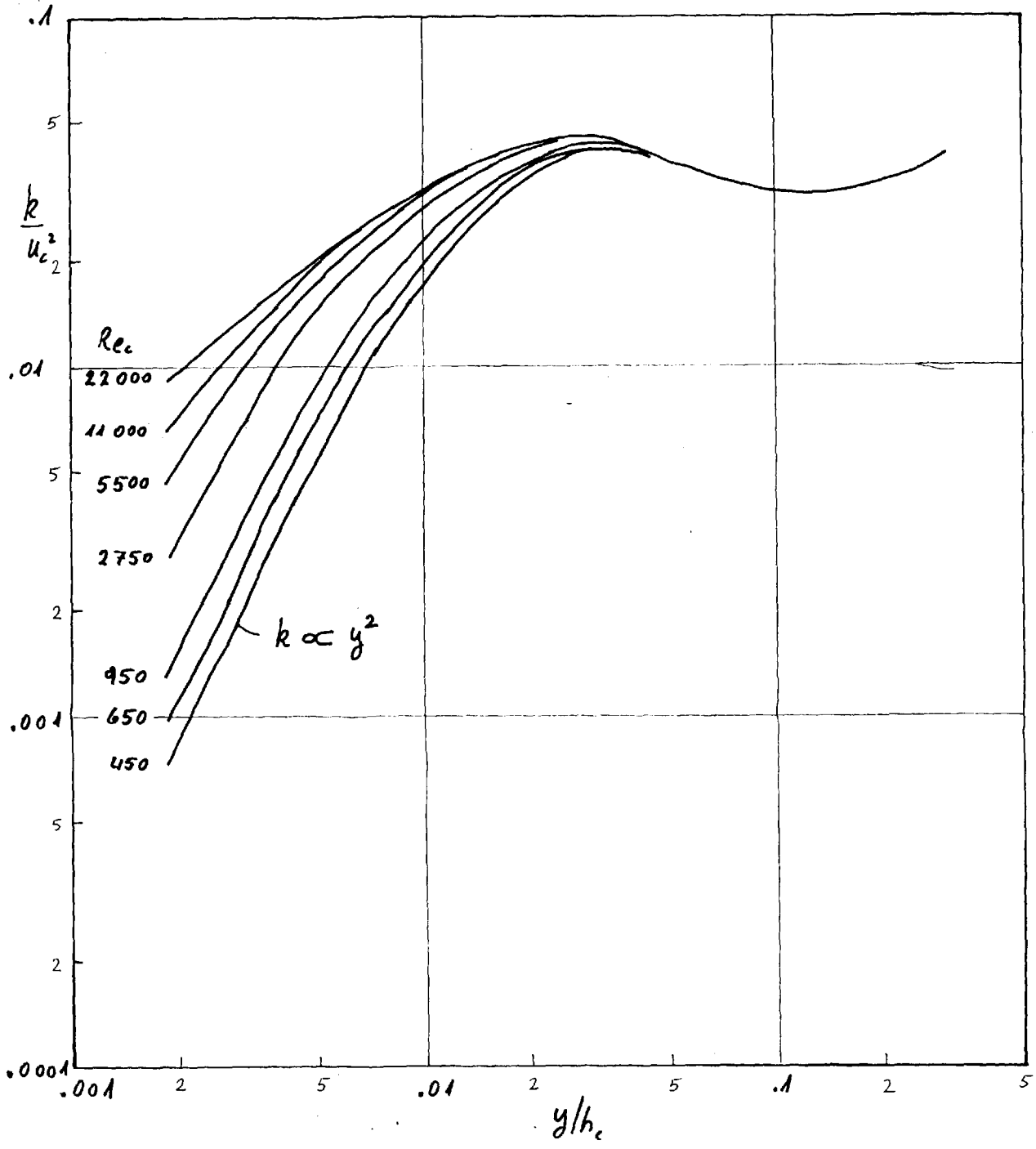

FIG 7.2-6: THE TURBULENCE ENERGY ON THE JET AXIS. $h_c/d_c = 8$

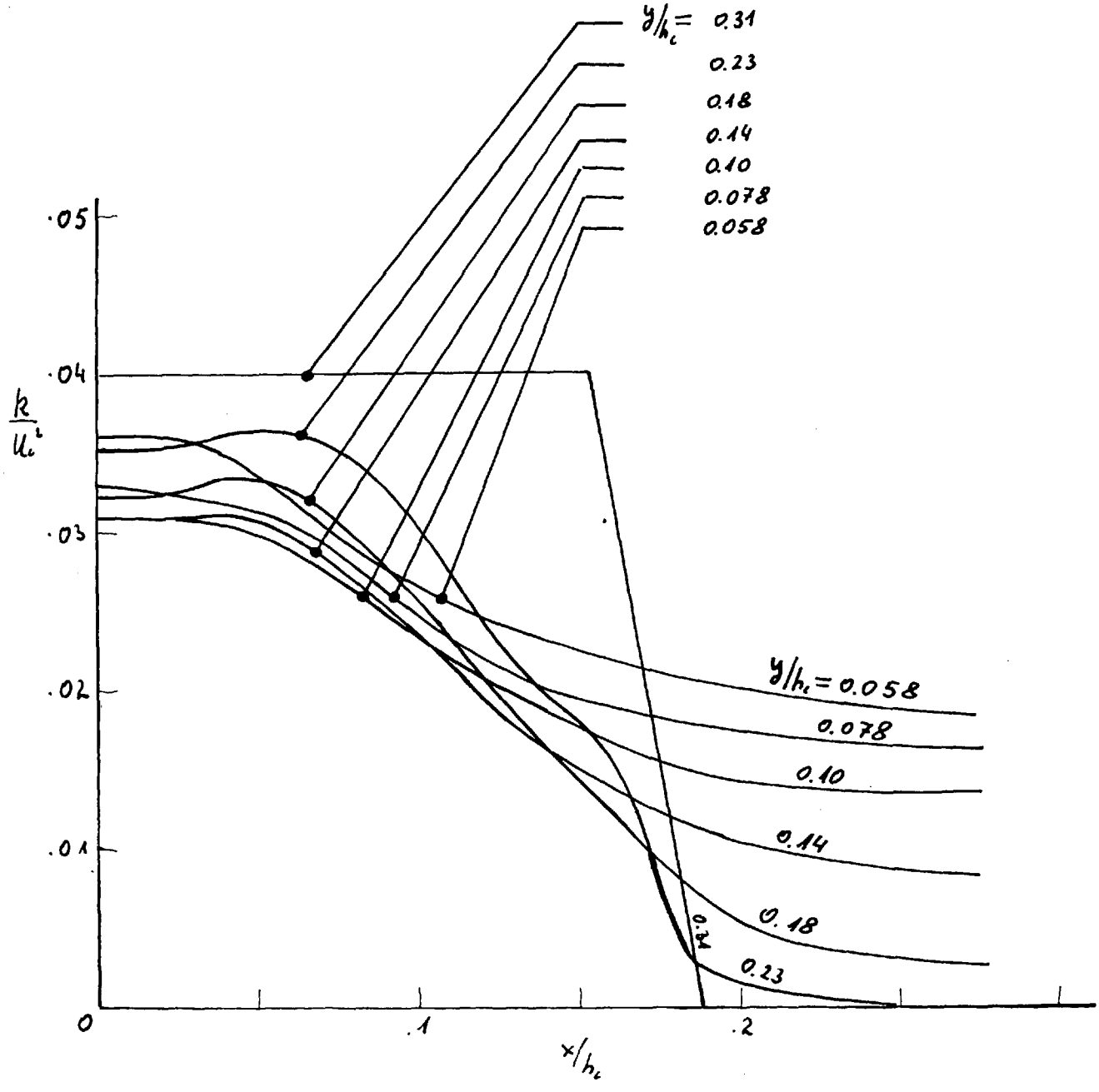

FIG 7.2-7 : THE TURBULENCE ENERGY PROFILE IN THE IMPINGEMENT REGION. Re_c = 11 000. h_c/d_c = 8. y STANDS FOR THE DISTANCE FROM THE SURFACE.

in the profiles for greater y/h_c in fig 7.2-7. However, when the stagnation point is approached, $\partial v/\partial y$ increases very considerably. Consequently, the maximum of the turbulence energy is shifted to the jet axis, due to the increased turbulence generation there. In this region the increase in the turbulence level is sufficiently large to create a maximum of the turbulence energy on the centre line as shown in fig 7.2-6. When the wall is further approached, the velocity decreases, until generation completely dies out, and the turbulence energy decays quickly. In the region of no generation we expect:

$$k = a\, y^{\alpha} \qquad (7.2\text{-}6)$$

where, it may be shown, by reference to eqns (5.6-23) and (6.3-7), that

$$\alpha = \frac{2}{3}\sqrt{\frac{1.5\, C_0\, \sigma_{k,turb}}{C_\mu}} = 1.38 \qquad (7.2\text{-}7)$$

in the fully turbulent region

and

$$\alpha = 0.5 + \sqrt{0.25 + C_0} = 1.32 \qquad (7.2\text{-}8)$$

in the laminar sublayer

As the two above values of α are very near to one another, it is impossible to learn from the above computations whether there is a "fully-turbulent no-generation" region

in the impinging jet system, or whether generation stops only in the viscous sublayer. Another interesting implication of figure 7.2-6 is that the no-generation layer, turbulent or viscous, as it may be, becomes thinner when the Reynolds number increases.

It has been suggested above that in the impingement region, turbulence is mainly generated by the normal stresses rather than the tangential ones; but does this represent true physical facts, or is it just an implication of the particular model of turbulence employed in the present paper? No definite answer to this question was obtained during the present research. In part IV, it will be suggested how such a definite answer may be obtained. However, before more research is done, we may get a partial answer by examining the plane, free jet data reported by Heskestad (1965), who measured the three fluctuating velocity components. Taking the squares of all the fluctuating components and summing these up, we get the solid line shown in fig 7.2-8, where the dotted line represents the mean velocity. As in the case of the computations described above, it will be difficult to explain the high turbulence level in the centre line if we assume that it is generated by the tangential stresses only.

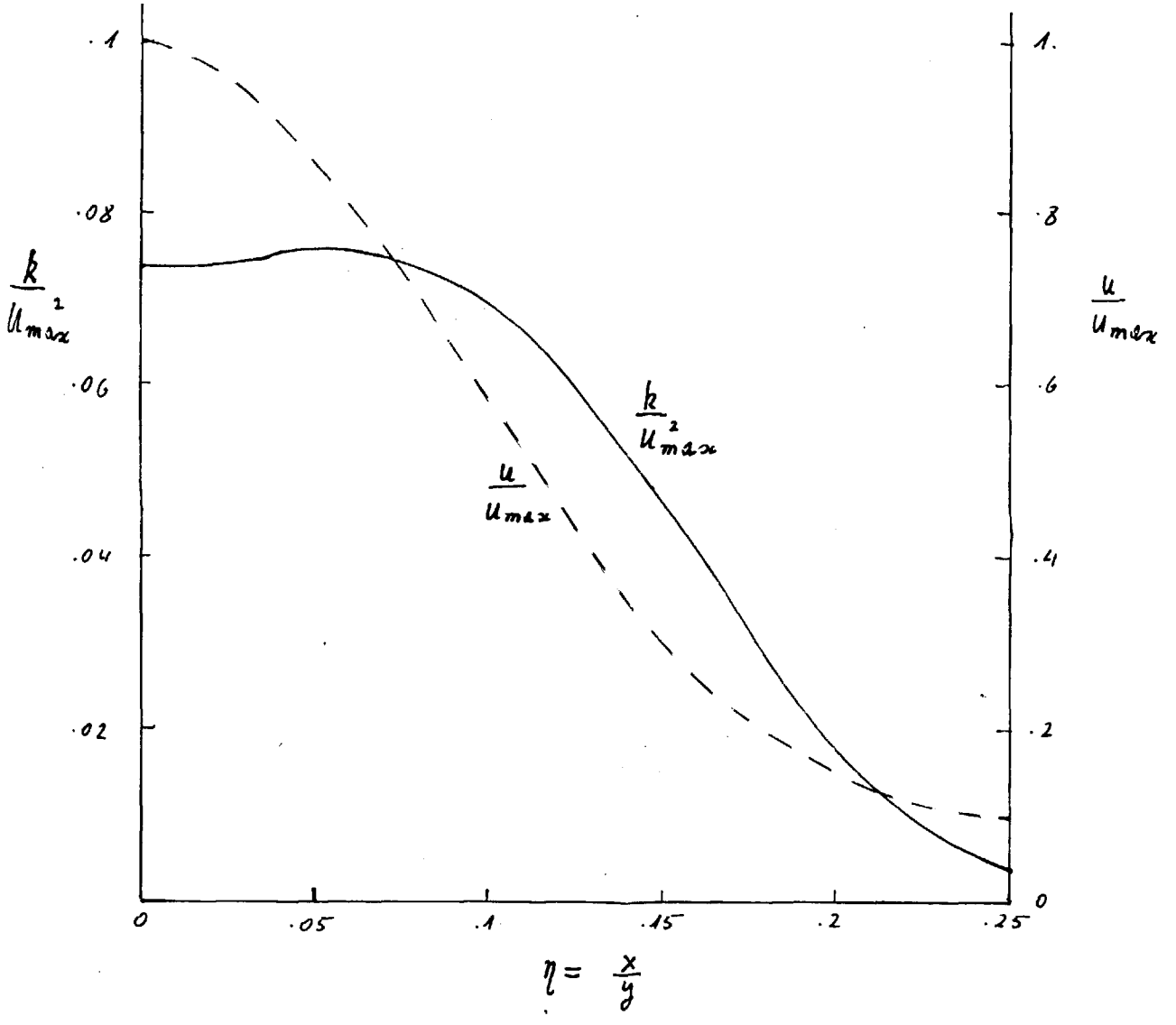

FIG 7.2-8 : THE TURBULENCE ENERGY DISTRIBUTION IN A PLANE FREE JET, BASED ON HESKESTAD'S DATA (1965).

7.3 The wall fluxes

In the present section we shall examine some predictions of the skin friction and Stanton number on the flat surface below the impinging jet. It should however be said from the very beginning, that in the previous two sections we were concerned mainly with the solution method and the viscosity law inside the control volume. At present, we shall have to consider mainly the wall functions. This distinction is rather important. Some of the solutions which will be presented will contain deficiencies. It is believed that these deficiencies result from deficient wall functions, rather than from the general method.

Many wall heat-flux measurements are available. Therefore we shall start by examining the Stanton number distribution, in section 7.3.1. In section 7.3.2 a short discussion of the skin-friction distribution follows.

7.3.1 The heat-transfer coefficient

The computation of the heat transfer from the surface to the impinging jet is probably the most interesting computation which we may perform in the impinging jet system. In the impingement region the conventional Reynolds analogy deteriorates completely as the skin-friction vanishes, while the heat-transfer reaches its maximum value.

Also the Prandtl mixing-length theory breaks down in the impingement region as it results in zero value for the turbulent viscosity (and therefore also the turbulent diffusivity) in this region. Therefore, the heat-transfer computations are a very useful tool to check the turbulent viscosity and diffusivity laws. Another aspect of these computations is to test the wall functions in this very particular region. On the other hand we are not likely to learn much on the general method; if the agreement with experimental results is not good, it is, most probably, a result of an unsuitable viscosity hypothesis, or wall functions. With this understanding we may now proceed towards the comparison with experiments. The most extensive experimental investigation available is that of Gardon and Akifrat (1965), for heat transfer from an isothermal surface to a plane impinging jet; their data, supplemented by some of Kroger and Krizek's results (1966), will be compared with computations in the present section.

The mesh

We must now choose a suitable mesh: the mesh point adjacent to the wall must be within the Couette flow region where the flow is nearly one dimensional. In other words, the number of mesh points, and the mesh non-uniformity parameter, ε_y, must be specified in such a way

as to ensure that the mesh point adjacent to the wall is not in the region of turbulence generation due to normal shear (discussed in section 7.2.3). Consulting fig 7.2-6, we see that the thickness of the no-generation layer on the jet axis decreases when the Reynolds number increases. Clearly, we have to refine the mesh when we increase the Reynolds number. If, on the other hand, we do not use a fine enough mesh, we are likely to assume too low a turbulence energy in the no-generation layer, which, in turn, will reduce the heat transfer rate.* Similar refinement of the mesh is necessary when we increase either h_t/d_t or σ. Thus, when we seek a solution for a higher Reynolds number case, we are penalised by having to use finer meshes, and spend more computer time.

In the present set of computations the meshes employed were sufficiently fine for Reynolds numbers up to and including 11000, for h_t/d_t of 8 and for σ of 0.7.

The influence of the Reynolds number

The results are shown in fig 7.3-1: St_o, the Stanton number in the stagnation point, is plotted versus Re_t, the slot Reynolds number, for $h_t/d_t = 8$ and $\sigma = 0.7$. Clearly the agreement is satisfactory until the Reynolds number

*Similar considerations prevail as well for the skin friction.

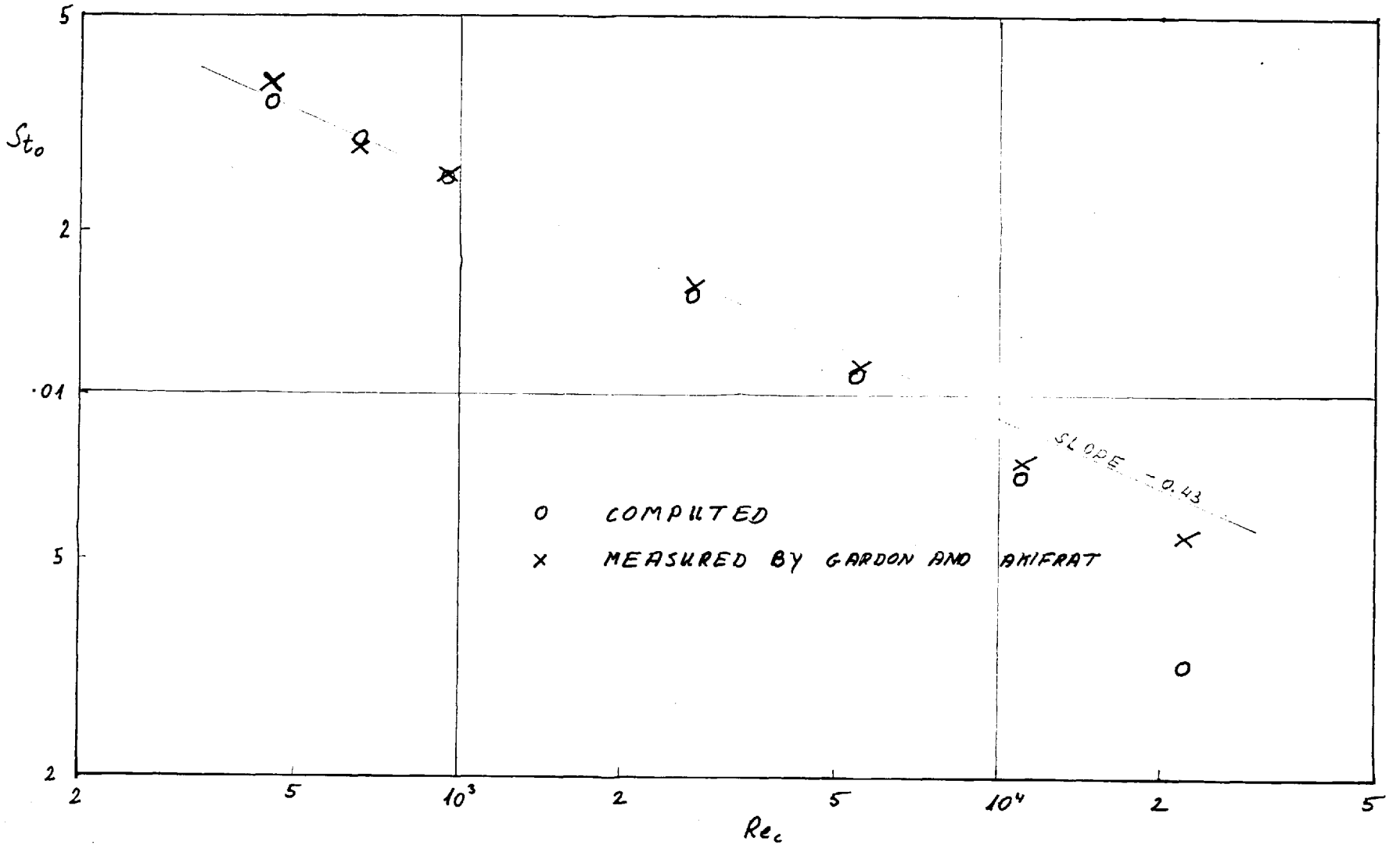

FIG 7.3-1 : THE STAGNATION POINT STANTON – NUMBER DEPENDENCE ON THE SLOT REYNOLDS NUMBER IN A TURBULENT IMPINGING JET.
$h_c/d_c = 8$. $\sigma = 0.71$

exceeds 11000. The point is even better emphasised in fig 7.3-2, where the lateral Stanton number variation is plotted, for $h_c/d_c = 8$ and the three Reynolds numbers, 2750, 11000 and 22000. For the lower Reynolds numbers the agreement is satisfactory at least qualitatively. For the higher Reynolds number, too low Stanton numbers are predicted on the jet axis. Away from the axis, where turbulence is generated by tangential rather than normal stresses, the Couette flow region becomes thicker and the agreement is qualitatively correct, as in the low Reynolds number case.

An interesting and important question is what is the power of Re_c in the relation

$$St_o \propto Re_c^{\alpha} \qquad (7.3\text{-}1)$$

The solutions presented in fig 7.3-1 do not support the value of -0.43 for α, which was reported in chapter 1. However, it was reported by Gardon and Akifrat (1965) that α may be fixed as -0.42 only when

$$\begin{aligned} 14 < h_c/d_c < 60 \\ 2000 < Re_c < 50\,000 \end{aligned} \qquad (7.3\text{-}2)$$

Because of the present limitations on the mesh distribution near the wall, solutions in the region specified by (7.3-2) were not obtained. Therefore the power in eqn (7.3-1) cannot be confirmed on the basis of the present computations.

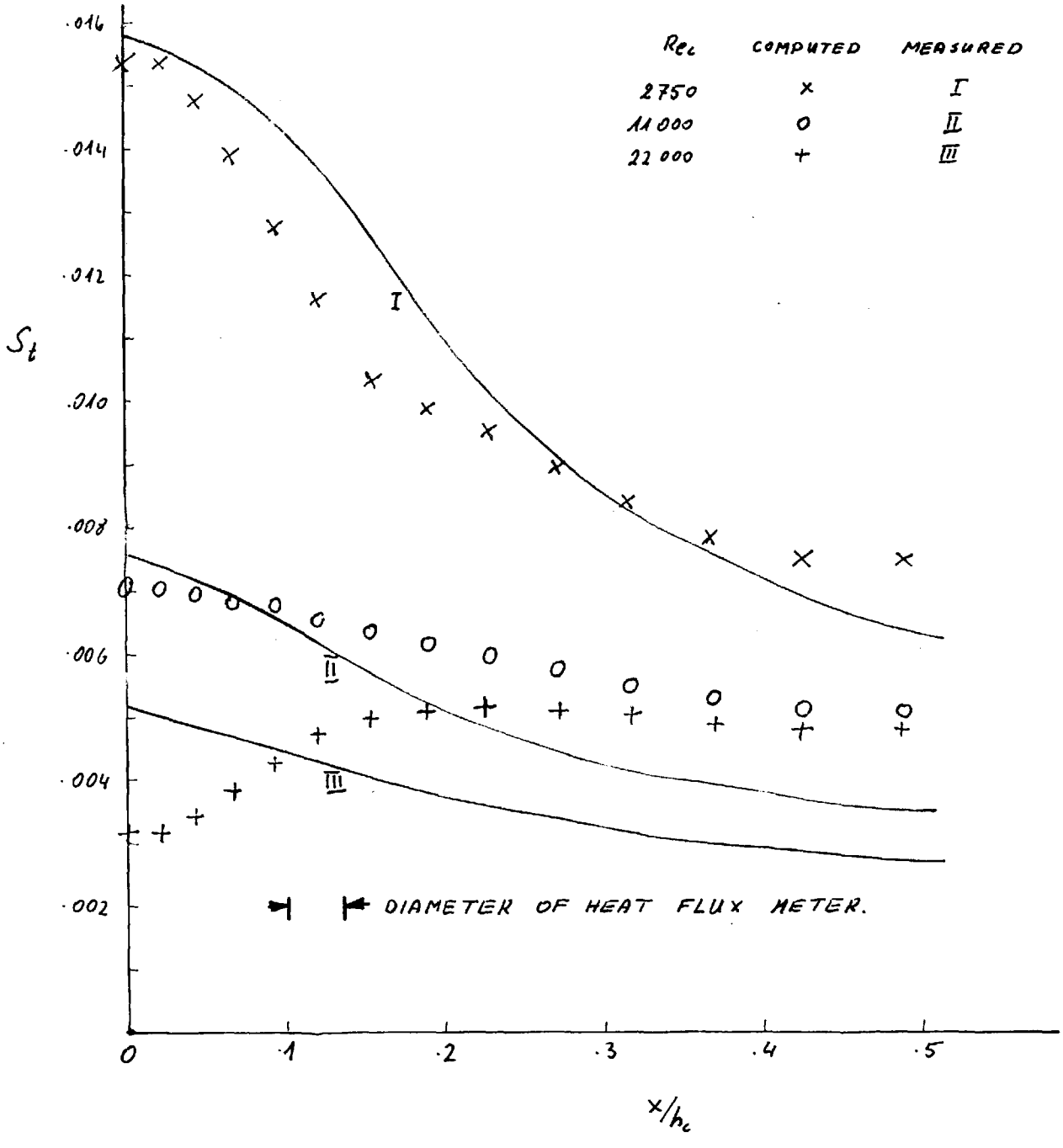

FIG 7.3-2 : A COMPARISON OF THE COMPUTED AND MEASURED LATERAL STANTON-NUMBER DISTRIBUTION IN THE IMPINGEMENT REGION. $h_L/d_L = 8$. $\sigma = 0.71$. EXPERIMENTAL DATA OF GARDON AND AKIFRAT (1965).

The influence of the Prandtl number

Here, again, we shall consider cases for which some experimental evidence is available. The data chosen is for a Reynolds number of 11000 and $h_c/d_c = 8$. Heat transfer measurements of Gardon and Akifrat (1965) are for $\sigma = 0.71$, while Kroger and Krizek (1966) measured mass transfer from a naphthalene surface to plane jet, with $\sigma = 2.5$. These experimental results are compared with the present computations in fig 7.3-3 and 7.3-4, where the Stanton number in the stagnation point and the lateral Stanton number distribution are displayed. It is worth noting, that Kroger and Krizek did not report the Reynolds number accurately, and this may cause some discrepancy between measurements and computation. An examination of fig 7.3-4 reveals that for a Schmidt number of 2.5 and Reynolds number of 11000, the mesh was not fine enough, and St_o was, therefore, too low.

7.3.2 The skin-friction distribution

The skin-friction distribution in the impingement region was measured by Schauer and Eustis (1963). The values of the parameters were

$$\begin{aligned} h_c/d_c &= 40 \\ Re_c &= 43000 \end{aligned} \qquad (7.2\text{-}2)$$

as in section 7.2.2.

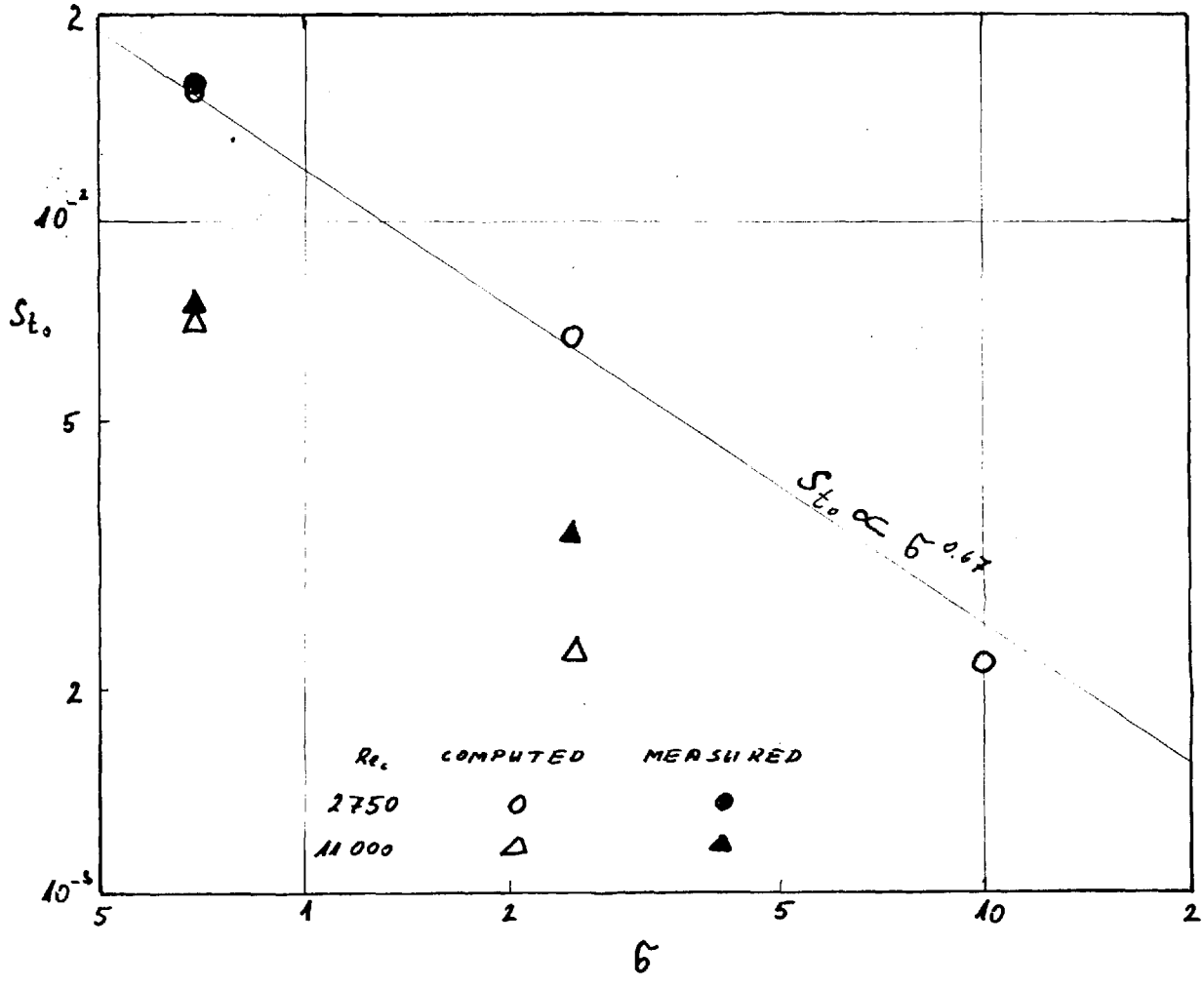

FIG 7.3-3 : THE INFLUENCE OF THE PRANDTL NUMBER ON THE STANTON NUMBER AT THE IMPINGEMENT POINT. $h_c/d_c = 8$. THE DATA FOR $\sigma = 0.7$ IS BY GARDON AND AKIFRAT (1965). THE DATA FOR $\sigma = 2.5$ IS BY KROGER AND KRIZEK (1966).

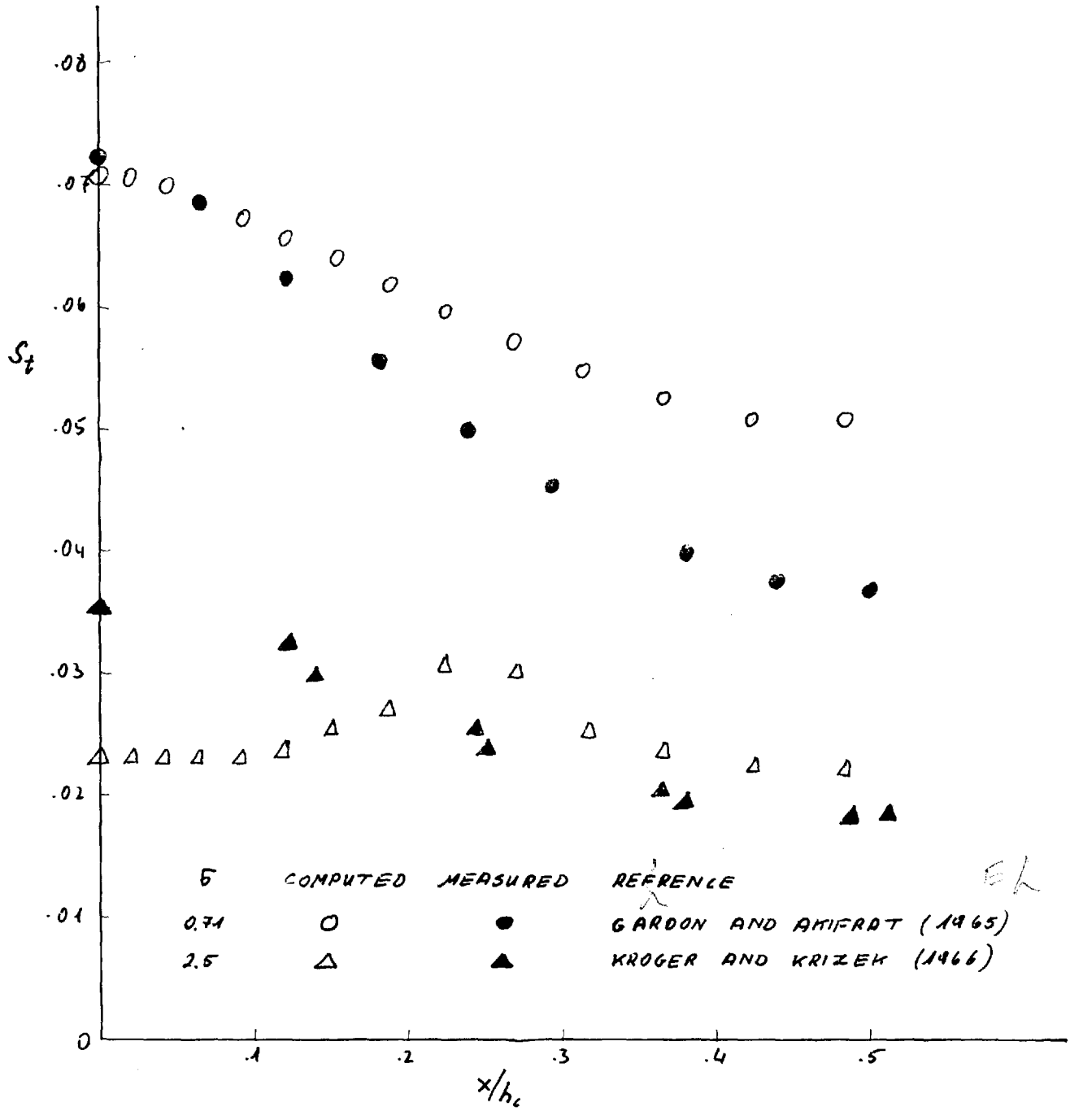

FIG 7.3-4: THE INFLUENCE OF THE PRANDTL NUMBER ON THE LATERAL DISTRIBUTION OF THE STANTON NUMBER.

$Re_c = 11000$. $h_c/d_c = 8$.

A comparison of Schauer and Eustis's experimental data with the present computations is shown in fig 7.3-5. The skin-friction is normalised by the nozzle velocity. As in the case of the maximum velocity growth, discussed in section 7.2.2, the computed skin-friction is qualitatively correct, but, it is consistently low. We may expect some connection between the skin-friction and the maximum velocity, and as we have seen that the maximum velocity is too low as well, we may expect to get better agreement, once that the influence of the velocity has been eliminated. This has been done in fig 7.3-6, where the skin friction was normalised by the local maximum velocity. The agreement is satisfactory.

7.4 A short discussion of chapter 7

In chapter 7, the vital task of testing the computing method and the physical input of viscosity law and wall functions was performed. It will be recalled that no attempt has been made to fit the method or the physical input to the impinging jet situation; they were derived from basic principles and Couette flow analysis. In the present section we shall now summarise the amount of success obtained as follows.

(i) Predictions of the main flow patterns such as contours and velocity profiles look very plausible. They

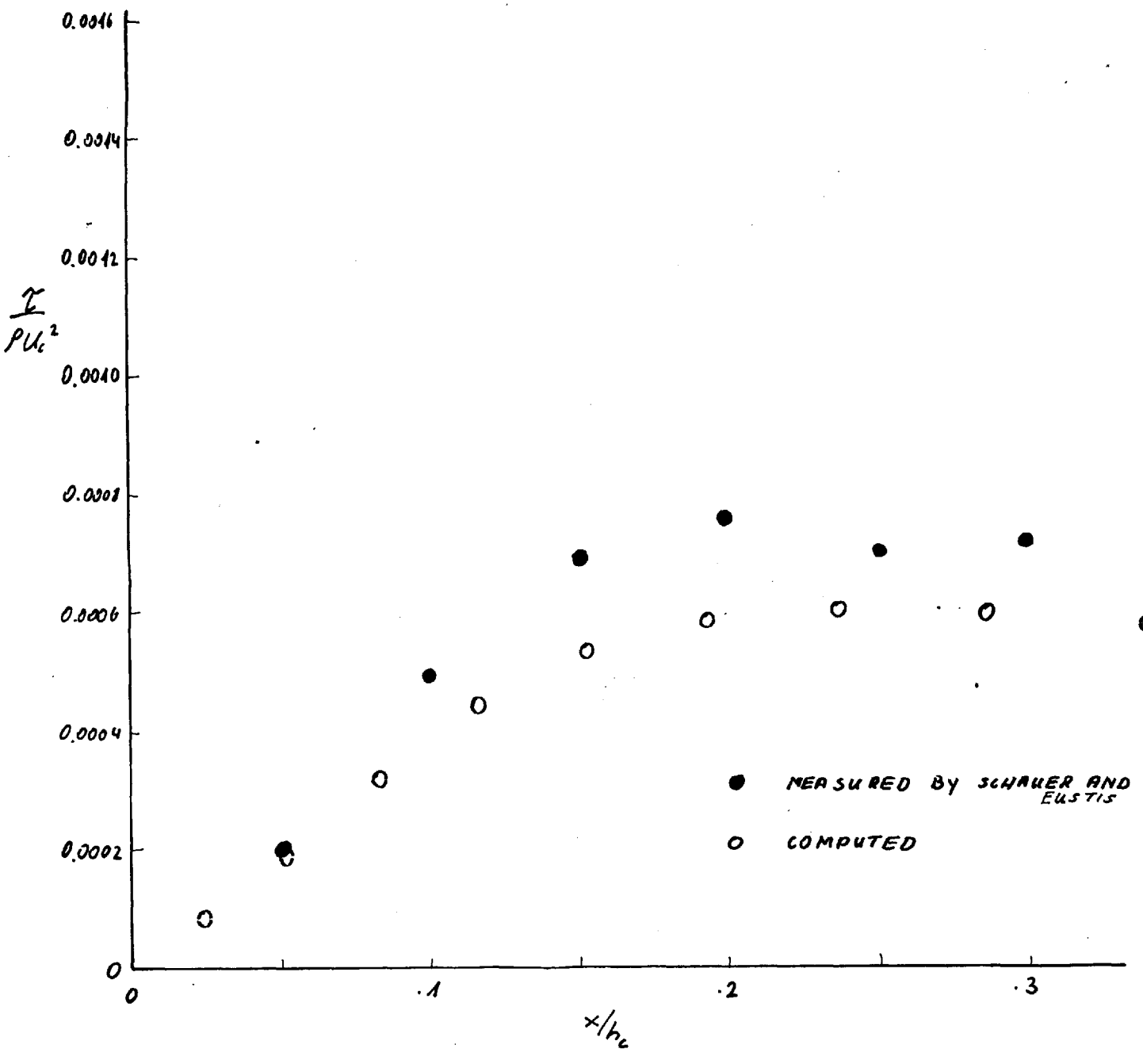

FIG 7.3-5 : THE SKIN FRICTION DISTRIBUTION IN THE IMPINGEMENT REGION, NORMALISED BY THE NOZZLE VELOCITY.

$Re_c = 43\,000$. $h_c/d_c = 40$. 14 × 16 MESH. $\xi_y = 1.5$.

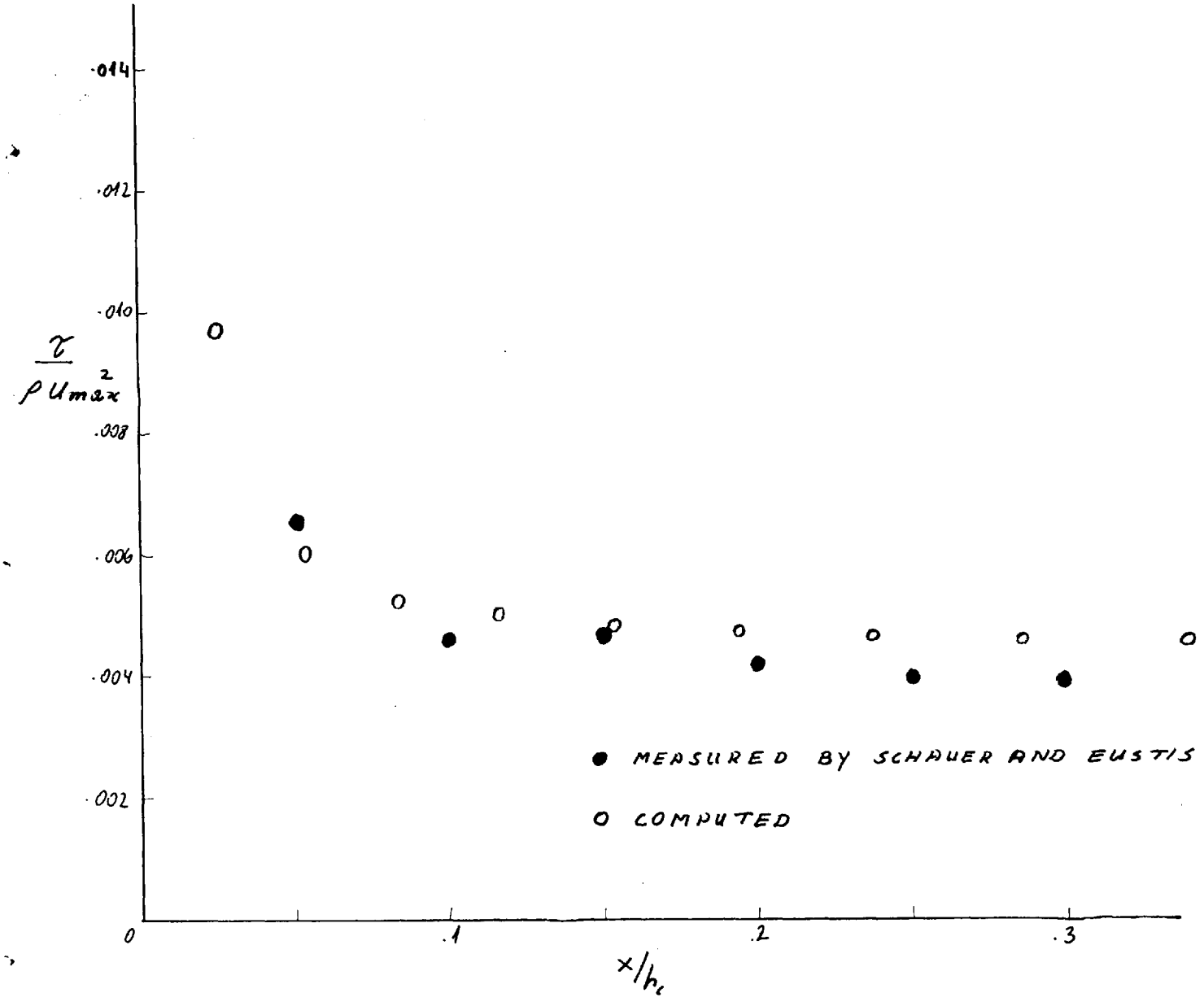

FIG 7.3-6: THE SKIN FRICTION DISTRIBUTION IN THE IMPINGEMENT REGION, NORMALISED BY THE LOCAL MAXIMUN VELOCITY. $Re_c = 43\,000$. $h_c/d_c = 40$. 14x16 MESH. $\xi_y = 1.5$.

do not contradict any available experimental information. Still the amount of experimental data existing at present is not sufficient to confirm the theory in a definite way.

(ii) The normal velocity on the jet axis is proportional to the distance from the wall as suggested by potential stagnation-flow theory. Very near to the wall, this velocity tends to become quadratic with the distance, as suggested by the laminar stagnation flow solution.

(iii) The static pressure and maximum velocity growth, in a high Reynolds number flow, are qualitatively correct, but a bit too low. It has been suggested, in the case of the maximum velocity growth, that this may have resulted from an inaccurate viscosity law.

(iv) The Stanton number predictions are reasonable for a low Reynolds number, and small nozzle-to-surface distance. When either of the two increases, the Stanton number predictions in the impingement region are too low, but they improve away from the stagnation point. The reason for this is believed to be the decrease in the width of the Couette flow layer near the stagnation point when either the Reynolds number or the nozzle-to-surface distance increase.

(v) The effect of the Prandtl number is predicted correctly for flows with a small Reynolds number. In the high Reynolds number cases an increase of the Prandtl

number is followed by too low Stanton number predictions near the stagnation point. The reason for this is believed to be the decrease in the thermal boundary-layer-thickness when the Prandtl number increases.

(vi) The skin-friction predictions are reasonable, especially when the influence of the local velocity is eliminated.

Closure to part III

In part III we dealt with some physical aspects of turbulent flows. First, in chapter 5, an extended version of the Kolmogorov-Prandtl hypothesis of turbulence was presented. It included the laws for the turbulent exchange coefficients and length scale distribution. Six empirical constants were fitted as to obtain good agreement with a variety of data on turbulent Couette flows. Then, in chapter 6, the behaviour of over-turbulent Couette flows was studied theoretically and algebraic forms for wall functions were suggested. Finally, in chapter 7, predictions of turbulent impinging jets were presented, using the constants and wall-functions which had been deduced from the Couette flow data. The results were in reasonable agreement with experimental data, provided that the mesh was fine enough.

Part IV : Discussion

8. Discussion

We have come to the final part of the thesis; now we have to examine the results, to estimate how good they are, and also to find out where expectations were not fulfilled. Then we wish to know which corrective measures may be taken, to overcome any failures. But the task in the present chapter is even wider. It must be realised that both the finite-difference method and the turbulent viscosity hypothesis are relatively new and fairly untried; therefore their generality must be established by further research. So suggestions for such research will be presented as well.

The chapter will be divided into two main sections. In section 8.1 we shall examine what has been done and where the results need further confirmation. Then, in section 8.2, suggestions for further work will be presented. A short closure to the chapter and indeed to the whole thesis will be presented in section 8.3.

8.1 Summary of the main results

The finite-difference method

The finite-difference method was presented in chapter 3. Its main innovations are:

(i) The preservation of the conservation laws in arbitrarily large or small control volumes.

(ii) The use of non-uniformly spaced meshes.

(iii) The inclusion of variable viscosity (and potentially variable density as well).

The present work was restricted to plane flows only, but the method can be easily extended to any axially-symmetrical flow, as was shown by Pun and Spalding (1967). The studies of accuracy, convergence and economy in chapter 4 showed that the method can, in fact, produce reasonably accurate results, without excessive computing times, whenever the distribution of the computed quantities is not highly non-linear between adjacent mesh points. The "smearing" of conserved properties was studied as well, and the amount of "smearing" in a uniform-velocity flow was related to local quantities.

The Kolmogorov-Prandtl hypothesis

In chapter 5 the general relations describing all the turbulent exchange coefficients and quantities were presented in a general form, applicable to any turbulent flow, in all its parts. Recommendations for the six necessary empirical constants were made on the basis of available data on Couette flow; the amount of such data and its reliability can not, however, be considered sufficient. Indeed, more work is necessary to confirm that these six constants are sufficient empirical input to the hypothesis, and to establish their values. Still,

it seems plausible that the general frame suggested here will prove useful in the future. The Kolmogorov-Prandtl hypothesis was used in chapter 6, when numerical solutions were obtained for a wide range of Couette flows with augmented turbulence. These solutions were later cast into correlations to be incorporated, as wall-functions, in the general method.

The impinging jet solutions

In chapter 7, the method as well as the wall-functions, were used to obtain solutions for the problem of a jet impinging normally to a flat isothermal surface. The following are the main conclusions resulting from these solutions:

(i) The contours, inside the field, of vorticity, stream-function, turbulence energy, conserved property and dynamic and static pressures look very plausible. Also the velocity profile on the downstream, wall-jet like, boundary, as well as the normal velocity decay on the jet axis, are qualitatively supported by all our previous knowledge. But no direct measurements are available for comparison.

(ii) The static pressure on the surface and the maximum-velocity growth along it are qualitatively right, but somewhat lower than the measured ones. The maximum difference between measured and computed values is of the

order of 10%. The reason is believed to be either an inaccurate specification of the boundary conditions on the upstream side or a deficiency in the present form of the turbulence hypothesis.

(iii) The predictions of the Stanton-number in the stagnation point are good in all cases when the mesh distribution near the wall is fine enough. Away from the stagnation point, they are not so good, and differences as large as 20% may be found. When either the Reynolds number, the nozzle-to-surface distance or the Prandtl number increase, the mesh should be refined near the wall. If this is not done the predictions become qualitatively wrong: a minimum of the Stanton number appears in the stagnation point, which may be removed only if the mesh is altered.

(iv) Skin-friction predictions show the right kind of behaviour, but they are too low. These low skin-friction values are very likely to be connected with the low maximum velocities computed.

(v) Computations of the turbulence energy suggest that there is a considerable generation of turbulence near the stagnation point, due to the gradient of the velocity in the y-direction. This generation diminishes only very near to the laminar sub-layer.

Conclusions

(i) The numerical methods seem to be powerful enough for the present needs.

(ii) Too few measurements of the flow in the impingement region of the impinging jet are available to enable a complete comparison of the measurements and predictions.

(iii) The turbulence energy equation, and the constants associated with it, may be established only after more research is done.

(iv) The use of wall-functions, based on a Couette flow model, in the impinging jet, did not eliminate completely the need for fine mesh near the stagnation point.

8.2 Recommendations for the future

The previous section was concluded with the suggestion that more research needs to be done. We shall now examine the possible paths, along which progress may be made:

The turbulence energy hypothesis

Three stages may be distinguished in the development of this hypothesis:

(i) As much information as possible must be extracted from existing measurements of turbulent quantities, in two-dimensional flows. Useful data has been reported by Heskestad (1965) on plane free jets, by Poreh

et el (1967) on radial wall-jet, and by Carmody (1964) on wake flow behind a blunt body. No doubt more papers of similar merits can be found by careful searching of the technical literature. Such data must be compared with predictions; then it will, very probably, become necessary to adjust the hypothesis. This stage of the work is not necessarily coupled with the present finite-difference method; many of the cases will be well described by the parabolic boundary-layer equations, which are much easier to solve than the present elliptic ones.

(ii) New measurements should be made to remove existing uncertainties and to supply new data, which may be easily compared with predictions. For instance, we would like to know what is the exact value of $k^{1/2}/\varepsilon$ in the outer part of a constant-shear non-diffusional Couette flow, or the constant K_o in eqn (5.6-2). There are some new situations, which have not been studied yet, but may prove rather interesting now. For instance, we may measure the turbulent exchange coefficient in a "thermal wake" which develops behind a linear heat source in a uniform velocity turbulent flow. Sure enough, the imaginative experimenter may find a large variety of other promising cases, from which new light may be thrown on the mechanism of turbulent transfer phenomena.

(iii) With such information as may become available after experiments have been performed, the turbulence energy hypothesis may be broadened to the very limits of its potential. One particular extension, which may, perhaps, be started even now, is the provision of a differential equation for the length scale. Suggestions for such an equation were made by Rotta (1951), and elaborated by Spalding (1967d). Once that such an equation is available, it will remove the present uncertainty, concerning the distribution of the turbulent length scale away from walls.

(iv) An additional point which needs clarification, is that of the generation of turbulence. At present, it has been assumed that turbulence is generated by normal as well as tangential stresses. The validity of this assumption should be confirmed, and it seems that a good starting point is the free jet, where data are available, and where normal shear is appreciable.

The wall-functions

The main deficiency of the wall-functions, in their present form, is that they apply to Couette flows only; therefore, when the Couette flow layer is very thin, as in the impingement region, we are still unable to use a coarse mesh even when the wall-functions are employed. However, in the impingement region the flow is very

similar to a stagnation flow. Therefore it is quite possible that the wall-functions may be extended, by incorporation of solutions for a turbulent stagnation flow.

Some of the disagreement between the impinging jet measurements and predictions may be attributed to imperfections of the wall-functions. This point needs careful examination. Of particular advantage may be some solutions, where the wall functions are not employed. A free turbulent shear flow may be studied first; then a test solution of the impinging jet problem with very fine mesh, but without the wall-functions, will probably prove to be an expensive, but worthwhile investment. After such tests have been performed, modifications to the present wall-functions are likely to become necessary.

Apart from all these extensions, the wall functions will have to be modified together with the turbulence hypothesis, as the latter is further developed.

The impinging jet

It is really difficult to separate the future work on impinging jets from the other future work already suggested. Clearly an improvement of the general hypothesis and relations will result in better impinging jet predictions as well. But some changes are likely to be

more influential than others. Most important for the impinging jet, are the following:

(i) The influence of the normal stresses on turbulence generation.

(ii) The incorporation of the turbulent stagnation flow solutions in the wall functions.

Experimental data will be needed to support these investigations. But some advance may be made even with the slight data available now.

Finally, a carefully planned set of measurementsof all turbulent quantities in the plane impinging jet seems very advisable. This is not a simple task, by any means: yaw-angle measurements, as well as a lot of hot wire anemometry will be needed. Still, such measurements will increase our confidence, and supply new and important data.

8.3 Closure

The present thesis has proceeded along the road from certainty towards optimistic guesswork of the future. The finite-difference method has been shown to enable reasonable predictions to be made. Thus our interest was stimulated, to attack complex problems, as the impinging jet, and to test new turbulent-property hypotheses. But now we are reaching the stage where our mathematical capabilities are larger than our physical understanding. In the present paper, the author has tried to describe some work on the physical side as well and to outline some future researches, which have become possible and necessary as a result of the recent developments. Some successes may be recorded, and old questions answered; but new problems have now been posed, which future research will have to solve. The author has found this widening of his horizon to be the major result of the work described in this thesis; he hopes that others will appreciate it in a similar way.

London,

November 1967.

Part V : Nomenclature and references

9. Nomenclature

9.1 Mathematical symbols

Symbol	Meaning	Defining eqn or eqn of first appearance
Latin characters		
A	- an occasional constant	
A_D	- a constant in the expression for ℓ_D	(5.4-6)
A_u	- a term in the finite difference equation for ϕ_p	(3.1-3)
A_μ	- a constant in the expression for ℓ_μ	(5.4-5)
A'	- a constant	(5.6-21)
a	- an occasional constant - in chapter 6, the turbulence-augmentation parameter	(6.4-1)
a_{ij}	- a coefficient in the finite-difference equation for ϕ_i	(4.5-1)
a_E, a_W, a_N, a_S	- coefficients in the finite-difference equation for ϕ_p	(3.1-5)
B, B'	- occasional constants	
c	- convergency criterion	(3.4-2)
c	$= \sqrt{u/r}$ in chapter 4	(4.4-5)
c	- a constant in chapter 6	(6.6-6)
c_D	- a coefficient in the turbulence energy dissipation term	(5.3-8)
c_E, c_W, c_N, c_S	- coefficients in the finite-difference equation for ϕ_p	(3.1-2)

c_f - $\tau_s/\rho u_*^2$

c_μ - a coefficient in the turbulent viscosity (5.3-3)

D - a constant (6.7-8)

d_c - the nozzle width

E - a constant (5.6-1)

F - a non-dimensional pressure gradient; (3.2-14)

- body force in chapter 5 (5.2-2)

f - pressure gradient correction (6.7-3)

$\underline{G}$ - the mass velocity vector (2.3-6)

g - a function of the Prandtl number (6.6-5)

h_c - the nozzle to surface distance

h - mesh size in section 4.4;

- distance between the flat surfaces in the Couette flow problem in section 4.1

$I_\phi, I_{\tau,1}, I_{\tau,2}, I_{p,1}, I_{p,2}$ - various integral functions, defined in eqns (3.2-19) to (3.2-23)

i - designates a coordinate (say x_i) when index notation is used; designates the number of nodes in the x-direction from the origin in finite-difference work

$\underline{J}$ - the ϕ-flux vector

J_j - the component of J in the x_j direction (2.1-5)

J_S - the component of J at a surface, normal to this surface (2.2-5)

J_ϕ - the ϕ-flux in a Couette flow (3.2-11)

$J_{\phi,S}$ - J_ϕ at a surface (3.2-10)

j - designates a coordinate (say x_j) when index notation is used; designates the number of nodes in the y-direction from the mesh origin in finite-difference work

K - $k\rho/\alpha_s$ (6.2-1)

K_o - a constant (5.6-2)

k - the turbulence energy (5.1-1)

k_F - k on the upstream boundary of the control volume in the impinging jet (7.1-5)

L - a typical length scale (4.4-12)

ℓ_D - the turbulence energy dissipation length scale (5.4-6)

ℓ_μ - the turbulent viscosity length scale (5.4-5)

M - the blowing Reynolds number in a Couette flow ($\equiv \frac{v h \rho}{\mu}$) (4.1-1)

m - the power in the $K \sim R$ relation (6.3-7)

P - the P-function, describing the resistance of the laminar sub-layer to heat-transfer (5.6-36)

P' - a dimensional function, similar to P (6.3-13)

p - the static pressure

p_d - the dynamic pressure (2.3-4)

$\overline{p}$ - the mean static pressure (5.2-4)

p' - the fluctuating static pressure in chapter 5 (5.2-4)

p' - the pressure gradient (3.2-6)

Q - a dimensionless stream-function (3.2-17)

R - Reynolds number, in general;

- Reynolds number of turbulence energy (5.4-2)

Re_ℓ - the nozzle Reynolds number of an impinging jet ($\equiv \frac{u_e \delta_e \rho}{\mu}$)

R_{eff} - Reynolds number based on the effective viscosity (4.4-13)

r - mesh non-uniformity parameter (3.2-25)

r_u - the convergency parameter (4.6-1)

S - dimensionless heat flux ($\equiv \frac{\sigma J_\phi y}{\mu(\phi - \phi_s)}$) (3.2-18)

- a source strength (4.4-6)

St - the Stanton number ($\equiv \frac{J_s}{\rho u_e(\phi_e - \phi_s)}$)

St_o - the Stanton number at the stagnation point of the impinging jet

$S_{u,p}$ - the source term in the finite-difference equation for ϕ_p (3.1-6)

S_ϕ - a ϕ-source (2.1-11)

S_ω - an ω-source (2.1-10)

s - dimensionless skin friction ($\equiv \frac{\tau_s y}{\mu u}$) (3.2-13)

s_o - the value of s when the pressure gradient is neglected (6.7-11)

t - time, in chapter 5;

- temperature

u - velocity in the x-direction

$\underline{u}$ - the velocity vector

u_+ - $u/\sqrt{\tau_s/\rho}$ in Couette flows (5.6-34)

u_e - the nozzle velocity in the impinging jet

u_i - the velocity component in the x_i-direction

u_i' - the fluctuating part of u_i (5.2-3)

$\overline{u}_i$ - the time-averaged part of u_i (5.2-3)

u_{max} - the maximum velocity in the wall jet

u_T - the top wall velocity in a Couette flow

V - the absolute velocity ($\equiv \sqrt{u^2+v^2}$) (2.3-2)

v - the velocity in the y-direction

v_{max} - the maximum velocity in the free jet

$v_{max,F}$ - v_{max} on the upstream boundary of the control volume

W - dimensionless vorticity (3.2-15)

x - a cartesian coordinate in cases of plane flow

x_G - the half width of the free jet when it crosses the boundary of the control volume

x_i - a general cartesian coordinate (i may take the values 1,2,3), in chapters 2 and 5;

- the value of x at the i^{th} node from the mesh origin (7.1-6)

x_M - the maximum length of the control volume in the x-direction, in the impinging jet

y - a cartesian coordinate in cases of plane flow

$y_{\frac{1}{2}}$ - the value of y when $\phi = \frac{1}{2}\phi_{max}$ (4.4-2)

y_+ - $y\sqrt{\tau_s \rho}/\mu$, in Couette flows (5.6-33)

y_F - the distance from the nozzle to the upstream boundary of the control volume, in the impinging jet

y_j - the value of y at the j^{th} node from the mesh origin (4.3-1)

Z - a velocity ratio (3.2-24)

Z_c - a term in the finite difference equation for ϕ_ρ (3.1-4)

Greek characters

α - the angle between the mesh and stream lines in chapter 4

- an occasional constant power elsewhere

Γ - diffusivity

Γ_{eff} - the effective diffusivity (5.5-1)

Γ_{false} - the false diffusivity (4.4-8)

Γ_{turb} - the turbulent diffusivity

Δy - a y-increment

δ - a power (6.7-8)

ε - μ_{eff}/μ , in chapter 3 (3.2-16)

ε_{turb} μ_{turb}/μ , in chapter 5 (5.5-4)

ε_x - the mesh non-uniformity parameter in the x-direction (7.1-6)

ε_y - the mesh non-uniformity parameter in the y-direction (4.3-1)

k - a constant (5.6-1)

μ - the viscosity (usually laminar)

μ_{eff} - the effective viscosity ($\equiv \mu + \mu_{turb}$)

μ_{turb} - the turbulent viscosity (5.3-3)

ρ - the density

σ - the Prandtl/Schmidt number

σ_{eff} - the effective Prandtl/Schmidt number (5.5-3)

σ_{turb} - the turbulent Prandtl/Schmidt number (5.5-2)

τ - the shear-stress in a Couette flow (3.2-3)

τ_{ij} - a component of the shear-stress in the general cartesian space (2.1-4)

τ_s - the skin friction (2.2-4)

τ_{xy}, τ_{yx} - the only non-zero shear-stress component in a plane flow (2.3-5)

ϕ - a conserved property

ϕ_+ - $\phi \sqrt{\tau_s \rho} / J_s$, in Couette flows (5.6-35)

ϕ_j - ϕ at a point j (4.5-1)

ϕ_{max} - the maximum absolute value of ϕ in the control volume in sections 3.4 and 4.6 (3.4-2)

- the ϕ-value on the center of a thermal wake, in section 4.4 (4.4-1)

ϕ_o - the value of ϕ at the source (4.4-1)

ϕ_s - the value of ϕ on a solid surface

ψ - the stream function (2.1-7)

ψ_F - ψ on the upstream boundary of the control volume in the impinging jet (7.1-4)

ψ_T - ψ on the top wall of a Couette flow (4.1-5)

ω - the vorticity (2.1-6)

ω_F - ω on the upstream boundary of the control volume in the impinging jet (7.1-3)

ω_T - ω on the top wall of the Couette flow (4.1-4)

Subscripts

C - in the nozzle of the impinging jet

F - in the upstream side of the control volume in the impinging jet

eff - effective, i.e. including laminar and turbulent contribution

n - after the n^{th} iteration

- sometimes, normal to

S - on a solid surface

s - slip value

T - on the top wall of a Couette flow

P,E,W,N,S - at the corresponding mesh points; P stands for the central point, and E,W,N,S stand for east, west, north and south respectively; (see fig 3.1-1)

$(\underline{\ })$ - designates a vector

$+$ - designates values non-dimensionalised by the shear velocity ($\sqrt{\tau_s/\rho}$) in a Couette flow

Upscripts

$\bar{(\ )}$ - the time-averaged part of

$(\ )'$ - the fluctuating part of

9.2 FORTRAN symbols

There are too many FORTRAN symbols to explain; therefore only the more important ones were included in the following list. Symbols which are not explained are usually dummy or local ones, and their meaning will become clear after inspection of the neighbouring statements. In some cases symbols are defined in specification statements without being used inside the programme; such symbols are not included in the following list.

Symbol	Meaning
A(I,J,K)	an array containing all the dependent variables, with I and J denoting the location in the x and y direction respectively and K denoting the variable
ADNM	the denominator in eqn (3.1-1)
AM(K)	an array containing the maximum value of A(I,J,K) for all I's and J's
ANAME(6,K)	an array containing a thirty six letter description of each of the variables denoted by K
ANUM	the numerator in eqn (3.1-1)
ASYMBOL(K)	an array containing a four letters name for each of the variables denoted by K
ATITLE(19)	an array containing a 114-letters heading for the problem

AU	the contribution of convection to ANUM, as defined in eqn (3.1-3)
A1	the rate of spread of the free jet in eqn (7.1-2)
A2	the constant in the free jet velocity decay equation (7.1-1)
C(I)	the s-function of eqn (3.2-13)
CA(I)	the turbulence-energy augmentation parameter as defined in eqn (6.4-1)
CC	the convergency criterion in eqn (3.4-2)
CE	the coefficient c_E in eqn (3.1-2)
CF(I)	the skin friction coefficient τ_S / u^2
CL1	the proportionality constant between the length scale and the width of the free jet
CL2	the proportionality constant between the turbulence energy and the square of the maximum velocity in the free jet
CMAX	the C(I)-value corresponding to a non-diffusional flow
CN	the coefficient c_N in eqn (3.1-1)
CS	the coefficient c_S in eqn (3.1-1)
CW	the coefficient c_W in eqn (3.1-1)
C2	the constant A_D in eqn (5.4-6)
C3	the constant A_μ in eqn (5.4-5)

DE,DN,DP,DS,DW

the coefficients Γ_E, Γ_N, Γ_P, Γ_S, Γ_W in section A.2-5

DFE, DFN,DFS,DFW

the coefficients a_E, a_N, a_S, a_W in eqn (3.1-3)

DV11 $\partial u/\partial x$

DV12 $\partial u/\partial y$

DV21 $\partial v/\partial x$

DV22 $\partial v/\partial y$

EX the mesh non-uniformity parameter in the x direction as defined in eqn (7.1-6)

EY the mesh non-uniformity parameter in the y direction as defined in eqn (4.3-1)

HE $x_{i+1}-x_i$

HN $y_{j+1}-y_j$

HS y_j-y_{j-1}

HW x_i-x_{i-1}

H1 $x_{i+1}-x_{i-1}$

H2 $y_{j+1}-y_{j-1}$

IE the number of conserved property equations to be solved

IFREE the index I, in the x-direction, of the mesh point on the edge of the free jet on the upstream boundary of the control volume

ILINE — the running number of lines already written since the last change in the index J

IN — the number of mesh points in the x-direction

INM — IN-1

IPAGE — the running number of lines already written from the beginning of the page

IPT — a control index for subroutine OUT specifying the form of the output listing

IV — the number of variables in the array A

JN — the number of mesh points in the y-direction

JNM — JN-1

NI(N) — an array containing output control information; when NITER equals NI(N) an output listing is generated

NITER — the running number of iterations

NMAX — the maximum permissible number of iterations

NPRIN — the number of variables for which an output listing is prepared

NDP,NF,NG1,NG2,NHS,NK,NML,NMU,NP,NRO,NT,NV1,NV2,NW — the index number of the following variables: dynamic pressure, stream function, mass velocity in the x-direction, mass velocity in the y-direction, conserved property, turbulence energy, length scale, turbulent viscosity, static pressure, density, shear stress, velocity in the x-direction, velocity in the y-direction, vorticity

PP,PP(I),PP(J)
: the pressure gradient

PR(N,K)
: an array containing the Prandtl numbers; N=1 corresponds to the laminar Prandtl number and N=2 corresponds to the turbulent Prandtl number

R(I)
: R, the turbulence Reynolds number of eqn (5.4-2),

REK
: the same as R(I)

RES
: the maximum absolute value of the convergency parameter r_u as defined by eqn (4.6-1), for all variables

ROC
: the nozzle density

RSDU(K)
: the maximum absolute value of the convergency parameter, r_u, as defined by eqn (4.6-1), for the variable with the index K

S(I)
: the S-function of eqn (3.2-18)

SIG
: the laminar Prandtl number

SIGO
: the turbulent Prandtl number

SOURCE
: the source term, S_{u_i}, in eqn (3.1-1)

ST(I)
: the Stanton number, S_t

T(I)
: the wall shear stress

TW
: the wall temperature

UC
: the nozzle velocity

XC
: half of the nozzle width

XG
: the half-jet width on the upstream boundary of the control volume

XM	the maximum permissible value of x
X1(I)	an array containing the x-coordinates of the mesh points
X2(J)	an array containing the y-coordinate of the mesh points
YC	the distance from the nozzle to the surface
YF	the distance from the nozzle to the upstream boundary of the control volume
ZA	the constant c_D of eqn (5.3-8)
ZB	the P-function of eqn (5.6-36)
ZC	the constant c of eqn (5.3-3)
ZCU	the contribution of convection to ADNM as defined in eqn (3.1-4)
ZJ(I)	the wall heat flux
ZL	the turbulence length scale for viscosity near the wall
ZLP	the turbulence length scale away from the wall
ZL3	the turbulence length scale for dissipation near the wall
ZK(I)	the K-function of eqn (6.2-1)
ZMU	the laminar viscosity
ZQ	that part of the source term which is a linear function of A(I,J,K) and may therefore be transferred from ANUM to ADNM

10. References

Alder B., Fernbach S. and Rotenberg M. (1964): "Methods in computational physics", volume 3, "Fundamental methods in hydrodynamics", Academic Press, New York and London.

Barakat H.Z. and Clark J.A. (1965): "Transient natural convection flows in closed containers", Univ. of Michigan, Mech. Eng. Dept., Heat Transfer Laboratory, Tech. Report No.2.

Burgraff O.R. (1966): "Analytical and numerical studies of the structure of steady separated flows", J. Fluid Mech., 24, 1, pp. 113-151.

Carmody T. (1964): "Establishment of the wake behind a disc", ASME Trans., J. of Basic Eng., pp. 869-882.

Chung P.M. and Viegas J.R. (1961): "Heat transfer at the reattachment zone of separated laminar boundary layers", NASA TN D-1072.

van Driest E.R. (1956): "On turbulent flow near a wall", J. Aero. Sci., 23, p. 1007.

Emmons H.W. (1954): "Shear flow turbulence", Proc. 2nd U.S. National Congress App. Mech., ASME.

Gardon R. and Akifrat J.C. (1965): "The role of turbulence in determining the heat transfer characteristics of impinging jets", Int. J. Heat Mass Transfer.

Glaser H. (1961): "Experimentelle Untersuchungen auf dem Gebiet der Wärme- und Stoffübertragung", Chemie-Ing.-Techn., 33, 3, pp. 146-155.

Glushko G.S. (1965): "Turbulent boundary layer on a flat plate in an incompressible fluid", (in Russian), Izv. Akad. Nauk SSSR, Mekh. No. 4, p. 13.

Golden J.T. (1965): "FORTRAN IV programming and computing", Prentice-Hall Inc., New Jersey.

Heskestad G. (1965): "Hot wire measurements in a plane turbulent jet", ASME Trans., J. App. Mech., paper No. 65-APM-H.

Kolmogorov A.N. (1942):

Izv. Akad. Nauk SSSR ser. phys. No. 1-2.

Kroger M. and Krizek F. (1966): "Mass-transfer coefficient in impingement flow from slotted nozzles", Int. J. Heat Mass Transfer, 9, pp. 1-8.

Metzger D.E. (1962): "Spot cooling and heating of surfaces with high velocity impinging air jets", Stanford Univ., Mech. Eng. Dept., Tech. Report No.52.

Patankar S.V. (1966): "Wall-shear-stress and heat-flux laws for turbulent boundary layers with pressure gradient: use of van Driest's eddy-viscosity hypothesis", Imperial College, Mech. Eng. Dept., Report No. TWF/TN/14.

Patankar S.V. (1967): "Heat and mass transfer in turbulent boundary layers", Imperial College, Mech. Eng. Dept., Report No. TWF/R/5.

Patankar S.V. and Spalding D.B. (1967): "A finite difference procedure for solving the equations of the two-dimensional boundary layer", Int. J. Heat Mass Transfer.

Patankar S.V. and Wolfshtein M. (1966): "A computer programme for hydrodynamic and heat-transfer calculations of turbulent boundary layer and wall jets", Imperial College, Mech. Eng. Dept., Report No. TWF/TN/16.

Poland R.A. (1967): "A normal impingement of an axially-symmetrical turbulent free jet on to a flat surface", Imperial College, Mech. Eng. Dept., M.Sc. Thesis.

Poreh M., Tsuei Y.G., and Cermak J.E. (1967): "Investigation of a turbulent radial wall jet", ASME Trans., J. App. Mech., paper No. 67-APM-10.

Prandtl L. (1925): "Bericht über Untersuchungen zur ausgebildeten Turbulenz", ZAMM, 5, p. 136.

Prandtl L. (1945): "Über ein neues Formelsystem für die ausgebildete Turbulenz", Nachrichten von der Akad. der Wissenshaften in Göttingen, pp. 6-19, Van den Loeck of Ruprecht, Göttengen.

Pun W.M. and Spalding D.B. (1967): "A procedure for predicting the velocity and temperature distribution in a confined, steady, turbulent, gaseous diffusion flame", Imperial College, Mech. Eng. Dept., Report No. SF/TN/11.

Runchal A.K., Spalding D.B., and Wolfshtein M. (1967): "The numerical solution of the elliptic equations for transport of vorticity, heat and matter in two-dimensional flows", Imperial College, Mech. Eng. Dept., Report No. SF/TN/2.

Runchal A.K. and Wolfshtein M. (1966): "A finite-difference procedure for the integration of the Navier-Stokes equations", Imperial College, Mech. Eng. Dept., Report No. SF/TN/1.

Runchal A.K. and Wolfshtein M. (1967): "A FORTRAN IV computer programme for the solution of the steady-state, two-dimensional equations of motion, energy and concentration", Imperial College, Mech. Eng. Dept., Report No. SF/TN/10.

Schauer J.J. and Eustis R.H. (1963): "The flow development and heat transfer characteristics of plane turbulent impinging jet", Stanford Univ., Mech. Eng. Dept., Tech. Rep. No.3.

Schlichting H. (1960): "Boundary layer theory", 4th Ed., McGraw-Hill, New York.

Spalding D.B. (1967a): "Heat transfer from turbulent separated flows", J. Fluid Mech., 27, 1, pp. 97-109.

Spalding D.B. (1967b): "Notes on the solution of the Navier-Stokes equations for steady, two-dimensional turbulent flow by numerical techniques", Imperial College, Mech. Eng. Dept., Report No. SF/TN/5.

Spalding D.B. (1967c): "Monograph on turbulent boundary layers", Chapter 2, Imperial College, Mech. Eng. Dept., Report No. TWF/TN/33.

Spalding D.B. (1967d): "The calculation of the length scale of turbulence in some turbulent boundary layers remote from walls", Imperial College, Mech. Eng. Dept., Report No. TWF/TN/31.

Spalding D.B. and Jayatillaka C.L.V. (1964): "A survey of theoretical and experimental information on the resistance of the laminar sub-layer to heat and mass transfer", Proc. 2nd All-Union Conf. on Heat Transfer, Minsk, B.S.S.R., U.S.S.R.

Strand T.(1962): "Inviscid-incompressible-flow of static two-dimensional solid jets in proximity to the ground", J. Aero. Sci., 29, 2, pp. 170-173.

Sutera S.P., Maeder P.F. and Kestin J. (1963): "On the sensitivity of heat transfer in the stagnation-point boundary layer to free-stream vorticity", J. Fluid Mech., 16, pp. 497-519.

Thom A. (1933): "The flow past circular cylinders at low speeds", Proc. Roy. Soc., London, A 141, p. 651.

Townsend A.A. (1961): "Equilibrium layers and wall turbulence", J. Fluid Mech., 11, p. 97.

Wolfshtein M. (1966): "Empirical correlations for the evaluation of Stanton number in impinging jets", ARC 27613, HMT 92.

Wolfshtein M. (1967): "The numerical solution of the equations of flow in the initial region of a wall jet", Imperial College, Mech. Eng. Dept., Report No. SF/TN/7.

Part VI : Appendices

Appendix A.1 : The derivation of the vorticity equation

Introduction: The purpose of the present section is to derive the equation for the conservation of vorticity, by elimination of the pressure from the equations for the conservation of momentum. The treatment will be restricted to steady, incompressible, variable viscosity, plane flow.

The momentum equations: Equations (2.1-1) and (2.1-2) may be explicitly written for plane flow as

$$\frac{\partial u}{\partial x} + \frac{\partial v}{\partial y} = 0 \qquad \text{(A.1-1)}$$

$$\rho u \frac{\partial u}{\partial x} + \rho v \frac{\partial u}{\partial y} + \frac{\partial p}{\partial x} = \frac{\partial \tau_{xx}}{\partial x} + \frac{\partial \tau_{xy}}{\partial y} \qquad \text{(A.1-2)}$$

$$\rho u \frac{\partial v}{\partial x} + \rho v \frac{\partial v}{\partial y} + \frac{\partial p}{\partial y} = \frac{\partial \tau_{yx}}{\partial x} + \frac{\partial \tau_{yy}}{\partial y} \qquad \text{(A.1-3)}$$

where by (2.1-4)

$$\tau_{xx} = 2\mu_{eff} \frac{\partial u}{\partial x} \qquad \text{(A.1-4)}$$

$$\tau_{yy} = 2\mu_{eff} \frac{\partial v}{\partial y} \qquad \text{(A.1-5)}$$

$$\tau_{xy} = \tau_{yx} = \mu_{eff} \left(\frac{\partial u}{\partial y} + \frac{\partial v}{\partial x} \right) \qquad \text{(A.1-6)}$$

Rearrangement of the equations. Now we introduce the vorticity, which was defined as

$$\omega = \frac{\partial v}{\partial x} - \frac{\partial u}{\partial y} \qquad (2.1\text{-}6)$$

By the use of this definition, and eqns (A.1-1), (A.1-4), (A.1-5) and (A.1-6), we may rearrange eqns (A.1-2) and (A.1-3), to get:

$$\frac{1}{2}\rho\frac{\partial V^2}{\partial x} - \rho v\omega + \frac{\partial p}{\partial x} = 2\frac{\partial}{\partial x}\left(\mu_{eff}\frac{\partial u}{\partial x}\right) + \frac{\partial}{\partial y}\left[\mu_{eff}\left(2\frac{\partial v}{\partial x} - \omega\right)\right] \qquad (A.1\text{-}7)$$

and

$$\frac{1}{2}\rho\frac{\partial V^2}{\partial y} + \rho u\omega + \frac{\partial p}{\partial y} = 2\frac{\partial}{\partial y}\left(\mu_{eff}\frac{\partial v}{\partial y}\right) + \frac{\partial}{\partial x}\left[\mu_{eff}\left(2\frac{\partial u}{\partial y} + \omega\right)\right] \qquad (A.1\text{-}8)$$

where $$V^2 = u^2 + v^2 \qquad (2.3\text{-}3)$$

Elimination of the pressure: In order to get the vorticity equation, we differentiate eqn (A.1-8) with respect to x, and subtract from it the derivative of eqn (A.1-7) with respect to y. The result is

$$\rho\frac{\partial(u\omega)}{\partial x} + \rho\frac{\partial(v\omega)}{\partial y} = \frac{\partial^2}{\partial x^2}\left[2\mu_{eff}\frac{\partial v}{\partial y} + \mu_{eff}\omega\right]$$

$$+ \frac{\partial^2}{\partial x\partial y}\left[2\mu_{eff}\left(\frac{\partial v}{\partial y} - \frac{\partial u}{\partial x}\right)\right] - \frac{\partial^2}{\partial y^2}\left[2\mu_{eff}\frac{\partial v}{\partial x} - \mu_{eff}\omega\right] \qquad (A.1\text{-}9)$$

Eqn (A.1-9) can be rearranged, by the use of (A.1-1), as

$$\rho u\frac{\partial\omega}{\partial x} + \rho v\frac{\partial\omega}{\partial y} = \left(\frac{\partial^2}{\partial x^2} + \frac{\partial^2}{\partial y^2}\right)\left(\mu_{eff}\omega\right) + 2\left[2\frac{\partial v}{\partial y}\frac{\partial^2\mu}{\partial x\partial y} + \frac{\partial u}{\partial y}\frac{\partial^2\mu}{\partial x^2} - \frac{\partial v}{\partial x}\frac{\partial^2\mu}{\partial y^2}\right]$$

(A.1-10)

or, simply

$$\rho u \frac{\partial \omega}{\partial x} + \rho v \frac{\partial \omega}{\partial y} = \nabla^2 (\mu_{eff} \omega) + S_\omega \qquad \text{(A.1-11)}$$

where

$$S_\omega = 2\left(2 \frac{\partial v}{\partial y} \frac{\partial^2 \mu}{\partial x \partial y} + \frac{\partial u}{\partial y} \frac{\partial^2 \mu}{\partial x^2} - \frac{\partial v}{\partial x} \frac{\partial^2 \mu}{\partial y^2}\right) \qquad \text{(A.1-12)}$$

Clearly, when the viscosity is uniform S_ω is zero; it may be easily shown that, in a boundary layer, S_ω may be neglected as well.

Appendix A.2 : The derivation of the finite-difference ϕ-conservation equation

A.2.1 : Purpose

In this appendix we shall be concerned with the derivation of the finite-difference counterpart of the equation

$$\rho u \frac{\partial \phi}{\partial x} + \rho v \frac{\partial \phi}{\partial y} = \frac{\partial}{\partial x}\left[\Gamma \frac{\partial}{\partial x}(\mu \phi)\right] + \frac{\partial}{\partial y}\left[\Gamma \frac{\partial}{\partial y}(\mu \phi)\right] + S \qquad \text{(A.2-1)}$$

which is the two-dimensional form of eqn (2.1-12). In eqn A.2-1 ϕ is the dependent variable and x and y are the independent variables; ρ, u, v, Γ, μ and S are arbitrary functions of ϕ, x and y. We shall not derive the finite-difference equation by a Taylor series expansion of eqn (A.2-1), as is, perhaps, more customary. Instead, we shall integrate eqn (A.2-1) over small control volumes. The advantages of such a treatment are (i) that it is more transparent physically, (ii) that we are more free to opt between various assumptions, and (iii) that we may rely on our understanding of the process when making these assumptions. All the points will become clearer later.

It will be more convenient to rearrange eqn (A.2-1). By the use of the continuity equation

$$\frac{\partial}{\partial x}(\rho u) + \frac{\partial}{\partial y}(\rho v) = 0 \qquad \text{(A.2-2)},$$

and after a small rearrangement, we get

$$\frac{\partial}{\partial x}\left[\rho u\phi - \Gamma \frac{\partial}{\partial x}(\mu\phi)\right] + \frac{\partial}{\partial y}\left[\rho v\phi - \Gamma \frac{\partial}{\partial y}(\mu\phi)\right] = S \qquad \text{(A.2-3)}$$

A.2.2 : The model

In fig A.2-1 a mesh point P is shown, which is surrounded by the four points N, S, E, W. The four points n, s, e, w are positioned halfway between P and N, S, E, W respectively. The control volume is the dotted quadrangle, with sides parallel to the x and y axes, and passing through the points n, s, e, w. We note that the points N, NE, E, SE, S, SW, W, NW are mesh points, where ϕ, ρ, u, v, Γ, μ, and S are known. But all these quantities are usually unknown in the points n, ne, e, se, s, sw, w, nw.

During the treatment we shall have to make assumptions on the distribution of some quantities. We shall list these assumptions here, as follows:

(i) Inside the control volume the ϕ-distribution is uniform, i.e.

$$\phi = \phi_p \qquad \text{(A.2-4)}$$

(ii) On the boundaries of the control volume the spatial derivatives are given by

$$\left(\frac{\partial(\phi\mu)}{\partial x}\right)_{x=x_w} = \frac{(\mu\phi)_p - (\mu\phi)_w}{y_p - y_w} \qquad \text{(A.2-5)}$$

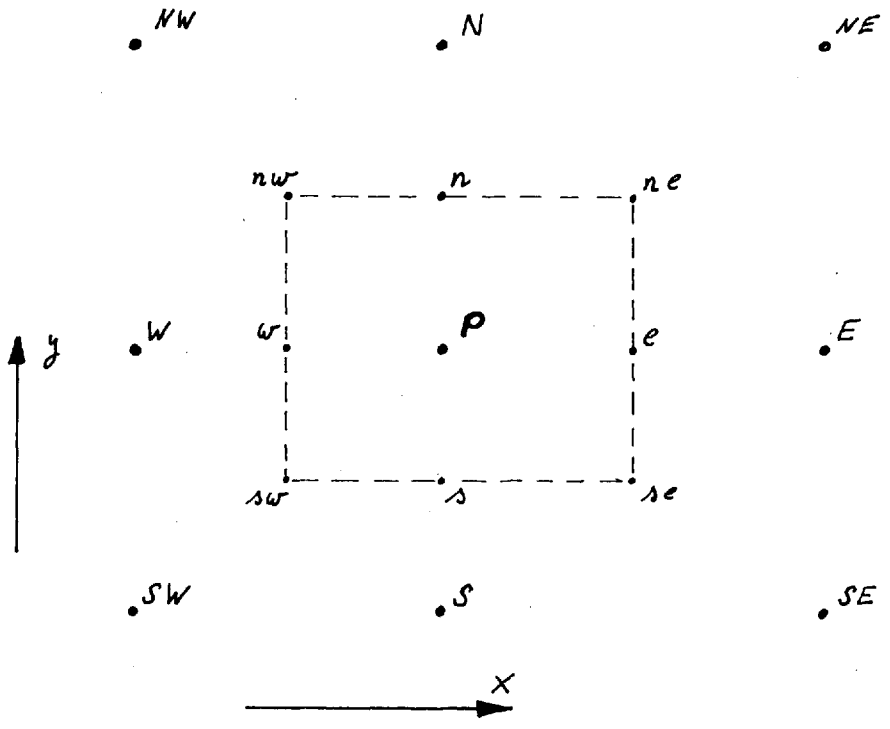

FIG A.2-1 : THE CONTROL VOLUME

$$\left(\frac{\partial(\phi\mu)}{\partial x}\right)_{x=x_e} = \frac{(\mu\phi)_E - (\mu\phi)_P}{y_E - y_P} \qquad \text{(A.2-6)}$$

$$\left[\frac{\partial(\mu\phi)}{\partial y}\right]_{y=y_s} = \frac{(\mu\phi)_P - (\mu\phi)_S}{y_P - y_S} \qquad \text{(A.2-7)}$$

$$\left[\frac{\partial(\mu\phi)}{\partial y}\right]_{y=y_N} = \frac{(\mu\phi)_N - (\mu\phi)_P}{y_N - y_P} \qquad \text{(A.2-8)}$$

(iii) In the corners of the control volume

$$4\psi_{nw} = \psi_{NW} + \psi_N + \psi_P + \psi_W \qquad \text{(A.2-9)}$$

$$4\psi_{sw} = \psi_{SW} + \psi_S + \psi_P + \psi_W \qquad \text{(A.2-10)}$$

$$4\psi_{se} = \psi_{SE} + \psi_S + \psi_P + \psi_E \qquad \text{(A.2-11)}$$

$$4\psi_{ne} = \psi_{NE} + \psi_N + \psi_P + \psi_E \qquad \text{(A.2-12)}$$

(iv) On the boundaries of the control volume

$$2\Gamma_w = \Gamma_P + \Gamma_W \qquad \text{(A.2-13)}$$

$$2\Gamma_e = \Gamma_P + \Gamma_E \qquad \text{(A.2-14)}$$

$$2\Gamma_n = \Gamma_P + \Gamma_N \qquad \text{(A.2-15)}$$

$$2\Gamma_s = \Gamma_P + \Gamma_S \qquad \text{(A.2-16)}$$

A.2.3 : First integration

Our task is to integrate eqn (A.2-3) over the control volume shown in fig A.2-1. Let us then do it formally:

$$\int_{y_s}^{y_n}\int_{x_w}^{x_e}\left[\frac{\partial}{\partial x}\left\{\rho u\phi - \Gamma\frac{\partial}{\partial x}(\mu\phi)\right\}\right]dx\,dy$$

$$+\int_{x_w}^{x_e}\int_{y_s}^{y_n}\left[\frac{\partial}{\partial y}\left\{\rho v\phi - \Gamma\frac{\partial}{\partial y}(\mu\phi)\right\}\right]dx\,dy = \int_{x_w}^{x_e}\int_{y_s}^{y_n} S\,dx\,dy \qquad \text{(A.2-17)}$$

We immediately see that each of the expressions on the left-hand side of eqn (A.2-17) can be integrated once exactly over either x or y. Such integration will yield

$$\int_{y_s}^{y_n}\left[\left\{\rho u\phi - \Gamma\frac{\partial(\mu\phi)}{\partial x}\right\}_e - \left\{\rho u\phi - \Gamma\frac{\partial(\mu\phi)}{\partial x}\right\}_w\right]dy$$

$$+\int_{x_w}^{x_e}\left[\left\{\rho v\phi - \Gamma\frac{\partial(\mu\phi)}{\partial y}\right\}_n - \left\{\rho v\phi - \Gamma\frac{\partial(\mu\phi)}{\partial y}\right\}_s\right]dx = \int_{x_w}^{x_e}\int_{y_s}^{y_n} S\,dx\,dy \qquad \text{(A.2-18)}$$

Generally, this is as far as we may proceed with exact integration. There are, however, some particular cases, when S is expressed in terms of x and y, or spatial derivatives of ϕ. In such cases we shall be able to carry out an exact integration on the right-hand side of eqn (A.2-18) as well. Still, we shall not include such cases in the present treatment, and therefore we can not proceed any more without applying our assumed distributions of section A.2.2.

A.2.4 : Integration and rearrangement of the convective terms

The convective terms are all those terms, in the left-hand side of eqn (A.2-18), which contain either u or v. Let us consider the first of them

$$\int_{y_s}^{y_n} (\rho u \phi)_e \, dy$$

Very clearly, this represents the complete ϕ flux into the control volume over the boundary se-e-ne. Therefore, if ϕ and γ are well-behaved functions, it may be written as

$$\int_{y_s}^{y_n} (\rho u \phi)_e \, dy = \phi_e \, (\gamma_{ne} - \gamma_{se}) \qquad \text{(A.2-19)}$$

where $(\gamma_{ne} - \gamma_{se})$ is the total mass flow into the control volume from direction E, and ϕ_e is the mean value of ϕ in this flow. But, before we determine the value of ϕ_e, let us write, on the basis of exactly similar arguments, the complete convective part of eqn (A.2-18) as

$$\phi_e (\gamma_{ne} - \gamma_{se}) - \phi_w (\gamma_{nw} - \gamma_{sw}) + \phi_n (\gamma_{ne} - \gamma_{nw}) - \phi_s (\gamma_{se} - \gamma_{sw}) \qquad \text{(A.2-20)}$$

Now, we shall try to determine what ϕ_e is. If we consult fig A.2-1, we see that when $\gamma_{ne} - \gamma_{se} > 0$ the flow direction is from P to E. But because of our assumed ϕ-distribution, eqn (A.2-4), we must then deduce that

in this case $\phi_e = \phi_P$. And similarly, if $\psi_{ne} - \psi_{se} < 0$, $\phi_e = \phi_E$. These assessments may be written in the form of the following equation:

$$\phi_e(\psi_{ne} - \psi_{se}) = \frac{\phi_P}{2}\left\{(\psi_{ne} - \psi_{se}) + |\psi_{ne} - \psi_{se}|\right\} + \frac{\phi_E}{2}\left\{(\psi_{ne} - \psi_{se}) - |\psi_{ne} - \psi_{se}|\right\} \tag{A.2-21}$$

Similar arguments hold for the other convective terms, and therefore we may replace eqn (A.2-20) by

$$a_E \phi_E + a_W \phi_W + a_N \phi_N + a_S \phi_S - \phi_P (a_E + a_W + a_N + a_S) \tag{A.2-22}$$

where

$$2a_E = +(\psi_{ne} - \psi_{se}) - |\psi_{ne} - \psi_{se}| \tag{A.2-23}$$

$$2a_N = -(\psi_{ne} - \psi_{nw}) - |\psi_{ne} - \psi_{nw}| \tag{A.2-24}$$

$$2a_W = -(\psi_{nw} - \psi_{sw}) - |\psi_{nw} - \psi_{sw}| \tag{A.2-25}$$

$$2a_S = +(\psi_{se} - \psi_{sw}) - |\psi_{se} - \psi_{sw}| \tag{A.2-26}$$

$$2b_E = +(\psi_{ne} - \psi_{se}) + |\psi_{ne} - \psi_{se}| \tag{A.2-27}$$

$$2b_N = -(\psi_{ne} - \psi_{nw}) + |\psi_{ne} - \psi_{nw}| \tag{A.2-28}$$

$$2b_W = -(\psi_{nw} - \psi_{sw}) + |\psi_{nw} - \psi_{sw}| \tag{A.2-29}$$

$$2b_S = +(\psi_{se} - \psi_{sw}) + |\psi_{se} - \psi_{sw}| \tag{A.2-30}$$

and γ_{ne} , etc. are given by eqns (A.2-9) to (A.2-12). A very straightforward addition shows that

$$a_E + a_W + a_N + a_S = b_E + b_W + b_N + b_S \qquad \text{(A.2-31)}$$

and therefore, we may finally write the convective terms as

$$a_E \phi_E + a_W \phi_W + a_N \phi_N + a_S \phi_S - \phi_P (a_E + a_W + a_N + a_S) \qquad \text{(A.2-32)}$$

A.2.5 : Integration and rearrangement of the diffusional and source terms

The diffusional terms are all those terms, in eqn (A.2-18) which contain Γ and μ. When we substitute the Γ values, from eqn (A.2-13) to (A.2-16), and the $(\mu\phi)$ derivatives, from eqns (A.2-5) to (A.2-8), the diffusional part becomes:

$$C_E(\mu\phi)_E + C_W(\mu\phi)_W + C_N(\mu\phi_N) + C_S(\mu\phi)_S - (C_E + C_W + C_N + C_S)(\mu\phi)_P \qquad \text{(A.2-33)}$$

where

$$C_E = \frac{\Gamma_e (y_n - y_s)}{x_E - x_P} = \frac{(\Gamma_E + \Gamma_P)(y_N - y_S)}{4(x_E - x_P)} \qquad \text{(A.2-34)}$$

$$C_W = \frac{\Gamma_w (y_n - y_s)}{x_P - x_W} = \frac{(\Gamma_W + \Gamma_P)(y_N - y_S)}{4(x_P - x_W)} \qquad \text{(A.2-35)}$$

$$C_N = \frac{\Gamma_n (x_e - x_w)}{y_N - y_P} = \frac{(\Gamma_N + \Gamma_P)(x_E - x_W)}{4(y_N - y_P)} \qquad \text{(A.2-36)}$$

$$C_s = \frac{\Gamma_s (x_e - x_w)}{y_p - y_s} = \frac{(\Gamma_s + \Gamma_p)(x_E - x_w)}{4(y_p - y_s)} \qquad \text{(A.2-37)}$$

Considering the source term, we may write

$$\int_{x_w}^{x_e}\int_{y_s}^{y_n} S \, dx \, dy = S_p (y_n - y_s)(x_e - x_w) = \frac{S_p (Y_N - Y_s)(X_E - X_w)}{4} = S_{u,p} \qquad \text{(A.2-38)}$$

A.2.6 : The final equation

Now we substitute the convective terms, eqn (A.2-32), the diffusional terms, eqn (A.2-33), and the source terms, eqn (A.2-38) into eqn (A.2-18). The result is

$$(a_E \phi_E + a_W \phi_W + a_N \phi_N + a_S \phi_S) - (a_E + a_W + a_N + a_S)\phi_P - (C_E \phi_E + C_W \phi_W + C_N \phi_N + C_S \phi_S) + (C_E + C_W + C_N + C_S)\phi_P = S_{u,P} \qquad \text{(A.2-39)}$$

or, after rearrangement

$$\phi_P = \frac{(C_E - a_E)\phi_E + (C_W - a_W)\phi_W + (C_N - a_N)\phi_N + (C_S - a_S)\phi_S + S_{u,P}}{(C_E + C_W + C_N + C_S) - (a_E + a_W + a_N + a_S)} \qquad \text{(A.2-40)}$$

where the a's are given by eqns (A.2-23) to (A.2-26); the c's are given by eqns (A.2-34) to (A.2-37); and $S_{u,P}$ is given by eqn (A.2-38).

Appendix A.3 : The solution of the conservation equation in a one-dimensional flow

In the present appendix, a non-iterative method for the finite-difference solution of the one-dimensional conservation equation will be presented. The method is based on Gauss's elimination technique which, for this particular case, reduces to straightforward recurrence formulae. The same technique was applied by Patankar (1967) to the boundary-layer equations with much success.

In a one-dimensional flow, eqn (A.2-1) of appendix A.2 reduces to

$$\rho u \frac{\partial \phi}{\partial y} = \frac{\partial}{\partial y}\left[\Gamma \frac{\partial \phi}{\partial y}\right] + S \qquad \text{(A.3-1)}$$

where y is the only spatial coordinate and ρ was assumed unity. In these conditions, the finite-difference equation, (A.2-40), reduces to

$$\phi_P = \frac{(C_N - a_N)\phi_N + (C_S - a_S)\phi_S + S_{P,u}}{(C_N + C_S) - (a_N + a_S)} \qquad \text{(A.3-2)}$$

If we now devise a one-dimensional mesh with N mesh points, we may now replace eqn (A.3-2) by

$$\phi_n = a_n \phi_{n+1} + b_n \phi_{n-1} + c_n \qquad \text{(A.3-3)}$$

where

$$a_n = \frac{C_{n+1} - a_{n+1}}{(C_{n+1} + C_{n-1}) - (a_{n-1} + a_{n-1})} \qquad \text{(A.3-4)}$$

$$b_n = \frac{c_{n-1} - a_{n-1}}{(c_{n-1} + c_{n-1}) - (a_{n-1} + a_{n-1})} \qquad \text{(A.3-5)}$$

$$c_n = \frac{S_n}{(c_{n-1} + c_{n-1}) - (a_{n-1} - a_{n-1})} \qquad \text{(A.3-6)}$$

It may be shown that, for this simple set of equations, the Gauss elimination yields

$$\phi_n = A_n \phi_{n-1} + B_n \qquad \text{(A.3-7)}$$

where, for $2<n<N$

$$A_n = \frac{a_n A_{n-1}}{A_{n-1} - b_n} \qquad \text{(A.3-8)}$$

$$B_n = \frac{A_{n-1}(b_n B_{n-1} + c_n)}{A_{n-1} - b_n} \qquad \text{(A.3-9)}$$

and

$$A_2 = a_2 \qquad \text{(A.3-10)}$$

$$B_2 = b_2 \phi_1 + c_2 \qquad \text{(A.3-11)}$$

So, we first compute A_n and B_n, going from n = 2 to n = N-1, and then we compute ϕ_n, going backwards from n=N-1 to n=2. It will be noted, that if a_n, b_n and c_n are not expressed in terms of ϕ, no iterations are necessary, and the solution is exact, to any degree of accuracy which the computer may yield.

Appendix A.4 : The computer programme for the impinging jet

Following is the listing of the computer programme which was used for the computations of the turbulent impinging jet. The important symbols are explained in section 9.2, and a flow diagram of the programme is shown in fig 3.4-1. Computer-control statements have been removed from the listing. The underlined names preceding each sub-programme are the subroutines names as used in fig. 3.4-1. The respective role of the various sub-programmes are:

HEAD : initiates the computations and controls the iterative cycle

INPDAT: supplies all necessary constants

INIT: generates the mesh distribution, initial values and boundary conditions

VROMU: computes the velocity components, the dynamic pressure and the turbulent visoosity

EQN: performs the finite-difference process in the internal mesh points

BOU: computes boundary values and wall fluxes

OUT: produces output listings

PRES: computes the static pressure in the internal mesh points

HEAD

```
      COMMON /CVRBLE/ A(14,16,14),X1(14),X2(16),IMIN(16),IMAX(16),RP(4),
     1   PR(2,4),IN,JN,IE,IV,IR
      COMMON /CNUMBR/NW,NF,NK,NHS,NVT,NML,NMH,NP,NG1,NG2,NMU,NRO
      COMMON /CN2/ NV1,NV2,NDP,NT
      COMMON/C/ANAME(6,14),ASYMBL(14),NI(50),NPRIN,INDG,CC,NMAX,INM,JNM
      COMMON /CPROP/ ZMU,ROG,TG,TW
      COMMON /CBOU/ ROC,TC,UC,ZKC,YC,XC,XM,EX,EY,IFREE
      COMMON /CTURB/ ZA,ZB,ZC,C1,C2,C3,ZLP
      COMMON SV,SHS,CF(41),ST(41)
      COMMON /CB1/ R(21),C(21),S(21),ZK(21),T(21),ZJ(21)
      DIMENSION RSDU(10),AM(10),ATITLE(19),FHS(81)
      DATA AM/10*10000./
      IPT=1
      IF (IN.GT.14) IPT=3
      READ (5,100) ATITLE
  100 FORMAT (12A6)
      WRITE (6,101) ATITLE,((ANAME(L,K),L=1,6),K=1,IE)
  101 FORMAT (12H1SOLUTION OF/1H0,19A6,3HFOR/(1H0,10X,6A6/))
      WRITE (6,102) NMAX,CC,IN,JN
  102 FORMAT (6HONMAX=,I4,3X,3HCC=,1PE11.4,3X,3HIN=,I3,3HJN=,I3)
      DO 200 K=1,IV
      DO 200 I=1,IN
      DO 200 J=1,JN
      A(I,J,K)=0.
  200 CONTINUE
      DO 201 I=1,IN
      DO 201 J=1,JN
      A(I,J,NRO)=ROC
  201 CONTINUE
      C1=PR(1,NHS)/PR(2,NHS)
      ZB=9.24*(C1**0.75-1.)*(1.+0.28*EXP(-0.007*C1))
      CALL INIT  (A,IMIN,IMAX,IN,JN,IE,IV,IPT,X1,X2)
  109 SV=0.
      RESSHS=0.
      RESSV=0.
      SHS=0.
      N=1
      NITER=1
      WRITE (6,103)
  103 FORMAT (1H1,3X,1HN,9X,5HRSTRM,7X,5HRVORT,7X,5HRESSV,8X,2HSV8X,4HRK
     1EN,14X,4HRENT,7X,6HRESSHS,7X,3HSHS)
1     CONTINUE
      CALL VROMU (A,IMIN,IMAX,IN,JN,IE,IV,IPT,X1,X2)
C***
C     THE ITERATION CYCLE
C***
      RES=0.
      SHSO=SHS
      SVO=SV
      DO 2 K=1,IE
```

```
      ES=0.
      RELAX=RP(K)
      CALL EQN (K, ES,RELAX,A,X1,X2,IMIN,IMAX,IN,JN,IE,PR,IV,AM)
      RSDU(K)= ES
    2 IF(ABS(RSDU(K)).GT.ABS(RES))RES=RSDU(K)
      CALL BOU (A,X1,X2,IMIN,IMAX,IN,JN,IE,PR,IV,AM)
      INMM=IN-2
      RESSV=1.-SVO/SV
      IF (IE.LT.NHS) GO TO 7777
      RESSHS=1.-SHSO/SHS
 7777 CONTINUE
      IF (NITER.NE.NI(N)) GO TO 301
      CALL OUT (A,IMIN,IMAX,IN,JN,IE,IV,1,X1,X2)
      WRITE (6,103)
      N=N+1
  301 WRITE (6,104) NITER,RSDU(NF),RSDU(NW),RESSX,SV,RSDU(NK),RSDU(NHS),
     1    RESSHS,SHS
  104 FORMAT (1H ,I5,5X,1P5E12.3,5X,3E12.3)
      IF(NITER.GT.NMAX) GO TO 5
      NITER=NITER+1
      IF(ABS(RES).GT.CC.OR.NITER.LE.5) GO TO 1
      CALL OUT (A,IMIN,IMAX,IN,JN,IE,IV,IPT,X1,X2)
      GO TO 1111
5     WRITE(6,106) NITER
106   FORMAT (32HOTHE PROCESS DID NOT CONVERGE IN,I5,13H   ITERATIONS)
      CALL OUT    (A,IMIN,IMAX,IN,JN,IE,IV,IPT,X1,X2)
1111  CONTINUE
      STOP
      END
```

INPDAT

```
      BLOCK DATA
      COMMON/C/ANAME(6,14),ASYMBL(14),NI(50),NPRIN,INDG,CC,NMAX,INM,JNM
      COMMON /CNUMBR/NW,NF,NK,NHS,NVT,NML,NMH,NP,NG1,NG2,NMU,NRO
      COMMON /CN2/ NV1,NV2,NDP,NT
      COMMON /CVRBLE/ A(14,16,14),X1(14),X2(16),IMIN(16),IMAX(16),RP(4),
     1    PR(2,4),IN,JN,IE,IV,IR
      COMMON /CTURB/ ZA,ZB,ZC,C1,C2,C3,ZLP
      COMMON /CBOU/ ROC,TC,UC,ZKC,YC,XC,XM,EX,EY,IFREE
      COMMON /CPROP/ ZMU,ROG,TG,TW
      COMMON /CIN/ HG,A1,POT,CL1,CL2,A2
      DATA IN,JN/14,16/
      DATA IMIN ,IMAX /16*1,16*14/
       DATA EX,EY /1.1,1.5/
      DATA NW,NF,NK,NHS,NML,NMU,NG1,NG2,NT,NDP,NP,NRO,NV1,NV2/
     1    1,2,3,4,5,6,7,8,9,10,11,12,13,14/
      DATA IE,IV,NPRIN/4,14,11/      ,INDG/1/
      DATA A1,A2,CL1,CL2/0.22,2.35,0.1,0.2/
      DATA NMAX,NI/250,100,200,48*300/    ,CC/0.00001/
      DATA XC,YC,XM,UC,ROC,ZMU,TW
     1    /.0625,.25,.25,1.,1.,.0000114,36./
      DATA PR(1,3),PR(2,3),PR(1,4),PR(2,4)/      1.,2.3,0.71,0.9/
```

```
      DATA ZA,ZC,C2,C3,PR(2,3),PR(2,4)/.416,.220,.263,.0160,1.53,0.9/
      DATA (ASYMBL(I),(ANAME(K,I),K=1,6),I=1,14)/
     1    4HVORT,6HTHE VO,6HRTICIT,6HY      ,6H       ,6H       ,6H       ,
     I    4HSTRM,6HTHE ST,6HREAM F,6HUNCTIO,6HN      ,6H       ,6H       ,
     O    4HKINE,6HTHE TU,6HRBULEN,6HT KINE,6HTIC EN,6HERGY   ,6H       ,
     4    4HTEMP,6HTHE TE,6HMPERAT,6HURE    ,6H       ,6H       ,6H       ,
     4    4HLENG,6HTHE TU,6HRBULEN,6HT SCAL,6HE      ,6H       ,6H       ,
     6    4HTURV,6HTHE TU,6HRBULEN,6HT VISC,6HOSITY ,6H       ,6H       ,
     7    4HG1  ,6HTHE MA,6HSS VEL,6HOCITY ,6HIN DIR,6H 1     ,6H       ,
     H    4HG2  ,6HTHE MA,6HSS VEL,6HOCITY ,6HIN DIR,6H 2     ,6H       ,
     I    4HSTR ,6HTHE SH,6HEAR ST,6HRESS   ,6H       ,6H       ,6H.      ,
     F    4HDYNA,6HTHE DY,6HNAMIC ,6HPRESSU,6HRE     ,6H       ,6H       ,
     K    4HPRES,6HTHE ST,6HATIC P,6HRESSUR,6HE      ,6H       ,6H       ,
     9    4HDENS,6HTHE ME,6HAN DEN,6HSITY   ,6H       ,6H       ,6H       ,
     7    4HU   ,6HTHE VE,6HLOCITY,6H COMPO,6HNENT I,6HP DIR ,6H1      ,
     8    4HV   ,6HTHE VE,6HLOCITY,6H COMPO,6HNENT I,6HN DIR ,6H2      /
      END
```

INIT

```
      SUBROUTINE INIT  (A,IMIN,IMAX,IN,JN,IE,IV,IPT,X1,X2)
      COMMON /CNUMBR/NW,NF,NK,NHS,NVT,NML,NMH,NP,NG1,NG2,NMU,NRO
      COMMON /CN2/ NV1,NV2,NDP,NT
      COMMON/C/ANAME(6,14),ASYMBL(14),NI(50),NPRIN,INDG,CC,NMAX,INM,JNM
      COMMON /CTURB/ ZA,ZB,ZC,C1,C2,C3,ZLP
      COMMON /CBOU/ ROC,TC,UC,ZKC,YC,XC,XM,EX,EY,IFREE
      COMMON /CPROP/ ZMU,ROG,TG,TW
      COMMON SV,SHS,CF(41),ST(41)
      COMMON /CIN/ HG,A1,POT,CL1,CL2,A2
      DIMENSION A(IN,JN,IV),IMIN(JN),IMAX(JN),X1(IN),X2(JN),ATITLE(19)
      INM=IN-1
      JNM=JN-1
C***
C     FIXED BOUNDARY CONDITIONS
C***
      YF=YC/(1.+2.*A1)
      XG=A1*YF
      UG=A2*UC/SQRT(YF/2./XC)
      XM=4.*XG
      X1(1)=0.
      X1(2)=1.
      DX1=1.
      DO 27 I=3,IN
      DX1=DX1*EX
   27 X1(I)=X1(I-1)+DX1
      DO 26 I=1,IN
   26 X1(I)=X1(I)*XM/X1(IN)
      IFREE=0
   37 IFREE=IFREE+1
      IF (X1(IFREE).LT.XG) GO TO 37
      DIV=XG/X1(IFREE)
      DO 38 I=1,IN
   38 X1(I)=X1(I)*DIV
      X2(1)=0.
```

```
      X2(2)=1.
      DX2=1.
      DO 7 J=3,JN
      DX2=DX2*EY
    7 X2(J)=X2(J-1)+DX2
      DO 6 J=2,JN
    6 X2(J)=X2(J)/X2(JN)
      DO 8  J=1,JN
    8 A(1,J,IV)=X2(J)
      DO 9 JJ=1,JN
      J=JN+1-JJ
      X2(J)=(1.-A(1,JJ,IV))*(YC-YF)
    9 A(1,JJ,IV)=0.
      DO 299 I=1,IFREE
      XI=X1(I)/XG
      A(I,1,NW)=3.*UG  *(XI*XI-SQRT(XI))/XG
      A(I,1,NF)=-XG*UG  *(XI-0.8*XI**2.5+0.25*XI**4) *A(I,1,NRO)
      A(I,1,NG2)= UG  *(1.-2.*XI*SQRT(XI)+XI*XI*XI) *A(I,1,NRO)
      A(I,1,NK)=UG*UG*CL2*CL2
  299 CONTINUE
      IFREE=IFREE+1
      DO 297 I=IFREE,IN
      A(I,1,NW)=0.
      A(I,1,NF)=A(IFREE-1,1,NF)
  297 CONTINUE
      DO 359 I=1,IN
  359 A(I,JN,NHS)=TW
      ZLP=CL1*(YC-YF)
      DO 202 I=2,INM
      DO 202 J=2,JNM
      IF (A(I,J,NK).NE.0.) GO TO 202
      A(I,J,NK)=1.
  202 CONTINUE
      WRITE (6,63) ZA,ZB,ZC,C2,C3,ZLP
      WRITE (6,63) ROC,ROG,UC
      WRITE (6,63) ZMU
      WRITE (6,63) CC
      WRITE (6,63) XC,UC  ,YC,EX,EY
      WRITE (6,63) YF,XG,UG
      WRITE (6,63) A1,A2,CL1,CL2
   63 FORMAT (1H0,1P8E14.4)
      WRITE (6,64) NW,NF,NK,NHS
      WRITE (6,64) NML,NMU,NRO
      WRITE (6,64) NP,NDP,NT
      WRITE (6,64) NG1,NG2,NV1,NV2
      WRITE (6,64) IE,IV,NPRIN
      WRITE (6,64) IN,JN,IFREE
      WRITE (6,64) NI
   64 FORMAT ( 1H0,25I4)
      WRITE (6,15) X1
      WRITE (6,16) X2
   15 FORMAT (4H0X1=,1P8E14.4)
   16 FORMAT (4H0X2=,1P8E14.4)
      RETURN
```

```
      END
```

VROMU

```
      SUBROUTINE VROMU (A,IMIN,IMAX,IN,JN,IE,IV,IPT,X1,X2)
      COMMON /CNUMBR/NW,NF,NK,NHS,NVT,NML,NMH,NP,NG1,NG2,NMU,NRO
      COMMON /CN2/ NV1,NV2,NDP,NT
      COMMON/C/ANAME(6,14),ASYMBL(14),NI(50),NPRIN,INDG,CC,NMAX,INM,JNM
      COMMON /CTURB/ ZA,ZB,ZC,C1,C2,C3,ZLP
      COMMON /CBOU/ ROC,TC,UC,ZKC,YC,XC,XM,EX,EY,IFREE
      COMMON /CPROP/ ZMU,ROG,TG,TW
      COMMON /CB1/ R(21),C(21),S(21),ZK(21),T(21),ZJ(21)
      COMMON SV,SHS,CF(41),ST(41)
      COMMON /CIN/ HG,A1,POT,CL1,CL2,A2
      DIMENSION A(IN,JN,IV),IMIN(JN),IMAX(JN),X1(IN),X2(JN)
C***
C     COMPUTATION OF THE VELOCITIES
C***
      DO 10 J=2,JNM
      HN=X2(J+1)-X2(J)
      HS=X2(J)-X2(J-1)
      A(1,J,NG2)=(A(1,J,NF)-A(2,J,NF))/(X1(2)-X1(1))
      A(IN,J,NG2)=(A(INM,J,NF)-A(IN,J,NF))/(X1(IN)-X1(INM))
      A(IN,J,NG1)=((A(IN,J+1,NF)-A(IN,J,NF))*HS/HN
     1   +(A(IN,J,NF)-A(IN,J-1,NF))*HN/HS)/(HS+HN)
      DO 10 I=2,INM
      HE=X1(I+1)-X1(I)
      HW=X1(I)-X1(I-1)
      A(I,J,NG1)=((A(I,J+1,NF)-A(I,J,NF))*HS/HN
     1   +(A(I,J,NF)-A(I,J-1,NF))*HN/HS)/(HN+HS)
      A(I,J,NG2)=((A(I-1,J,NF)-A(I,J,NF))*HE/HW
     1   +(A(I,J,NF)-A(I+1,J,NF))*HW/HE)/(HE+HW)
   10 CONTINUE
      DO 11 I=2,INM
      HE=X1(I+1)-X1(I)
      HW=X1(I)-X1(I-1)
      A(I, 1,NG2)=((A(I-1, 1,NF)-A(I, 1,NF))*HE/HW
     1   +(A(I, 1,NF)-A(I+1, 1,NF))*HW/HE)/(HE+HW)
      A(I,1,NG1)=(A(I,2,NF)-A(I,1,NF))/(X2(2)-X2(1))
   11 CONTINUE
      DO 12 I=1,IN
      DO 12 J=1,JN
      A(I,J,NV1)=A(I,J,NG1)/A(I,J,NRO)
      A(I,J,NV2)=A(I,J,NG2)/A(I,J,NRO)
   12 A(I,J,NDP)=(A(I,J,NG1)*A(I,J,NG1)+A(I,J,NG2)*A(I,J,NG2))
     1   /A(I,J,NRO)  *0.5
C***
C     COMPUTATION OF THE DENSITY AND THE VISCOSITY
C***
   21 DO 32 J=1,JNM
      DO 32 I=1,IN
      IF (A(I,J,NK).LT.0.) A(I,J,NK)=0.
      IF (X2(JN)-X2(J  )-ZLP) 40,41,41
   41 ZL=ZLP
```

```
      GO TO 42
   40 Y=X2(JN)-X2(J)
      REK=A(I,J,NRO)*SQRT(A(I,J,NK))*Y/ZMU
      ZL =Y*(1.-EXP(-C3*REK))
   42 A(I,J,NML)=ZL
   32 A(I,J,NMU)=ZC*A(I,J,NRO)*SQRT(A(I,J,NK))*ZL
      RETURN
      END
```

EQN

```
      SUBROUTINE EQN (K,RES,RELAX,A,X1,X2,IMIN,IMAX,IN,JN,IE,PR,IV,AM)
      COMMON /CNUMBR/NW,NF,NK,NHS,NVT,NML,NMH,NP,NG1,NG2,NMU,NRO
      COMMON /CN2/ NV1,NV2,NDP,NT
      COMMON/C/ANAME(6,14),ASYMBL(14),NI(50),NPRIN,INDG,CC,NMAX,INM,JNM
      COMMON /CTURB/ ZA,ZB,ZC,C1,C2,C3,ZLP
      COMMON /CBOU/ ROC,TC,UC,ZKC,YC,XC,XM,EX,EY,IFREE
      COMMON /CPROP/ ZMU,ROG,TG,TW
      COMMON SV,SHS,CF(41),ST(41)
      COMMON /CB1/ R(21),C(21),S(21),ZK(21),T(21),ZJ(21)
      DIMENSION A(IN,JN,IV),X1(IN),X2(JN),IMIN(JN),IMAX(JN),PR(2,IE)
      DIMENSION AM(IE)
      GAMA=ZMU/PR(1,K)
      AMAX=AM(K)
      AM(K)=0.
      JI=2
      JNMM=JNM
      IF (K-NW) 102,101,102
  101 JNMM=JNM-1
  102 CONTINUE
   39 DO 40 J=2,JNMM
      DO 40 I=JI,INM
      H1=X1(I+1)-X1(I-1)
      H2=X2(J+1)-X2(J-1)
      HE=X1(I+1)-X1(I)
      HW=X1(I)-X1(I-1)
      HN=X2(J+1)-X2(J)
      HS=X2(J)-X2(J-1)
C***
C     SOURCE TERMS
C***
      SOURCE=0.
      ZQ=0.
      IF (K.NE.NK) GO TO 789
      Y=X2(JN)-X2(J)
      DV21=((A(I+1,J,NV2)-A(I,J,NV2))*HW/HE
     1    +(A(I,J,NV2)-A(I-1,J,NV2))*HE/HW)/(HE+HW)
      DV12=((A(I,J+1,NV1)-A(I,J,NV1))*HS/HN
     1    +(A(I,J,NV1)-A(I,J-1,NV1))*HN/HS)/(HN+HS)
      A(I,J,NT)=(A(I,J,NMU)+ZMU)*(DV12+DV21)
   81 DV11=((A(I+1,J,NV1)-A(I,J,NV1))*HW/HE
     1    +(A(I,J,NV1)-A(I-1,J,NV1))*HE/HW)/(HE+HW)
      DV22=((A(I,J+1,NV2)-A(I,J,NV2))*HS/HN
```

```
     1    +(A(I,J,NV2)-A(I,J-1,NV2))*HN/HS)/(HN+HS)
      IF (A(I,J,NK).LT.0.) A(I,J,NK)=0.
  834 VISC=A(I,J,NMU)
      GEN=(2.*(DV11*DV11+DV22*DV22)+(DV12+DV21)*(DV12+DV21))*VISC
   82 IF (Y-ZLP) 51,52,52
   52 ZL3=ZLP
      ZL3=A(I,J,NML)
      GO TO 53
   51 REK=A(I,J,NRO)*SQRT(A(I,J,NK))*Y/ZMU
      ZL3=Y*(1.-EXP(-C2*REK))
   53 DIF=ZA*A(I,J,NRO)              *SQRT(A(I,J,NK))/ZL3
      SOURCE=GEN
      ZQ=DIF
  789 IF (K.EQ.NF) SOURCE=A(I,J,NRO)*A(I,J,NW)
C***
C     CONDUCTIVE TERMS
C***
      IF (K-NF) 65,62,65
   65 IF (K-NW) 63,62,63
   62 CE=H2/2./HE
      CW=H2/2./HW
      CN=H1/2./HN
      CS=H1/2./HS
      GO TO 25
   63 DP  =A(I  ,J  ,NMU)/PR(2,K)+GAMA
      DE  =A(I+1,J  ,NMU)/PR(2,K) +GAMA
      DN  =A(I  ,J+1,NMU)/PR(2,K) +GAMA
      DW  =A(I-1,J  ,NMU)/PR(2,K) +GAMA
      DS  =A(I  ,J-1,NMU)/PR(2,K)+GAMA
   35 CE=H2*(DE+DP)/(4.*HE)
      CW=H2*(DW+DP)/(4.*HW)
      CN=H1*(DN+DP)/(4.*HN)
      CS=H1*(DS+DP)/(4.*HS)
   25 ADNM=CE+CW+CN+CS
      IF (K-NW) 42,94,42
   94 CE=CE*(A(I+1,J,NMU) +ZMU)
      CW=CW*(A(I-1,J,NMU)   +ZMU)
      CN=CN*(A(I,J+1,NMU)  +ZMU)
      CS=CS*(A(I,J-1,NMU)   +ZMU)
      ADNM=ADNM*(A(I,J,NMU)  +ZMU)
   42 ANUM=CE*A(I+1,J,K) +CW*A(I-1,J,K) +CN*A(I,J+1,K) +CS*A(I,J-1,K)
     2              +SOURCE  *H1*H2 /4.
      ADNM=ADNM+ZQ*H1*H2/4.
      IF (K-NF) 41,44,41
C***
C     CONVECTIVE TERMS
C***
   41 ZCU=0.
      AU=0.
      DFW=(A(I,J+1,NF)+A(I-1,J+1,NF)-A(I,J-1,NF)-A(I-1,J-1,NF)) /4.
      DFN=-(A(I-1,J,NF)+A(I-1,J+1,NF)-A(I+1,J,NF)-A(I+1,J+1,NF))/4.
      DFS=-(A(I+1,J,NF)+A(I+1,J-1,NF)-A(I-1,J,NF)-A(I-1,J-1,NF))/4.
      DFE=(A(I,J-1,NF)+A(I+1,J-1,NF)-A(I,J+1,NF)-A(I+1,J+1,NF)) /4.
      IF (DFW) 911,912,913
  911 ZCU=-DFW+ZCU
```

```
      GO TO 912
  913 AU=AU+DFW*A(I-1,J,K)
  912 IF (DFE)  921,922,923
  921 ZCU=ZCU-DFE
      GO TO 922
  923 A U =A U +DFE*A(I+1,J,K)
      IF (I.EQ.INM) CE=CE+DFE
  922 IF (DFS) 931,932,933
  931 ZCU=ZCU-DFS
      GO TO 932
  933 AU=AU+DFS*A(I,J-1,K)
  932 IF (DFN) 941,942,943
  941 ZCU=ZCU-DFN
      GO  TO 942
  943 AU=AU+DFN*A(I,J+1,K)
  942 CONTINUE
C***
C     COMPUTATION OF THE NEW VALUES
C***
      ADNM=ADNM+ZCU
      ANUM=ANUM+AU
   44 Z=A(I,J,K)
      A(I,J,K)=ANUM/ADNM
      IF (I.EQ.INM) A(I,J,K)=(ANUM-CE*A(IN,J,K))/(ADPM-CE)
      IF (ABS(A(I,J,K)).GT.ABS(AM(K))) AM(K)=A(I,J,K)
      RS=(A(I,J,K)-Z)/AMAX
  377 FORMAT (1H ,3I3,1X,1P12E10.2/13E10.2)
   40 IF(ABS(RS).GT.ABS(RES)) RES=RS
      RETURN
      END
```

BOU

```
      SUBROUTINE BOU (              A,X1,X2,IMIN,IMAX,IN,JN,IE,PR,IV,AMAX)
      COMMON /CNUMBR/NW,NF,NK,NHS,NVT,NML,NMH,NP,NG1,NG2,NMU,NRO
      COMMON /CN2/ NV1,NV2,NDP,NT
      COMMON/C/ANAME(6,14),ASYMBL(14),NI(50),NPRIN,INDG,CC,NMAX,INM,JNM
      COMMON /CTURB/ ZA,ZB,ZC,C1,C2,C3,ZLP
      COMMON /CBOU/ ROC,TC,UC,ZKC,YC,XC,XM,EX,EY,IFREE
      COMMON /CPROP/ ZMU,ROG,TG,TW
      COMMON SV,SHS,CF(41),ST(41)
      COMMON /CB1/ R(21),C(21),S(21),ZK(21),T(21),ZJ(21)
      DIMENSIONA(IN,JN,IV),X1(IN),X2(JN),IMIN(JN),IMAX(JN),PR(2,IE)
      DIMENSION AMAX(IE)
      DIMENSION CA(21)
      DATA CMIN /0.155/
      DATA T /21*1./
      HN=X2(JN)-X2(JNM)
      HS=X2(JNM)-X2(JN-2)
C***
C     THE VARYING BOUNDARY CONDITIONS
C***
      DO25 K=1,IE
```

```
      DO25 J=2,JN
   25 A(IN,J,K)=A(IN-1,J,K)
      DO26 K=3,IE
      DO26 J=2,JNM
   26 A(1,J,K)=A(2,J,K)
      DO 116 I=IFREE,IN
  116 A(I,1,NF)=A(I,2,NF)
      RO=ROC
      SIG=PR(1,NHS)
      SIGO=PR(2,NHS)
      DO 71 I=1,IN
      T(I)=A(I,JN,NT)
      IF (A(I,JNM,NK).LT.0.) A(I,JPM,NK)=0.
      R(I)=SQRT(A(I,JNM,NK))*(X2(JN)-X2(JNM))*RO/ZMU
      CMAX=0.0565*(R(I)+5.)**0.895
      IF (R(I)-19.8 ) 50,50,53
   53 IF (T(I)) 54,55,5
   55 ZK(I)=10000.
      GO TO 56
   54 ZK(I)=A(I,JNM,NK)*RO/ABS(T(I))
   56 CONTINUE
      CA(I)=ZK(I)/R(I)**0.827
      CAA=0.097/CA(I)**0.34
      IF (CAA-CMIN) 60,60,59
   59 C(I)=CAA *(R(I)+5.)**0.58
      IF (C(I).GT.CMAX) GO TO 63
      GO TO 64
   60 C(I)=CMIN *(R(I)+5.)**0.58
      GO TO 64
   50 C(I)=1.
      S(I)=SIG/SIGO/(1./CMAX+1.8*ZB/ R(I))
      A(I,JN,NK)=-A(I,JNM,NK)
      GO TO 67
   63 C(I)=CMAX
   62 S(I)=SIG/SIGO/(1./C(I)+1.8*ZB/ R(I))
      A(I,JN,NK)=A(I,JNM,NK)
      GO TO 61
   64 S(I)=SIG/SIGO/(1./C(I)+0.45*ZB/ R(I)**0.6)
      A(I,JN,NK)=-A(I,JNM,NK) *0.39
   61 CONTINUE
   67 CONTINUE
      IF (S(I).GT.1.) GO TO 65
      S(I)=1.
      A(I,JN,NK)=-A(I,JNM,NK)
   65 CONTINUE
   99 CONTINUE
      A(I,JN,NT)=-C(I)*ZMU*A(I,JNM,NG1)/HN
      PP=(A(I,JN,NT)+A(I,JN-2,NW)*(A(I,JN-2,NMU)+ZMU))/(HN+HS)
      A(I,JNM,NT)=A(I,JN,NT)-PP*HN
      A(I,JNM,NW)=-A(I,JNM,NT)/(ZMU+A(I,JNM,NMU))
      CF(I)=A(I,JN,NT)/RO/UC/UC
   71 CONTINUE
      IF (IE.LT.NHS) GO TO 9876
      DO 81 I=1,IN
      DT=A(I,JNM,NHS)-TW
```

```
      H=X2(JN)-X2(JNM)
      ZJ(I)=S(I)*ZMU*DT/SIG/H
      A(I,JN,NHS)=A(I,JNM,NHS)-S(I)*DT/(1.+A(I,JNM,NMU)/ZMU*SIG/SIGO)
      TEM=A(1,1,NHS)-TW
      ST(I)=ZJ(I)/RO /UC/TEM
   81 CONTINUE
 9876 SHS=0.
      SV=0.
      DO 391 I=2,IN
      SV=SV+0.5*(CF(I-1)+CF(I))*(X1(I)-X1(I-1))
  391 SHS=SHS+0.5*(ST(I-1)+ST(I))*(X1(I)-X1(I-1))
      SV=SV/X1(IN)
      SHS=SHS/X1(IN)
      RETURN
      END
```

OUT

```
      SUBROUTINE OUT    (A,IMIN,IMAX,IN,JN,IE,IV,IPT,X1,X2)
      COMMON/C/ANAME(6,14),ASYMBL(14),NI(50),NPRIN,INDG,CC,NMAX,INM,JNM
      COMMON /CN2/ NV1,NV2,NDP,NT
      COMMON /CNUMBR/NW,NF,NK,NHS,NVT,NML,NMH,NP,NG1,NG2,NMU,NRO
      COMMON /CTURB/ ZA,ZB,ZC,C1,C2,C3,ZLP
      COMMON /CBOU/ ROC,TC,UC,ZKC,YC,XC,XM,EX,EY,IFREE
      COMMON /CPROP/ ZMU,ROG,TG,TW
      COMMON /CB1/ R(21),C(21),S(21),ZK(21),T(21),ZJ(21)
      DIMENSION A(IN,JN,IV),IMIN(JN),IMAX(JN),X1(IN),X2(JN)
      COMMON SV,SHS,CF(41),ST(41)
      JX=JN/14
      IX=IN/14
      IF (IX.LT.1) IX=1
      IF (JX.LT.1) JX=1
      IF (NP.GT.NPRIN) GO TO  205
      CALL PRES  (A,IMIN,IMAX,IN,JN,IE,IV,IPT,X1,X2)
  205 CONTINUE
C***
C     GEOMETRICAL DISPLAY OF THE RESULTS
C***
      IF (IPT.EQ.2) GO TO 201
      DO 10 K=1,NPRIN
      WRITE(6,100) (ANAME(L,K),L=1,6)
100   FORMAT(1H1,30X,21HTHE DISTRIBUTION OF  ,6A6//4H   J//)
      DO 2 J=1,JN,JX
    2 WRITE(6,111) J,(A(I,J,K),I=1,IN,IX)
  111 FORMAT (1H0,I2,2X,1P14E 9.2)
      WRITE(6,112) (I,I=1,IN,IX)
  112 FORMAT (1H0/4H  I=    ,13(I2,7X),I2)
      IF (K-NW) 21,22,21
   22 WRITE (6,233) (CF(I),I=1,IN,IX)
      WRITE (6,233) (R (I),I=1,IN,IX)
      WRITE (6,233) (C (I),I=1,IN,IX)
      WRITE (6,233) (T (I),I=1,IN,IX)
      WRITE (6,233) (X1(I),I=1,IN,IX)
```

```
   21 IF (K-NK) 23,24,23
   24 WRITE (6,233) (ZK(I),I=1,IN,IX)
      WRITE (6,233) (X1(I),I=1,IN,IX)
   23 IF (K-NHS) 25,26,25
   26 WRITE (6,233) (S(I),I=1,IN,IX)
      WRITE (6,233) (ZJ(I),I=1,IN,IX)
      WRITE (6,233) (ST(I),I=1,IN,IX)
      WRITE (6,233) (X1(I),I=1,IN,IX)
  233 FORMAT (1H0,4X,1P14E 9.2)
   25 CONTINUE
   10 CONTINUE
  201 IF (IPT.EQ.1) RETURN
C***
C      TABULAR DISPLAY OF THE RESULTS
C***
      IPAGE=0
      DO 12 J=1,JN
      ILINE=0
      DO 1 I=1,IN
      IF (IPAGE.EQ.0) WRITE (6,101) (ASYMBL(K),K=1,NPRIN)
101   FORMAT(10H1 I       J,7(9X,A6))
      IF (ILINE.EQ.0) WRITE (6,103)
103   FORMAT(1H )
      WRITE(6,102) I,J,(A(I,J,K),K=1,NPRIN)
102   FORMAT(1H ,I2,5X,I2,7(1PE15.5))
      ILINE=ILINE+1
      IPAGE=IPAGE+1
      IF (IPAGE.GE.40) IPAGE=0
1     IF(ILINE/5*5.EQ.ILINE)WRITE(6,103)
   12 WRITE (6,103)
      RETURN
      END
```

PRES

```
      SUBROUTINE PRES  (A,IMIN,IMAX,IN,JN,IE,IV,IPT,X1,X2)
      COMMON/C/ANAME(6,14),ASYMBL(14),NI(50),NPRIN,INDG,CC,NMAX,INM,JNM
      COMMON /CN2/ NV1,NV2,NDP,NT
      COMMON /CNUMBR/NW,NF,NK,NHS,NVT,NML,NMH,NP,NG1,NG2,NMU,NRO
      COMMON /CTURB/ ZA,ZB,ZC,C1,C2,C3,ZLP
      COMMON /CBOU/ ROC,TC,UC,ZKC,YC,XC,XM,EX,EY,IFREE
      COMMON /CPROP/ ZMU,ROG,TG,TW
      DIMENSION A(IN,JN,IV),IMIN(JN),IMAX(JN),X1(IN),X2(JN)
      COMMON /CB1/ R(21),C(21),S(21),ZK(21),T(21),ZJ(21)
      DIMENSION PP(41)
      DATA PO/0./
      A(2,2,NP)=PO
      J=2
      DO21 I=2,INM
      HE=X1(I+1)-X1(I)
      HN=X2(J+1)-X2(J)
      HS=X2(J)-X2(J-1)
      HW=X1(I)-X1(I-1)
      DI=A(I,J,NDP)*((A(I+1,J,NRO)-A(I,J,NRO))*HW/HE
```

```
     1    +(A(I,J,NRO)-A(I-1,J,NRO))*HE/HW)/(HE+HW)
          DII=A(I,J,NG2)*A(I,J,NW)
          DIII=((A(I,J+1,NT)-A(I,J,NT))*HS/HN
     1    +(A(I,J,NT)-A(I,J-1,NT))*HN/HS)/(HN+HS)
          DPDX=DI+DII+DIII
          PP(I)=DI+DII+DIII
   21     CONTINUE
          DO22 I=3,INM
   22     A(I,2,NP)=(PP(I-1)+PP(I))*0.5*(X1(I)-X1(I-1))+A(I-1,2,NP)
          DO23 I=2,INM
          HE=X1(I+1)-X1(I)
          HW=X1(I)-X1(I-1)
          DV11=((A(I+1,2,NV1)-A(I,2,NV1))*HW/HE
     1    +(A(I,2,NV1)-A(I-1,2,NV1))*HE/HW)/(HE+HW)
   23     A(I,2,NP)=A(I,2,NP)-A(I,2,NDP)+2.*(A(I,2,NMU)+ZMU)*DV11
          DO27 I=2,INM
          HN=X2(3)-X2(2)
          HS=X2(2)-X2(1)
          DV22=((A(I,3,NV2)-A(I,2,NV2))*HS/HN
     1    +(A(I,2,NV2)-A(I,1,NV2))*HN/HS)/(HN+HS)
          A(I,2,NP)= A(I,2,NP)+A(I,2,NDP)-2.*(A(I,2,PMU)+ZMU)*DV22
          DO25 J=2,JNM
          HE=X1(I+1)-X1(I)
          HW=X1(I)-X1(I-1)
          HS=X2(J)-X2(J-1)
          HN=X2(J+1)-X2(J)
          DI=A(I,J,NDP)*((A(I,J+1,NRO)-A(I,J,NRO))*HS/HN
     1    +(A(I,J,NRO)-A(I,J-1,NRO))*HN/HS) /(HN+HS)
          DII=-A(I,J,NG1)*A(I,J,NW)
          DIII=((A(I+1,J,NT)-A(I,J,NT))*HW/HE
     1    +(A(I,J,NT)-A(I-1,J,NT))*HE/HW)/(HE+HW)
          DPDY=DI+DII+DIII
          PP(J)=DPDY
   25     CONTINUE
          DO26 J=3,JNM
   26     A(I,J,NP)=A(I,J-1,NP)+(PP(J)+PP(J-1))*0.5*(X2(J)-X2(J-1))
          DO27 J=2,JNM
          HS=X2(J)-X2(J-1)
          HN=X2(J+1)-X2(J)
          DV22=((A(I,J+1,NV2)-A(I,J,NV2))*HS/HN
     1    +(A(I,J,NV2)-A(I,J-1,NV2))*HN/HS)/(HN+HS)
          A(I,J,NP)=A(I,J,NP)-A(I,J,NDP)+2.*(A(I,J,NMU)+ZMU)   *DV22
   27     A(I,J,NP)=A(I,J,NP)-A(INM,2   ,NP)
          RETURN
          END
```